4-2020

Design, Development and Evaluation of Dual Drug Nanomedicine for Non-Small Cell Lung Cancer

Elham Hatami
University of Tennessee Health Science Center

Design, Development and Evaluation of Dual Drug Nanomedicine for Non-Small Cell Lung Cancer

Abstract

Resistance to conventional chemotherapy is a big challenge in the treatment of cancer including non-small cell lung cancer (NSCLC). A combination of natural chemo sensitizer agents with chemotherapy offers unique advantages over monotherapy alone. However, free unbound drugs, (in combination or as a single agent), lack tumor-targeted accumulation and therefore can be easily eliminated from the patient body. Moreover, some drugs are hydrophobic, and their organic solvents cause in vivo toxicity, thereby limiting their capability in clinical translation. Herein, dual loaded biocompatible and biodegradable nanoparticles (NPs) using Gemcitabine (Gem)a pyrimidine nucleoside antimetabolite and Gambogic acid (GA) (a highly hydrophobic chemo sensitizer agent)- were developed on human serum albumin-tannic acid nano-platform (HTA) for targeted treatment of NSCLC.Our in vitro results demonstrate that Gem and GA combination therapy has tremendous potential due to their high efficacy on NSCLC, and GA sensitize NSCLC to Gem therapy. However, GA used in combination with Gem suffers from limited solubility which subsequently leads to a decline in therapeutic efficacy. Therefore, in order to overcome this, in the present study GA and Gem were encapsulated in human serum albumin-tannic acid nanoparticles by the solvent evaporation method. In this platform, HTA is a biocompatible nanocarrier that binds to both GA and Gem. Physico chemical characterizations studies revealed that GA and Gem are successfully encapsulated in HTA NPs with uniform spherical morphology. These nanoparticles were readily taken up by NSCLC cells (A549 and H1299) in a concentration and time-dependent manner. Apart from an increase in GA solubility, encapsulated GA and Gem subsequently manifested elevated therapeutic efficacy, which was confirmed by cell viability, colony formation, migration and invasion studies. Furthermore, in vivo and ex vivo imaging analysis demonstrated notable tumor-targeting behavior of our uniquely designed HTA NPs in mice bearing A549 xenograft tumors. These findings clearly illustrate that our dual loaded NPs can be efficiently utilized to improve cancer therapy and tumor eradication.

Document Type

Dissertation

Degree Name

Doctor of Philosophy (PhD)

Program

Pharmaceutical Sciences

Research Advisor

Murali M. Yallapu Ph.D.

Keywords

Cancer, Combination, Drug Delivery, drug resistance, Nano medicine, Pharmaceutical Scinces

Subject Categories

Analytical, Diagnostic and Therapeutic Techniques and Equipment | Medicine and Health Sciences

UNIVERSITY OF TENNESSEE HEALTH SCIENCE CENTER

DOCTOR OF PHILOSOPHY DISSERTATION

Design, Development and Evaluation of Dual Drug Nanomedicine for Non-Small Cell Lung Cancer

Author:
Elham Hatami

Advisor:
Murali M. Yallapu, Ph.D.

A Dissertation Presented for The Graduate Studies Council of
The University of Tennessee Health Science Center
in Partial Fulfillment of the Requirements for the
Doctor of Philosophy degree from
The University of Tennessee

in

Pharmaceutical Sciences: Pharmaceutics
College of Graduate Health Sciences

May 2020

DEDICATION

To my lovely parents: Ali and Aghdas, with heartfelt love and gratitude. I am where I am because of your endless love, care and sacrifices. Thank you for teaching me to believe in myself.

To Elnaz: for all the time she was there for me, and for zillion reasons she knows so well.

To Babak: for his endless support.

ACKNOWLEDGEMENTS

I would like to express my sincere gratitude to everyone who supported me throughout my Ph.D. journey at University of Tennessee Health Science Center. I would like to thank my mentor Dr. Murali M. Yallapu for providing me the opportunities to conduct my doctoral research in his laboratory. His guidance and help have made this dissertation possible.

I would also like to express my sincere thanks to my committee members, Dr. Liza Makowski, Dr. Santosh Kumar, Dr. Subhash C. Chauhan, Dr. Wei Li and Dr. Yi Lu for their valuable support, suggestions and directions for the successful completion of this dissertation project.

I also want to convey my sincere thanks to the dean of the graduate school, Dr. Donald B. Thomason and director of pharmaceutical sciences program Dr. Hassan Almoazen for their continuous support and encouragement. My special thanks should also go to my colleagues for their assistance at various stages of the project, Dr. Prashanth K. B. Nagesh for providing constructive suggestions and his invaluable and critical guidance and help in conducting biological assays as well as biochemical and *in vivo* techniques and Advait B. Shetty, Pallabita Chowdhury, Deanna N. Shields and Sumeet Chauhan for their assistance in various stages of this project. I am also immensely grateful for the UTHSC and NIH funding's for my research. I also welcome this opportunity to acknowledge Dr. Brian M Peters, Dr. Frank Park and Dr. Wei Li for their help with FACs machine, EVOS® FL Imaging System Keyence microscope and FTIR spectroscopy. Also, I would like to thank Dr. Amali Samarasinghe for providing lung fluid and Dr. Sheema Khan for her valuable consultations. Additionally, I would like to acknowledge UTHSC core and animal facility staff.

I would like to thank Pharmaceutics Journal, for granting permission to use my published work in this dissertation.

Finally, I express my sincere gratitude and thank to my parents Mr. Ali Hatami and Mrs. Aghdas Hatami for their love and care. I am forever grateful for my mother's blessings and prayers that gave me strength to complete this journey. I would like to convey my heartiest appreciation to my sister Elnaz for her love, support and constant encouragement and I am very grateful to my lovely brothers Amir and Afshin. Also, I want to thank my beloved fiancé Babak for his endless love, support, and understanding.

ABSTRACT

Resistance to conventional chemotherapy is a big challenge in the treatment of cancer including non-small cell lung cancer (NSCLC). A combination of natural chemo-sensitizer agents with chemotherapy offers unique advantages over monotherapy alone. However, free unbound drugs, (in combination or as a single agent), lack tumor-targeted accumulation and therefore can be easily eliminated from the patient body. Moreover, some drugs are hydrophobic, and their organic solvents cause *in vivo* toxicity, thereby limiting their capability in clinical translation. Herein, dual loaded biocompatible and biodegradable nanoparticles (NPs) using Gemcitabine (Gem)a pyrimidine nucleoside antimetabolite and Gambogic acid (GA) (a highly hydrophobic chemo-sensitizer agent)-were developed on human serum albumin-tannic acid nano-platform (HTA) for targeted treatment of NSCLC.

Our *in vitro* results demonstrate that Gem and GA combination therapy has tremendous potential due to their high efficacy on NSCLC, and GA sensitize NSCLC to Gem therapy. However, GA used in combination with Gem suffers from limited solubility which subsequently leads to a decline in therapeutic efficacy. Therefore, in order to overcome this, in the present study GA and Gem were encapsulated in human serum albumin-tannic acid nanoparticles by the solvent evaporation method. In this platform, HTA is a biocompatible nanocarrier that binds to both GA and Gem. Physico-chemical characterizations studies revealed that GA and Gem are successfully encapsulated in HTA NPs with uniform spherical morphology. These nanoparticles were readily taken up by NSCLC cells (A549 and H1299) in a concentration and time-dependent manner. Apart from an increase in GA solubility, encapsulated GA and Gem subsequently manifested elevated therapeutic efficacy, which was confirmed by cell viability, colony formation, migration and invasion studies. Furthermore, *in vivo* and ex vivo imaging analysis demonstrated notable tumor-targeting behavior of our uniquely designed HTA NPs in mice bearing A549 xenograft tumors.

These findings clearly illustrate that our dual loaded NPs can be efficiently utilized to improve cancer therapy and tumor eradication.

TABLE OF CONTENTS

LIST OF TABLES

LIST OF FIGURES

LIST OF ABBREVIATIONS

μ	Micro
ALP	Alkaline phosphatase test
ALT	Alanine transaminase
AST	Aspartate aminotransferase bromide
BUN	Blood urea nitrogen
C6	Coumarin 6
Create	Creatinine
DDS	Drug delivery system
DLS	Dynamic light scattering
EGFR	Epidermal growth factor receptor
EPR	Enhanced permeation and retention effect
FTIR	Fourier transform infrared spectroscopy
GA	Gambogic Acid
Gem	Gemcitabine
G-G@HTA NPs	Gambogic acid and Gemcitabine encapsulated in human serum albumin-tannic acid nanoparticles
GGT	Gamma-glutamyl transpeptidase
GLDH	Glutamate dehydrogenase
Glu	Glucose
h(s)	Hour(s)
HAS	serum albumin
HTA NPs	human serum albumin-tannic acid nanoparticles
LF	Lung fluid

MDR	Multi-drug resistant
MFI	Mean fluorescence intensity
ml	Milliliter(s)
MTS	3-(4,5-dimethylthiazol-2-yl)-5-(3-
MTT	3-(4,5-Dimethylthiazol-2-yl)-2,5-diphenyltetrazolium
nM	Nano molar
nm	Nanometer
NP(s)	Nanoparticle(s)
NSCLC	Non-small cell lung cancer
OS	Overall survival
PBS	Phosphate buffered saline
PDI	Polydispersity index
PFS	Progression-free survival
PK/PD	Pharmacokinetics/pharmacodynamics
RES	Reticulo-endothelial system
Rh123	Rodamin123
RPM	Revolutions per minute
RR	Ribonucleotide reductase
RT	Room temperature
SA(s)	Self-assemblie(s)
siRNA	Small interfering ribonucleic acid
TA	Tannic Acid
Tbili	Total bilirubin

TEM	Transmission electron microscopy
TEM	Transmission electron microscopy
UV	Ultraviolet
VEGFR	Vascular endothelial growth factor receptor

CHAPTER 1. INTRODUCTION

Non-Small Cell Lung Cancer

Lung cancer, also known as bronchogenic carcinoma, is the leading cause of cancer-related mortality among both men and women in the United States and throughout the world[1] [2] [3]. In the United States alone, an estimated 228,150 new cases have been diagnosed in 2019 and 142,670 patients have died from lung cancer[4] [5]. In the present year, it is predicted that lung cancer will lead to more deaths than breast, prostate, and colon cancers combined together[4]. Based on the histopathological appearance and morphology under the microscope, lung cancer is divided into two categories: 1) Small cell lung cancer (SCLC) and 2) Non-small cell lung cancer (NSCLC)[6] [7].

NSCLC represents about 85% to 90% of all lung cancer cases (~194 K new cases in 2019). This category is further subcategorized as squamous cell carcinoma, large cell carcinoma, adenocarcinoma and a mixture of undifferentiated carcinomas. NSCLC is mainly asymptomatic in its initial stage; therefore, the majority of NSCLC patients are often diagnosed at advanced stages, contributing to a five-year survival rate as low as 19%[8]. Unfortunately, by the time of diagnosis, 55% of NSCLC cases have developed distant metastases throughout the patient's body [9] [10] [11].

Available Treatment Options

Treatment options range from standard therapies currently implemented in clinical practice to investigational treatments undergoing clinical trials. **Table 1-1** lists the stages of NSCLC and associated treatment strategies[12] [13]. These options include:

- **Surgery**: Consisting of pneumonectomy, lobectomy, segmentectomy or wedge resection, and sleeve resection. Depending on the tumor size and the affected area of the lungs, surgeons will remove either the entire lung or a segment of it. However, one must bear in mind that resection of the lung, regardless of the quantity of tissue removed, will lead to decline in lung function.
- **Radiofrequency ablation (RFA)**: RFA utilizes high-energy radio waves to heat and burn the tumor. Usually patients who have low surgery tolerance and small tumors located by the edge of the lung can take advantage of this procedure.
- **Radiation**: Depending upon the stage of the cancer (localization and size) radiotherapy might be considered as a primary treatment, pre/post surgery therapy.
- **Chemotherapy**: The chemotherapeutic agents can be the only treatment option remaining based on the stage of the cancer and overall health of the patient. We will cover chemotherapy in more detail.
- **Targeted therapies**: These treatment strategies could be designed to identify certain molecular biomarkers on cancer cells and efficiently target and attack those cells. For instance, epidermal growth factor receptor (EGFR) mutations are the most commonly

Table 1-1. Different stages of NSCLC and tumor localization with associated treatment options.

Stage	Tumor localization	Treatment	%Diagnosis	%Survival
Occult	Tumor is hidden, cannot visualized by imaging	-	-	-
0	Carcinoma *in situ*	Surgery	-	-
IA & IB	Only in lung without evidence of regional lymph node or distance metastasis	Surgery	15	75- 55
IIA & IIB	Spread to lymph nodes associated to lung, no evidence of distance metastasis	Surgery	-	50-40
IIIA & IIIB	Lymph nodes in tracheal area, or pop lung and neck, no evidence of distance metastasis	Surgery, chemotherapy, radiation or combination	22	35-5
IV	Metastasis (regional and distance) beyond chest	Chemotherapy	55	<5

Source: Silvestri GA, Gonzalez AV, Jantz MA, et al. Methods for staging non-small cell lung cancer: diagnosis and management of lung cancer, 3rd ed: American College of Chest Physicians evidence-based clinical practice guidelines. Chest 2013; 143: 211–250

occurring mutations in NSCLC cells. Thus, targeted therapy with an EGFR inhibitor (such as erlotinib, afatinib, gefitinib, etc.), could efficiently attack cancer cells by attaching to EGFR receptors which are abundant on the surface of NSCLC cells. Unfortunately, EGFR inhibitors may cause severe side effects such as acneiform rash, which causes skin infections and hematologic toxicity, in addition to the rapid development of resistance[14].

- **Immunotherapy**: The goal of immunotherapy is to establish and create personalized therapy for NSCLC patients by exploring the immune checkpoints response. However, this approach is associated with immune-mediated toxicity issues, e.g. colitis, nephritis, pneumonitis and endocrinopathy[15 16].

Targeted therapies and immunotherapy are among the most recent developments in treating NSCLC. Over past few decades, substantial progress has been made, in all possible respects, in improving the survival rate of lung cancer patients[17 18].Currently, the most desirable treatment strategy in clinical practice utilizes a combination of therapies[19]. For initial stages of NSCLC, physicians generally suggest starting with local resection and radiation therapy, followed by chemotherapy. However, as previously stated, the majority of cases have reached advanced stages (III &IV) by the time of diagnosis, precluding surgical intervention. Thus, the most elite treatment option remaining for these stages is chemotherapy[20]

Chemotherapeutic Treatments for NSCLC and Their Drawbacks

To date, conventional chemotherapeutic anticancer agents, administrated either orally or intravenously, is the most effective therapeutic regimen for NSCLC[21]. Depending on the phase and stage of cancer, the chemotherapy can be administrated pre-surgery (neoadjuvant), post-surgery (adjuvant) or as the predominant regimen (advanced stages). The most common chemotherapeutic agents for NSCLC include:

- Paclitaxel and albumin-bound paclitaxel (nab-paclitaxel, Abraxane)
- Platinum-based agents (e.g. carboplatin and cisplatin).
- Gemcitabine
- Docetaxel
- Irinotecan
- Vinorelbine
- Etoposide
- Pemetrexed

Table 1-2 shows the result of a systematic research from ClinicalTrials.gov, a publicly accessible website. This data was acquired by utilizing the advanced search option and searching the term of "NSCLC" for the past decade (2009-2019), the search was further narrowed by applying "completed" and "with result" filters. Of 184 trials found in this analysis, we excluded those that did not reported "overall survival (OS)" and "Progression free survival (PFS)". Finally, the major chemotherapeutic agent

Table 1-2. Clinical trials on NSCLC.

Chemotherapeutic agent	Combined anticancer agent	OS (months)	PFS (months)
Gemcitabine	Zactima (ZD6474) + Vandetanib	8.9	9.15
	Pemetrexed and Bevacizumab	8.78	5.56
	Necitumumab	14.92	4.21
	Custirsen sodium	14.1	4.3
	Docetaxel	30	13.6
	Cisplatin + axitinib	14.2	6.2
	Cisplatin+ radiation	27.9	11.4
Irinotecan	Oxaliplatin+ Etoposide+ Carboplatin	12.9	8.95
	Pegylated irinotecan	7.00	2.66
Paclitaxel	Carboplatin	11.2	5.8
	Cetuximab	10.3	6.4
	pemetrexed	7.7	3.8
	Imatinib mesylate	7.3	3.6
	Ramucirumab	16.85	7.85
	Olaratumab + carboplatin	12.8	4.77
Nab- Paclitaxel	Carboplatin	12.1	6.3
Carboplatin	TRC105	NA	3
	Necitumumab +Paclitaxel+ Carboplatin	13.2	5.4
	Bevacizumab-EU	16.02	7.62
	nab-paclitaxel	14.52	3.8
	ABP 215	6.6	NA
	OGX-427	10.8	6
	Hydroxychloroquine	NA	4.2
	Bevacizumab+ Carboplatin+ Pemetrexed	20.3	12.6
	Belotaxel	10.6	3.6
	Ipilimumab+ Paclitaxel+ Carboplatin	10.7	5.5
	Pemetrexed + Cixutumumab	NA	8
	Ramucirumab + Gemcitabine	10.4	5.6
	Panitumumab+ Pemetumumab	17.02	5.75
	Olaratumab + Paclitaxel	12.8	4.77
	Gefitinib+Gemcitabine +Carboplatin	NA	9.7
Docetaxel	Alectinib + Pemetrexed	27.8	10.9
	Atezolizumab	15.7	2.8
	Lurbinectedin	5.5	16.7
	Gemcitabine + Lurbinectedin	7.2	6.1
	mogamulizumab	8.88	1.87

Table 1-2. (Continued).

Chemotherapeutic agent	Combined anticancer agent	OS (months)	PFS (months)
	GSK3052230	NA	4.6
	Ramucirumab	15.15	5.22
	Erlotinib	7.1	1.6
	Eribulin Mesylate	9.5	3
	Tivantinib + Erlotinib	6.8	7.3
	Erlotinib [Tarceva]	5.61	2.33
	LY2181308	7.9	2.8
	Erlotinib+ Bevacizumab+ Erlotinib	11.86	4.01
Vinorelbine	Eribulin	9.5	3
Etoposide	Cisplatin	10.3	NA
Pemetrexed	Zoledronic acid + Denosumab	10.9	5.7
	GSK3052230+ Carboplatin	4.1	NA
	OGX-427+ Placebo	10.8	6
	Erlotinib	5.8	1.8
	Gefitinib	10.8	4.0
	Eribulin	9.5	3.0
	Tivantinib+ Erlotinib	6.8	7.3
	Bevacizumab, Carboplatin,	20.3	12.6
	Cisplatin + Cixutumumab	10.68	5.45
	Cisplatin+ Folic acid	34.6	12.4
	Cisplatin+ LY2603618	12.9	4.7
	Ramucirumab + Carboplatin +Gemcitabine	10.4	5.6

Source: U.S. National Library of Medicine. https://clinicaltrials.gov/ct2 accessed October 19, 2019.

that the studies utilized[259]. **Table 1-2** demonstrates that the major trial studies conducted in the past ten years are combination studies of chemotherapeutic agents with another anticancer agent in order to increase patient OS and PFS.

As shown in **Table 1-2**, most of the chemotherapeutic agents have achieved only modest survival improvements due to limitations such as chemo-resistance, relapse, cancer recurrence, intolerable toxicities (as a result of excessive drug usage), and severe side effects. Chemotherapeutic side effects are often due to unspecific targeting, in which the drug attacks healthy cells as well as cancer cells. Since cancer cells are derived from normal cells, conventional agents are unable to differentiate between them. For instance, they can attack neurons and damage nerves, causing peripheral neuropathy. However, gemcitabine (Gem) has shown a safer toxicity profile than other available chemotherapy agents for NSCLC therapy, with improved PFS and OS with Gem/platinum treatment rather than taxol/platinum treatments[22 23]. The clinical benefit of Gem, which has the highest average OS rate (~17 months) among chemotherapy options, while carboplatin and docetaxel have ~12 months and ~10 months average OS respectively, are placed in the second and third best positions.

Moreover, a review on 37 randomized phase III clinical trials with more than 15,000 participants, conducted by Langer et al. to investigate the effect of Gem as first line therapy for NSCLC patients, revealed that Gem as a monotherapy showed similar effects to platinum-based monotherapy for advanced and/or metastatic NSCLC, but with the advantage of having less toxicity. According to this analysis, Gem combination shows a statistically significant benefit-risk ratio with regard to OS and PFS in comparison to platinum-based drug combinations[24]. However, there is a risk of rapid development of resistance to Gem and also of systemic toxicities when combined with other chemotherapeutic agents, we will cover this subject in more detail.

There is an emerging need for optimization and validation of new therapeutic strategies to make the most of Gem therapy for NSCLC and to circumvent its associated difficulties.

Gemcitabine and Its Mechanism of Action

Gemcitabine (Gem) [2'-deoxy-2',2'-d ifluorocytidine monohydrochloride misomer); dFdC] is a potent chemotherapeutic anticancer agent (**Figure 1-1a**). Approved as a cancer therapy by the Food and Drug Administration (FDA) in 1998, Gem has been used as a first and second-line treatment of NSCLC, both as a single agent and in combination regimens[25 26]. Due to its unique mechanism of action, Gem is the most commonly used chemotherapeutic agent for treating advanced NSCLC [27].

Gem, a prodrug, is a nucleotide (deoxycytidine) analog falling under the category of antimetabolite anticancer agents. Upon internalization to cancer cells, the drug converts to its active form *via* a phosphorylation process catalyzed by deoxycytidine

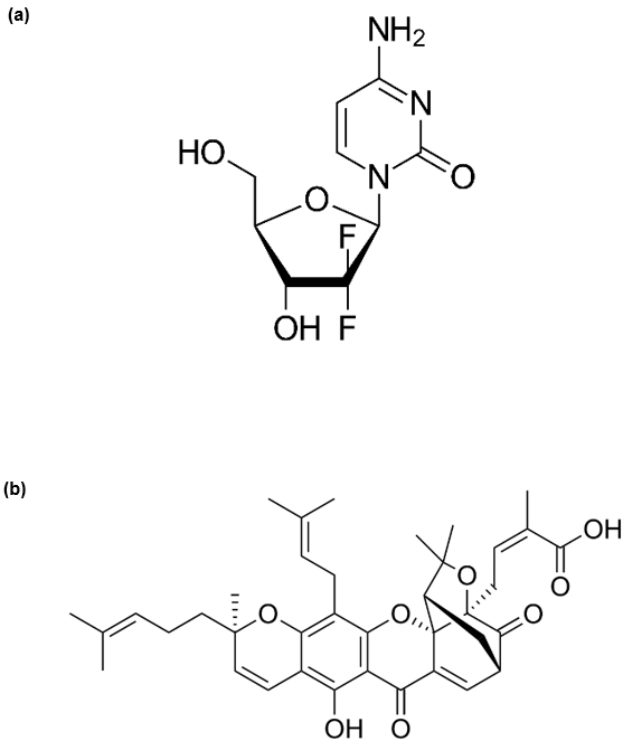

Figure 1-1. Chemical structure of (a) gemcitabine and (b) gambogic acid.
(a) Chemical name of Gem is (2'-deoxy-2',2'-d ifluorocytidine monohydrochloride misomer); dFdC, with chemical formula of $C_9H_{11}F_2N_3O_4$.
(b) Chemical name of GA is (Z)-4-[12-hydroxy-8,21,21-trimethyl-5-(3-methylbut-2-enyl)-8-(4-methylpent-3-enyl)-14,18-dioxo-3,7,20-trioxahexacyclo[15.4.1.02,15.02,19.04,13.06,11]docosa-4(13),5,9,11,15-pentaen-19-yl]-2-methylbut-2-enoic acid, with chemical formula of $C_{38}H_{44}O_8$.

kinase. The kinase converts it to the diphosphate and triphosphate forms. The triphosphate metabolites compete with deoxycytidine triphosphate and promote termination of the DNA chain synthesis. Therefore, Gem acts as an inhibitor of DNA replication, leading to DNA fragmentation, and ultimately causing cell death and apoptosis. Once Gem has been activated inside the cells, self-potentiating activities of its di- and triphosphate forms initiate. This process enhances its anticancer effect by increasing its intracellular concentration above the level of deoxycytidine triphosphate, its competitor in DNA synthesis.

Gem advantages as compared to other nucleoside analogues in NSCLC therapy include 1) active transport through the cell membrane, 2) efficient phosphorylation, 3) ability to self-potentiate, 4) slower elimination rate, 5) good pharmacokinetics profile, 6) increased cell permeability and 7) lower toxicity[28 29]. Moreover, extensive amount of data from phase II studies supports that Gem (Gemzar) has response rate of 21% on NSCLC as a single drug and also it was able to escalate the median survival rate of NSCLC patients by 20-25%, or approximately 9 months[27] . Taken together, this evidence would suggest that Gem is an ideal chemotherapeutic candidate for NSCLC therapy.

Challenges of Gemcitabine Monotherapy

Despite the promising results associated with Gem therapy for NSCLC, the drug may not achieve optimal therapeutic efficacy due to the development of resistance by cancer cells. Initially, patients may respond favorably to Gem-based chemotherapy but will eventually experience a significant decline in response [30 31]. In general, cancer cells develop resistance by a number of mechanisms, including 1) reduction of drug uptake or increase in drug efflux by cells, 2) increased tolerance and fast repair of damaged DNA in cancer cells, or 3) altered drug activation factors by intracellular elements[32 33]. Evidence suggests that mechanisms of resistance cause a drastic decrease in cellular uptake of Gem[34]. Cells may develop resistance to Gem either by intrinsic or acquired pathways involving molecular and cellular variations, such as changes in nucleotide metabolism enzymes, apoptosis pathways, and induction of ATP-binding cassette transporter expression [35]. Furthermore, it has been reported that Gem-related chemoresistance is associated with reduced cellular uptake due to defective human concentrative nucleoside transporter 1 (hCNT1) and human equilibrative nucleoside transporter 1 (hENT1), which are required for Gem influx, as well as overexpression of ribonucleotide reductase activity and decrease in deoxycytidine kinase (DCK) expression [36 37]. Another important factor for the development of chemoresistance is the deamination of Gem by cytidine deaminase (CDA), which plays a critical role in Gem metabolism. Deamination converts Gem to its inactive form, and studies support that the over-expression of CDA is associated with Gem resistance [38]. Moreover, significant number of studies indicate that the over-expression of the ribonucleotide reductase (RR) enzyme, which is directly associated with Gem's self-potentiating process and is responsible for conversion of nucleotide diphosphates (NDPs) to deoxyribonucleoside triphosphates (dNDPs) during DNA synthesis, has great impact on cell resistance to Gem therapy [39 40 41 42 43].

Gemzar® is the chemically modified version of Gem (a hydrochloride salt form) produced by Eli Lilly and Company in the expectation of increased potency, but, along with a slight increase in side effects, it is also more susceptible to deamination, decreasing its half-life to 15 minutes [44].

To date, anticancer agents have been used both as single agents and in combination regimens. Combination therapies are continuously being explored and have already gained significant attention. The synergistic effect of combining therapeutic agents improves patient response and reduces the development of drug resistance by cancer cells. Particularly for lung cancer therapy, an increasing body of evidence suggests that the utilization of a single anticancer drug confers a high failure rate as a consequence of the complex nature of this cancer[19 45]. Thus, devising effective combination regimens that overcome the multivdrug resistance (MDR) phenomenon remains desirable in the clinical setting.

As Gem exhibits mild toxicity, it is a superior candidate for combination therapy regimens. The copious literature available on PubMed on Gem combinations with other anticancer agents for NSCLC therapy supports the importance of the co-administration of Gem in order to elevate its level of efficacy **(Figure 1-2**). Combination therapy not only will help to maximize the therapeutic efficacy of Gem, but also minimize the development of intrinsic and acquired resistance toward Gem therapy, while reducing overlapping side effects for enhanced tolerability[28]. These are all feasible as usually combined drugs have distinct molecular mechanisms of action.

Current Gemcitabine-Combination Therapies and Their Drawbacks

Currently, there are multiple preclinical and clinical trials designed to enhance Gem therapy outcome by combining it with other therapeutic agents. As shown in **Figure 1-2** most of the combination therapy studies with Gem have been conducted with cisplatin; five phase II investigations have been carried out with different dosages and scheduling, with a median response rate of 38-54% and elevated median OS rate to 8.4-14.3 months [46]. In another randomized phase III clinical trial, Cardenal et al (1997) studied in 136 NSCLC patients, to compare and investigate the combination of cisplatin with Gem and etoposide. Unsurprisingly, the Gem group had a response rate as high as 46% with lower toxicities, while the etoposide group had a 22% response rate[47].

Furthermore a combination of cisplatin and Gem e led to a 46% reduction in drug resistance[48]. However, this type of combination regimen is associated with clinically relevant adverse effects such as neutropenia, neuropathy, thrombocytopenia, myelosuppression, and nephrotoxicity. These side effects were around 3 or 4 with respect to the World Health Organization grading system. Grade 3 accounts for severe adverse effects and grade 4 for life threatening or disabling adverse effects[49]. Therefore, future directions on NSCLC therapy are more focused on less toxic, particularly non-platinum

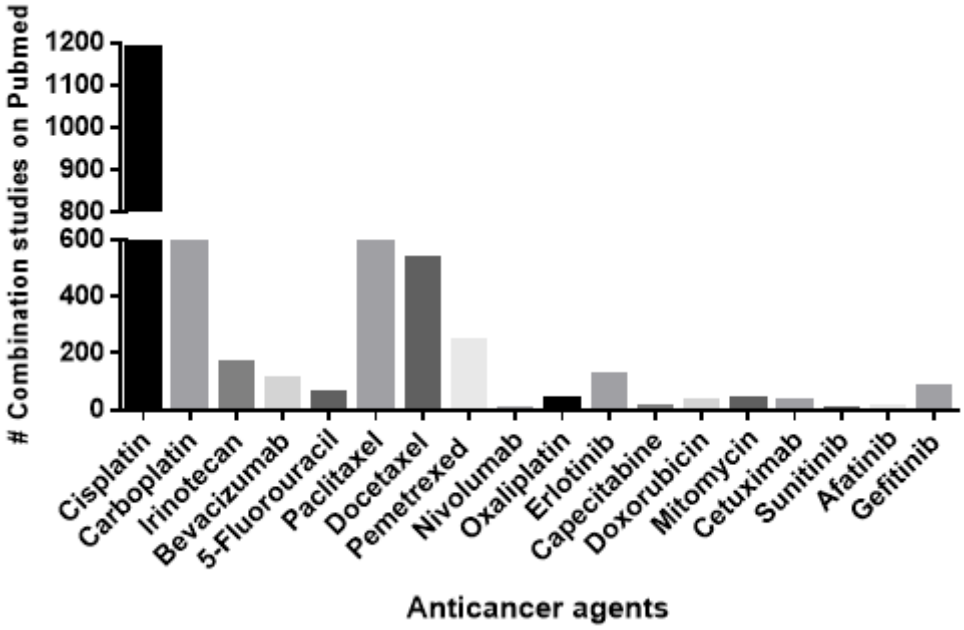

Figure 1-2. Graphical representation of number of peer-reviewed articles, book chapters and reviews, published on Gem combination with different anticancer drugs to treat NSCLC cancer.
This data was compiled from PubMed (1994 -2019).

combinations, as their risks are higher than their benefits especially for unfit patients with compromised health issues. Hence, we speculate that the combination of Gem with a chemo-sensitizer/anticancer agent with a more favorable safety profile, would open up a new horizon for the future of NSCLC therapy. A combination such as this may achieve greater treatment efficacy, delay or eliminate development of drug resistance, and reduce toxicity.

Use of Natural Compounds in Cancer Therapy

Since ancient times, natural compounds have shown a broad range of therapeutic potential for the treatment of various diseases. Currently, there are a multitude of these natural products available on the market. Therapeutic applications relate to antiviral, anti-inflammatory, chemo-preventive and chemo-sensitization properties, etc.[50] Most common categories of natural compounds that have shown to have anticancer properties include polyphenols, phytochemicals, and xanthonoid.

According to a statistical electronic search on PubMed, there are around ten thousand studies conducted on effects of natural compounds on cancer since 1981. However, the majority of these compounds have exhibited a decline in interest during drug discovery due to lack of potency. For example, tannic acid and curcumin have shown very promising inhibitory results on multiple oncogenic signaling cascades and in different cancer types. Unfortunately, their use in this context is unfeasible due to the high concentration required to achieve sufficient potency Interestingly, gambogic acid is among a few natural compounds that demonstrates somewhat potent anticancer properties within an acceptable dosage range[50]. For better **Table 1-3** , shows the half-maximal inhibitory concentration (IC50) in A549 and H1299 (NSCLC cell lines) of resveratrol, tannic acid, flavonoids, curcumin, epigallocatechin gallate (EGCG) and mangiferin.

Among above mentioned studies approximately seven thousand of them are related to combinations of natural compounds with either chemotherapeutic drugs or other anticancer compounds. Not surprisingly, around 3,500 of these combination studies were conducted in last five years, indicating the emerging interest in using natural compounds as a co-treatment agent to act synergistically or additively toward better anticancer efficacy. **Figure 1-3** presents a graphical representation of the number of publications conducted on combinations of known natural compounds with commonly used chemotherapeutic agent in NSCLC. We have focused on combination studies conducted using the natural compounds mentioned above with our drug of interest, Gem, on NSCLC therapy published in the past five years, and a total of three studies have emerged. In one, Mirza et al. (2017) investigated the effect of curcumin in combination with Gem on NSCLC, and their results curcumin remarkably decreases the self-renewal ability of stem cells and, when combined with Gem, was able to decrease the IC50 of NSCLC cell lines compared to Gem alone. They suggested that this is due to induced DNA damage and/or inhibition of repair mechanisms by curcumin [51]. Another study by Zhang et al. (2018) developed a liposomal curcumin dry powder inhaler, and they

Table 1-3. Range of IC50 for different natural compounds on NSCLC cell lines (A549 and H1299).

Natural compound	IC 50 on NSCLC(μM)		Ref.
	A549	H1299	
Resveratrol	<90	45-51	[52]
Tannic acid	20-30	15-27	-
Vitamin D	50-60	35-45	[53]
Curcumin	48-53	20-30	[54,55]
EGCG	<300	170-210	[56]
Gambogic acid	1.2-1.55	0.9-1.2	[57]

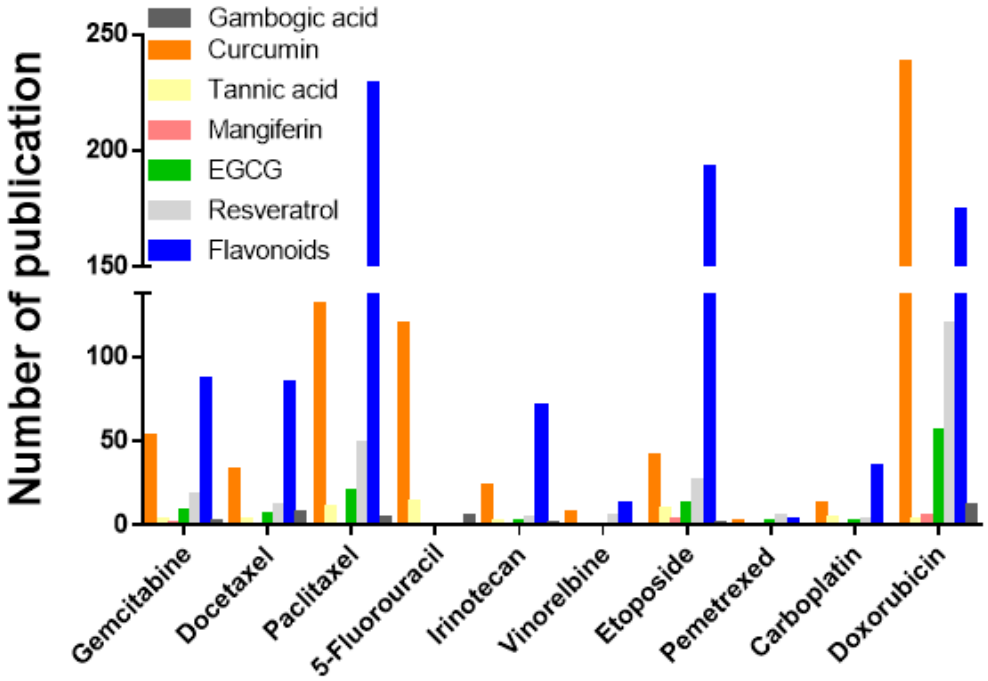

Figure 1-3. Graphical representation of number of publications compiled on frequently used natural compounds in NSCLC therapy.
Flavonoids, resveratrol, epigallocatechin gallate, Mangiferin, tannic acid, curcumin, gambogic acid with chemotherapeutic agents that are commonly employed in NSCLC.

sprayed the powder, curcumin, and Gem on the lungs of rats with lung cancer. Their results indicated that liposomal curcumin dry powders had higher antitumor efficacy, modulating the expression of VEGF, malondialdehyde, TNF-α, caspase-3, and BCL-2[58]. However, both studies mentioned low water solubility, weak bioavailability and rapid metabolism as the main limitations of curcumin. Moreover, Lee et al. (2015) investigated the chemo-sensitization ability of quercetin, a bioflavonoid, on lung cancer. They demonstrated that not only does quercetin decreases cell growth in lung cancer, but it also sensitizes them to Gem therapy through inhibiting HSP70 expression. At the same time, quercetin increased side effects such as headache, nausea and vomiting, kidney damage, numbness and tingling of fingers, and shortness of breath[59]. Interestingly, gambogic acid is among a few natural compounds that demonstrates somewhat potent anticancer properties within an acceptable dosage range, with safer toxicity profile [60], therefore, setting forth a suitable component for successful combination therapy.

Natural Chemo-Sensitizer Agent: Solution for Gemcitabine-Combination Therapy

Gambogic acid (GA, chemical formula: $C_{38}H_{44}O_8$) is a small molecule isolated from the brownish/orange gamboge resin of the *Garcinia hanburyi* tree (**Figure 1-1b**) [61]. Due to easy isolation, GA supply is abundant. Previous studies reported that GA has antineoplastic effects and is a potent apoptosis inducer[62]. It also has a favorable safety profile and large therapeutic index[63 64]. On one study, due to emerging interest to use GA as an anticancer agent general pharmacological aspects, toxicity and analgesic properties of GA investigated on dogs and mice to check the effect of GA on cardiovascular, respiratory and central nervous system (CNS), which suggested minimal effect on blood pressure, heart rate and respiratory system. Beside administrating really high dosage of GA(>16mg/kg) exhibited minor and insignificant side effects on CNS in mice. In addition GA showed high analgesic activity which could be connected to its anti-inflammatory nature[65].

Furthermore, GA is amenable to chemical modification, has been approved for phase II clinical trials in solid tumor therapy, and is approved by china food and drug administration (CFDA) as an anticancer agent for lung cancer therapy specially NSCLC[66 67 68].

Accumulated preclinical and clinical evidence indicates that GA has a significant anticancer effect on various types of cancers including NSCLC, breast cancer, and prostate cancer, by targeting different molecular pathways (**Table 1-4)**. This evidence demonstrates the broad range of mechanisms of action and excellent potency of GA. Its anti-tumor effects include, but are not limited to, induction of apoptosis, accumulation of reactive oxygen species, autophagy, cell anti-proliferation, and inhibition of enzymes (e.g. telomerase) and growth factors (e.g. VEGF), and interception of NF-κB signaling pathways. In addition to all of that, Duan et al. (2013) have reported that healthy cells exhibit less sensitivity to GA compared to cancer cell lines, presumably due to redox homeostasis[69].

Table 1-4. Molecular targets of gambogic acid.

Molecular target category	Effects on biomarkers
Kinases	↓Akt, ↓ JNK1, ↓CDk7, ↓ p34, ↓ p38-MAPK, ↓PI3K, ↓ SRC3, ↓pMET, ↓pERK1/2, ↓ ERK, ↓ Focal Adhesion Kinase, ↑p21waf/cip1, ↓CDC2, ↓Tyrosine Kinase
Growth factor signaling	↓VEGF, ↓EGF, ↑ p21, ↑p27, ↓PDGF
Receptors	↓VEGFR, ↓VEGFR2, ↓ EGFR, ↓PDGFR, ↓KDR/FLK1
Apoptotic proteins	↓Bcl2, ↑ Bax, ↑ Caspase3,8 &9, ↓c-FLIP, ↓Survivin, ↓Bad, ↓Bid
Transcription factors	↓HlF-1α, ↓ NF-ƙb, ↓ hTERT, ↓MYC, ↑FOXO3, ↓STAT3
Enzymes	↓Telomerase, ↓ MMP-2, -9, ↓Thioredoxin reductase, ↓ PHD-2, ↓PARP
Oncoproteins and tumor suppressor gene	↓cMYC, ↓ MDM2, ↓ P MET, ↓P53
Others	↑ LRIG1, ↑ROS, ↑SIRT1, ↑ DOX, ↑DRS, ↑ BCR-AB1, ↑ RECK, ↓CYCLIN D1, ↓CD31, ↓CALUMENIN, ↓HSP90, ↓PXR, ↓IL-5

Source: Banik, K. *et al.* Therapeutic potential of gambogic acid, a caged xanthone, to target cancer. *Cancer Lett.* **416**, 75–86 (2018).

Most importantly, GA has shown chemo-sensitization properties in different types of cancers[70] [63] . In general, chemo-sensitizers are small molecules that make cancer cells more sensitive to chemotherapeutic agents, thus improving the therapeutic index and antitumor effects of these agents. These compounds are also known as resistance modulators, which inhibit or block drug efflux from cancer cells *via* the P-glycoprotein (P-gp) pump and elevate the concentrations of therapeutic agents inside MDR cells[71].

Previously, GA has been combined with other chemotherapy drugs, to enhance the antitumor efficacy synergistically or additively, such as its combination with 5-fluorouracil (5-FU) on gastric cancer treatment, exhibiting significant effect of tumor regression. Also, cotreatment with low dose of GA, elevated the efficacy of docetaxel on docetaxel-resistant gastric cancer cell lines *via* down regulation of survivin[72]. These findings support the concept of using GA as a chemo-sensitizier agent for conventional chemotherapy. GA not only serves as a P-glycoprotein inhibitor to reduce MDR *via* the post-translational proteasome signaling pathway, but also down-regulates the expression of ribonucleotide reductase enzyme subunit-M2 (RRM2) *via* (ERK)/E2F1 signaling pathway. As discussed previously these are two main causes of development of resistance toward Gem [73] [74] [75].

Altogether, combination therapies such as this may combat drug resistance. However, side effects in healthy cells resulting from off target toxicity remain a challenge. Further, GA is a hydrophilic molecule, which leads to limited passive diffusion, and its organic solvents cause severe systemic toxicity *in vivo*. Moreover, based on its relatively low molecular weight, GA is eliminated quickly from the body after administration, leading to a short half-life in the blood. These limitations are also obstacles to the use of GA monotherapy. Hence, there is an urgent need to improve current treatment strategies and to develop appropriate drug delivery systems that will produce more robust therapeutic effects and promote successful utilization of natural compounds in chemotherapeutic co-therapies in clinical practice.

Nanomedicine

Nanomedicine and nano-drug delivery systems (NDDS) have been employed to conquer the disadvantages of conventional drugs. The value of nano drugs expected to be developed by 2025 has been estimated at $350.8 billion according to a report released by grand view research, Inc. To date, over 75 nanomedicine formulations have been approved by the FDA, and they are currently being utilized in clinical practice[76].

Nanoparticle formulations for cancer therapies have gained significant attention, as chemotherapeutic drugs loaded on nanocarriers have shown several advantages over conventional formulations. Nanoparticle (NP) delivery systems reduce the side effects of conventional chemotherapy *via* more efficient drug delivery to the tumor site. They also lower the dosage needed for administration and reduce the possibility of acquiring drug resistance toward chemotherapeutic agents.

The rationale behind using NPs is based on their delivery approach, which increases accumulation at the tumor site *via* the enhanced permeation and retention (EPR) effect[77 78 79]. NPs prolong circulation time and improve tolerability concerns by decreasing toxicity issues. These advantages relate to their appropriately designed size (~100-400nm), which allows them to easily bypass the reticuloendothelial system (RES) yet take advantage of the EPR effect due to leaky tumor vasculature. These deformed blood and lymphatic vasculatures arise from irregularities in their membranes upon rapid angiogenesis during the development of tumor tissues [80 81].

Consequently, the pharmacokinetic, pharmacodynamic and bioavailability profiles of therapeutic agents encapsulated in NPs is favorably enhanced by expanding their half-life and blood circulation time. NPs allow the drug enough time to be in close contact with the tumor microenvironment to efficiently penetrate and accumulate in tumor tissues and release the drug cargo at the tumor site. [82 83 84]. The other physicochemical properties of NPs, such as surface charge, are an important factor for utilization of any designed NPs for a drug delivery system. During development, it is highly desirable to achieve a negative zeta potential that decreases the risk of systemic toxicity and formation of NP aggregates, while also increasing the internalization of NPs within cancer cells. Moreover, nanoparticles can increase the water solubility of hydrophobic drugs. Although Gem is a water-soluble agent, GA suffers from water insolubility, and organic solvents of hydrophobic drugs cause *in vivo* toxicity, thereby limiting their clinical use[85]. Furthermore, NPs can reverse MDR, as they can promote the efficient uptake of drugs by cancer cells [86 87 88], Also, combination regimens with chemotherapeutic agents often suffer from poor bioavailability and off-target toxicity, drastically decreasing their efficacy, whereas nanotechnology strategies promotes targeted and efficient delivery of anticancer cargo.

In general, nanomedicine for cancer therapy consists of a carrier vehicle and a drug. Some NPs may be conjugated with a targeting moiety as well. There are various types of carrier designs, which can be utilized in NCLC therapy that are listed below their schematic representation are shown in **Figure 1-4**.

Lipid-based nanocarriers: This group of nanoparticles are composed from phospholipids; they are consisting from two major groups; liposomes and micelle. Lipid based nanoparticles can encapsulate both hydrophobic and hydrophilic drug due to their lipid layer and aqueous core, respectively. They can increase the blood circulation time and reduce the RES clearance. By conjugating with polyethylene glycol (PEG), this liposome can reach to higher tumor accumulation, enhanced the permeability and retention effect, and excellent biocompatibility[89].

Polymer-based nanocarriers: This category of NPs is synthesized from polymers, major groups in this category consists of polymeric micelles, polymersomes, polyplexes, polymer-lipid hybrid systems, and protein systems. Polymeric nanoparticles can be developed by self-assembly formation between two or more polymers. Accumulated data indicates that they are able to co-delivery hydrophobic and hydrophilic drugs and improve the anticancer effect, due to increased tumor penetration of drugs [90].

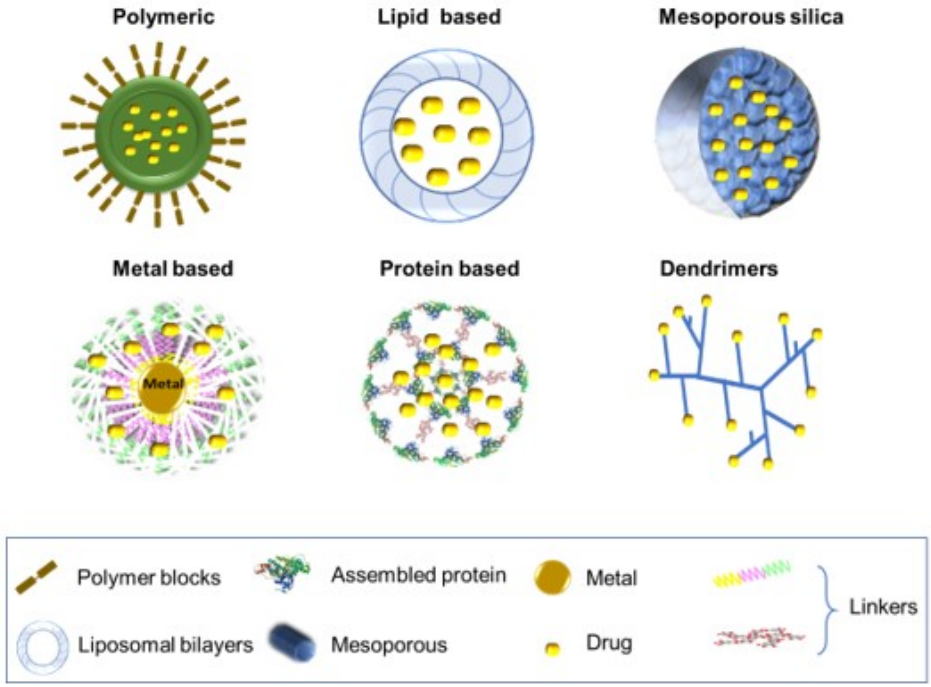

Figure 1-4. Schematic representation of different types of nanoparticles that have been used in NSCLC therapy.

Protein-based self-assemblies are also being investigated for NSCLC therapies as they are biodegradable, biocompatible, and can be conjugated to drugs and release them easily in the tumor environment. A successful example in this group is Abraxane, an FDA-approved albumin-bonded paclitaxel for NSCLC and also other cancers such as breast and ovarian cancer[91 92].

Metal-based nanocarriers: Another category of the nanocarriers are metal NPs designed mostly with silver and gold, recently they have been widely used in biomedical application more focused on diagnostic studies, for instance, discrimination of the histological aspects of lung cancer and healthy cells. Magnetic nanoparticles, fails under this category and generally shown the encouraging properties for cancer therapy[93].

Other nanocarriers: Other NPs, such as mesoporous silica, commonly used in drug delivery studies due to their loading capacity and drug release properties. Their main mechanism for internalization to NSCLC is *via* endocytosis. Due to their multifunctional properties, these NPs can also be used in intercellular labeling and magnetic resonance imaging investigations.

Dendrimers nanoparticles is a class of nanocarriers with broad functional properties, ranging from drug delivery to nanodevice. For drug delivery applications, they can either entrap the drug *via* noncovalent interactions (formulation approach), or covalently couple with drugs (nano-construct approach). Dendrimers consist of multiple branches, providing enough surfaces for drug conjugations. They have been used frequently for platinum-drug delivery, and have been able to increase solubility and loading payload and also decrease the toxicity and selective penetration of the drug in tumor tissue, leading to improvement in anticancer efficacy[94 95 96].

Table 1-5 gives detailed information on nanocarriers designed especially for targeting NSCLC and their outcome.

Passive Targeting and Active Targeting

Nanoparticles usually target cells through two main mechanisms: 1) Passive targeting; whereby nanoparticles are able to take advantage of the EPR effect and passively diffuse to the tumor site and accumulate in tumor tissue due to enhanced circulation time, and 2) active targeting; whereby attaching specific affinity ligands to the nanoparticle surface facilitates its recognition by receptors on the cancer cell surface and assists its uptake by tumor cells *via* a receptor-mediated endocytosis mechanism. It is noteworthy to mention that there is usually a possibility to modify the surface of nanoparticles with ligands to promote active targeting in order to more precisely recognize the tumor cells and increase their uptakes by tumor cells.

Table 1-5. Examples of various types of nanocarriers studies in preclinical and clinical trials leading to improved antitumor efficiency of different chemotherapeutic drugs on NSCLC.

Nano-carrier type	Drug conjugated	Study results	Ref.
Lipid-based nanoparticle (Lipoplatin)	Cisplatin	Phase II and III clinical trial, similar OS to Cisplatin (59.22% vs. 42.2%) plus significantly lower toxicity.	[97], [98]
Lipid-based nanoparticle (Lipusu)	Paclitaxel	Higher efficacy in comparison to plain Paclitaxel, also clinical studies conducted on its premedication on solid tumors, including 60 NSCLC patient, supporting the elevated level of antitumor potency.	[99], [100]
Lipid-based nanoparticle (Liposomal Paclitaxel)	Paclitaxel	A phase I clinical trial and PK study showed lower toxicity and better PK profile, with OS rate of 54.5%.	[101]
Lipid-based nanoparticle (Self-assembled platinum)	Cisplatin	Harnessing structure-activity relationship (SAR) for localized drug release, improved cisplatin efficacy on inhibiting the tumor growth, and remarkably reducing the toxicity.	[102]

Table 1-5. (Continued).

Nano-carrier type	Drug conjugated	Study results	Ref.
Polymeric Micelles (NK012)	Irinotecan	Increased accumulation of Irinotecan in tumor cells, and enhancement of antitumor activity was observed.	[103]
Polymeric Micelles (Genexol-PM)	Carboplatin+ Paclitaxel	Phase II clinical trial exhibited significant efficacy improvement as a first line treatment, OS rate= 35.7% Currently is in market in Korea.	[104,105]
Polymeric Micelles (Pluronic P123/F127 mixed micelles)	Paclitaxel	*In vitro* and *in vivo* studies showed elevated level of antitumor efficacy, decreasedIC50, and tumor volume on a A549 xenograft tumor.	[106]
Metal-based nanocarrier (Gold nanoparticle (AuNP))		Improved tumor necrosis factor related apoptosis inducing ligand (TRAIL) sensitivity *via* dynamin-related protein 1 (Drp1) apoptosis.	[107]
Polyacrylic acid (PAA)-coated cerium oxide nanoparticles (PNC)	Doxorubicin (Doxo) and Hsp90 inhibitor ganetespib (GT)	Synergistic antitumor effect of Doxo and GT was observed, *via* increase ROS, and 80% cell death on *in vitro* assays.	[108]

Table 1-5. (Continued).

Nano-carrier type	Drug conjugated	Study results	Ref.
Lipid-based nanoparticle (Lipid/Calcium/Phosphate nanoparticle (LCP)	Gemcitabine	Co-delivery of siRNA targeting VEGFs and gemcitabine, *in vitro* and *in vivo* studies supports escalated level of tumor cell apoptosis.	[109]
Gelatin nanocarriers (GNCs) cross-linked with Genipin (Gem-GNCs)	Gemcitabine	Developed through Taguchi design, decreased IC50 of NSCLC cell lines by 5-fold.	[110]
Polymeric- based Nanocarriers (Albumin-bound paclitaxel)	Paclitaxel	FDA approved for NSCLC therapy Good safety profile. Elevated antitumor efficacy,	[111]
(lipid Nanocapsule-based gel)	Gemcitabine	Lipid based nanogel targeted the lymph nodes, less toxicity and better biodistribution.	[112]
Dendrimer (4 PAMAM-dendrimer)	N2, N4-dibenzylquinazoline-2,4-diamine (DBeQ)	DBeQ was successfully encapsulated in dendrimer and significantly decreased in cell proliferation, migration and tumor growth.	[95]

Nontechnology-Based Gemcitabine Therapeutics

Literature evidence support that NP-mediated delivery of Gem is able to reverse the associated resistance in various cancer types mainly through following aspects: 1) increasing Gem uptake by cells *via* EPR effect and overcoming the deficiency of nucleoside transporters [113], 2) reducing the ribonucleotide reductase(RR) enzyme expression[114 115], 3) reducing the deamination process by conjugation to either a fatty acid or another chemotherapeutic agent (e.g. paclitaxel) to protect the Gem from CDA enzyme and inhibit deamination[91 116 117 118] .

Accordingly, nanomedicine has had some positive impact in increasing the efficacy of Gem on NSCLC, supported by rising numbers of preclinical and clinical studies in this regard. Wonganan et al. (2012), studied the co-delivery of RRM1-specific small interfering RNA (siRNA), conjugated with polyethyleneimine, which was able to significantly enhance the tumor regression in the mice bearing RRM1-overexpressing tumors. Likewise, Khatri et al. (2015) investigated the sensitization effect of cyclic arginine-glycine-aspartic conjugated siRNA nano-constructs on Gem in NSCLC, and their results indicates that with successful delivery of siRNA facilitated by nanoformulation, they were able to lower the IC50 of A549 cells compare to Gem alone, and reduce the expression of the RR subunit[119].

Furthermore, two phase II clinical research was conducted on Gem delivery to NSCLC by Genexol-PM nanoformulation. Genexol-PM is a cremophor-free nano-formulation of paclitaxel developed with PEG and polylactic acid for treatment of lung cancer. In one study, 43 patients were subjected to 230 mg/m^2 and Gem 1,000 mg/m^2 for a three-week period, as a first line treatment. The results showed overall survival rate was 46.5%, and average OS and PFS were 14.8 and 4.0 months respectively, with side effects of anemia, asthenia, myalgia and peripheral pneumonia[120]. A similar phase II trial was performed utilizing Genexol-PM in combination with cisplatin, in which the median dose of Genexol-PM was higher, but the OS rate was lower (37.7%). In addition, given the concerns about the side effects associated with the platinum-based therapy, co-delivery of Gem with Genexol-PM was more satisfactory in NSCLC patients[105].

Self-Assembly Nanocarriers

Artificial nanoparticles have been utilized in drug delivery for many years and were able to serve their purpose, more or less. There are numerous nano delivery systems developed every year in laboratories, however, when exposed to more complicated *in vivo* modeling for preclinical and clinical trials, they often encounter some limitations leading clinical failure. These limitations involve stability in systemic circulation, immune responses, and issues with compatibility and degradation. Therefore, there is an emerging necessity to use more stable, biocompatible and biodegradable materials for drug delivery systems, with fewer immunogenicity and toxicity issues, in order to achieve a superior approach for encapsulation of therapeutic drugs.

Hence, protein-based self-assemblies (SAs) are being utilized for nanocarrier development. Proteins are non-toxic and can easily degrade into their subunits (amino acids), which can eventually be reused by peripheral tissue[121]. These self-assembly-based nanoparticles are easily fabricated and tailored designed methods can provide stable platforms. In addition, we should not forget that SAs can extend a drug's half-life and blood circulation time, as well as readily benefit from passive targeting. They can also be modified for active targeting. SAs often form covalent conjugations, which enhance the hydrophobicity of proteins and convert SAs to more complex nanoparticles. Taken together, SAs have been recommended as convenient and suitable scaffolds for nanoparticle design. Further, SAs are composed of cell bases, which promotes higher tolerability compared to chemically based nanoparticles.

Advantage of Using Human Serum Albumin as a Drug Delivery Platform

Human serum albumin (HSA) consists of three homologous domains known as I, II, and III, with multiple hydrophobic subdomains. HSA is responsible for transporting drugs, hormones and other metabolic substrates; therefore, due to its unique merit, HSA can serve as a versatile platform to transport hydrophobic as well as hydrophilic drugs simultaneously.

HSA is an abundant plasma protein in human blood. It is produced by the liver and has a half-life of 19 days. One of the most desirable advantages of using HSA is the fact that it can be actively internalized within cancer cells *via* 60kDa glycoprotein (gp60) and caveolin-1-mediated transcytosis receptors. Thus, nanoparticles designed from HSA can benefit from these natural transporting pathways[122]. In addition, while evidence shows that the main process responsible for HAS NPs penetration in the tumor site is due to the enhanced permeability and retention (EPR) effect, and by targeting tumor-derived secreted proteins (SPARC) for the successful accumulation of HAS NPs in tumor sites[78 123]. Furthermore, SPARC proteins are overexpressed by many tumors such as breast, lung, prostate etc. In short, HSA provides a bioavailable, biocompatible, and biodegradable platform, with low immunogenicity, low toxicity, and capacity for dual loading. Thus, HSA is ideal for the development and design of novel nanocarriers.

Utilization of an HSA platform increases the solubility of hydrophobic drugs, mostly due to the negatively charged surface of HSA, which makes it a highly water-soluble biomolecule. HAS NPs can form *via* aggregation and or crosslinking of HSA molecules and creation of intermolecular disulfide bonds[44]. In addition, hydrophobic agents can induce the self-assembly of HSA proteins and make them even more stable. Albumin-bound paclitaxel NPs (Abraxane®) is an FDA-approved nanomedicine for metastatic breast cancer, which was able to significantly increase OS by ten weeks[124].

In the present investigation, we aimed to study the development and characterization of stable HSA-based nanoparticles using simple self-assembly by the solvent evaporation method. The solvent evaporation method is the most frequently used

method in nanoparticle preparation. It is less complex and more time-efficient than other methods, making it promising for manufacturing purposes. Therefore, we hypothesize that nanoparticle-mediated drug delivery using an HSA basis will effectively improve drug uptake into tumor cells, enhance anticancer activity, and lower undesirable side effects.

Use of Natural Small Molecules as Crosslinkers and Stabilizers

Indeed, in forming the perfect NDDS, there is an urgent need to employ and select pharmaceutical excipients wisely. Pharmaceutical excipients are used to enhance aqueous solubility, improve long term stability, increase bioavailability, and increase therapeutic value and other favorable characteristics, while also ensuring the safety of the finished product. The selection of nanoparticle excipients will determine the physicochemical and biological fate of designed nanomedicine formulations in *in vitro* and *in vivo* models, and ultimately in patients' bodies[125 126]. Therefore, it is necessary to design relatively simple, yet safe and stable self-assemblies in order to transport therapeutic drugs to the tumor site. It is also important to be cognizant of toxicity that may result from residual chemical crosslinking agents. Herein, we decided to choose a natural stabilizing compound that would exhibit better binding affinity to plasma proteins and biofluids, while also assisting in efficient penetration to the tumor site, without jeopardizing the safety of healthy tissues.

Recently, tannic acid (TA, $C_{76}H_{52}O_{46}$), a natural polyphenol extracted from different types of plants (e.g. green tea), has gained attention as an additive natural compound. TA has various beneficial therapeutic properties. It was previously known as a potent antioxidant, an anti-inflammatory agent, and it has also been used as an anticancer and chemo-sensitizing agent[127 128 129]. However, this compound lacked sufficient potency. Thus, scientists have begun to use TA as a stabilizer and crosslinker in nanoparticle formation [76 130]. The structure of TA has hydroxyl and carboxyl functional groups, which provide secure binding sites to proteins and DNA [131]. It is also a water-soluble compound with low viscosity (favorable in the formulation procedure) and an excellent biocompatibility profile. Furthermore, it easily binds to different drugs *via* hydrophobic interactions.

Based on these promising characteristics, we determined that using TA as a stabilizer to develop Human serum albumin-tannic acid nanoparticles (HTA NPs), might also produce a higher binding affinity of HTA NPs in lung fluids. Thus, HTA NPs will not only enrich the chemotherapeutic efficiency of loaded drugs, but also decrease off-target toxicity.

Therefore, human serum albumin nanoplatforms with tannic acid as a stabilizer (HTA) will have a safer toxicity profile and will overcome previously mentioned limitations of simple multifunctional nanoparticles. This nanoparticle is speculated to provide a dual loading platform for co-delivery of the hydrophobic and hydrophilic drugs, as well as potentiate their synergistic effect on NSCLC.

This approach efficiently eliminates limitations in multicomplex methods of nanoparticle synthesis. It also eliminates the need for organic solvents for hydrophobic drugs and reduces toxicity issues involved in using chemical excipients in nanomedicine formulations. Indeed, it could revolutionize the development of multidisciplinary strategies for NSCLC therapy.

Hypothesis and Specific Aims

Despite the establishment of several therapeutic strategies, Lung cancer (LC) stands as the main source of cancer-related mortality among both males and females in the United States and worldwide, with the overall 5-year survival rates for advanced stages with distance metastasis is less than 5% [4]. Statistics estimate approximately 228,150newly diagnosed LC cases and 142,670 deaths in the United States in 2019 alone[8]. Based on the histopathological phenomenon, LC is categorized to small cell lung cancer (SCLC) and non-small cell lung cancer (NSCLC). Around 85-90% of the LC cases fall under the category of NSCLC, roughly 194,000 new NSCLC cases in 2019.

Surgery, radiation, chemotherapy, targeted treatments and immunotherapy—alone or in combination—are the current options for treating NSCLC. By a considerable margin, conventional chemotherapy, such as gemcitabine, carboplatin, cisplatin, paclitaxel and irinotecan, have shown to be the most effective regimens for NSCLC; however, they have resulted in only modest survival improvements due to limitations such as chemo-resistance, relapse, cancer recurrence, and intolerable toxicities from high drug dosage and other adverse effects. Therefore, there is an emerging need for optimizing and validating new therapeutic strategies to circumvent these problems.

Among other chemotherapeutic agents, Gem has an outstanding profile. Gem is a pyrimidine nucleoside antimetabolite and has been used widely for different types of cancer therapy, specifically NSCLC, for decades [29]. Gem was able to increase the median survival rate of NSCLC patients by 20-25% (9 months)[25 132], however, the main clinical drawback of Gem therapy is the development of the resistance by NSCLC tumor cells, either by P-gp-mediated efflux, or other involved pathways[133]. Currently, there is a diverse range of clinical trials for Gem in combination with other chemotherapeutic agents. For instance, a combination of cisplatin with Gem causes a 46% reduction in drug resistance in tumors (with highly resistant and intermediate level) in comparison to Gem therapy alone[48]. However, clinical applications of this type of combination are often associated with disadvantages due to adverse side effects such as neutropenia, neuropathy, myelosuppression, and nephrotoxicity. Hence, a combination of Gem with a sensitizer/anticancer agent having a more favorable safety profile is highly desired. Such a combination could achieve higher treatment efficacy, procrastinate /eliminate the development of drug resistance, and reduce side effects and toxicity issues. Therefore, we selected Gambogic acid (GA) with the chemical formulation of $C_{38}H_{44}O_8$, a natural compound isolated from the gamboge resin of *Garcinia hanburyi* tree. Selection of GA was based on previous studies that have identified GA as a potent apoptosis inducer, an

anticancer agent and chemo-sensitizer in different types of cancer, and its favorable safety profile [34] [134]. However, GA is relatively water insoluble, which increases the *in vivo* toxicity. Moreover, traditional delivery of this combinatorial therapy may result in limited therapeutic efficacy and severe side effects due to unspecific targeting. Nanomedicine and the development of novel nanocarriers are gaining attention for cancer therapy. Nanocarriers can efficiently deliver therapeutic drugs to the tumor site, increasing drug concentration within tumor cells, thereby lowering the total required dose and significantly reducing side effects. There has been enormous investigation in loading chemotherapeutic agents in nanoparticles. One of the most successful of these nanomedicines is Abraxane (albumin bonded paclitaxel), which was approved by the FDA in 2005 for metastatic breast cancer. Since then, it has gained FDA approval for other cancer types (e.g. NSCLC, ovarian, and pancreatic cancers).

Furthermore, albumin, the primary component of human serum proteins, is proven to be an excellent nanocarrier for drug delivery. Albumin is biocompatible, biodegradable, has low immunogenicity and low toxicity, and it serves as a transporter in the body[85] [135]. Studies reported that HSA has the ability for dual loading. Furthermore, another study revealed that GA, a highly hydrophobic chemo-sensitizer agent for NSCLC, can bind to human serum albumin (HSA) *via* hydrophobic interactions formed between the drug molecule and the hydrophobic subdomains of HSA [85] [136] [137]. This unique platform can create a stable self-assembly with hydrophobic molecules. It has several advantages, such as the ability to carry multiple, large therapeutic payloads, a desirable size and zeta potential, surface functionality with the ability to attach to different targeting ligands (enabling targetability and specificity), and increased water solubility of hydrophobic molecules. It can also readily bypass RES clearance and take advantage of the EPR effect [138] [85]. Furthermore, it also has an excellent drug release profile and good serum stability [139] [121]. In the present study, we investigated the anti-tumor effect of HTA formulation loaded with a GA and Gem (G-G) combination in *in vitro* and *in vivo* systems, using non-small cell lung cancer cell lines and a xenograft mouse model. The schematic representation for preparation of proposed nanoparticle is shown in **Figure 1-5 .** The NP core was composed of HSA, an abundant plasma protein, and TA, a stabilizer crosslinker. TA is a natural compound and FDA-approved food and drug additive, which was utilized as a stabilizer and crosslinker in this NP formulation. Both HSA and TA are biocompatible and biodegradable. Finally, Gem and GA were loaded by the solvent evaporation method to the HTA NPs, referred to as G-G@HTA NPs.

Based upon our *in silico* data, through docking studies, we predicted that GA and Gem can successfully interact with HSA while, they fit perfectly into the HSA binding site (with 1195 and 596.40 interact surface and -7.81 and -6.25 kcal/mol estimated free energy of binding respectively) (**Figure 1-6**). We computationally docked the chemical structure of GA into the HSA binding site, revealing that 42 residues on the conformational structure of HSA interacted with GA and similarly 36 residues interacted in case of Gem and HSA structure, these data further contributed in preparation of nanoparticles and determination of the loading capacity ratio of the drugs to the HSA(w/w).

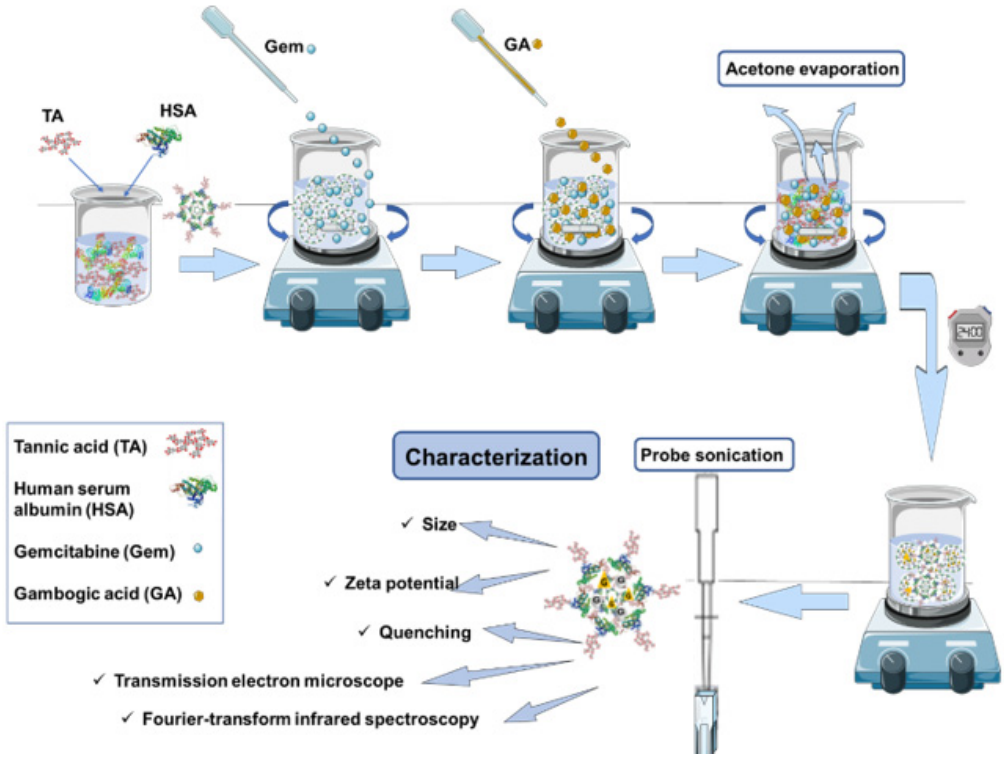

Figure 1-5. Schematic representation of the steps involved in HTA NPs loaded with Gem and GA synthesis.

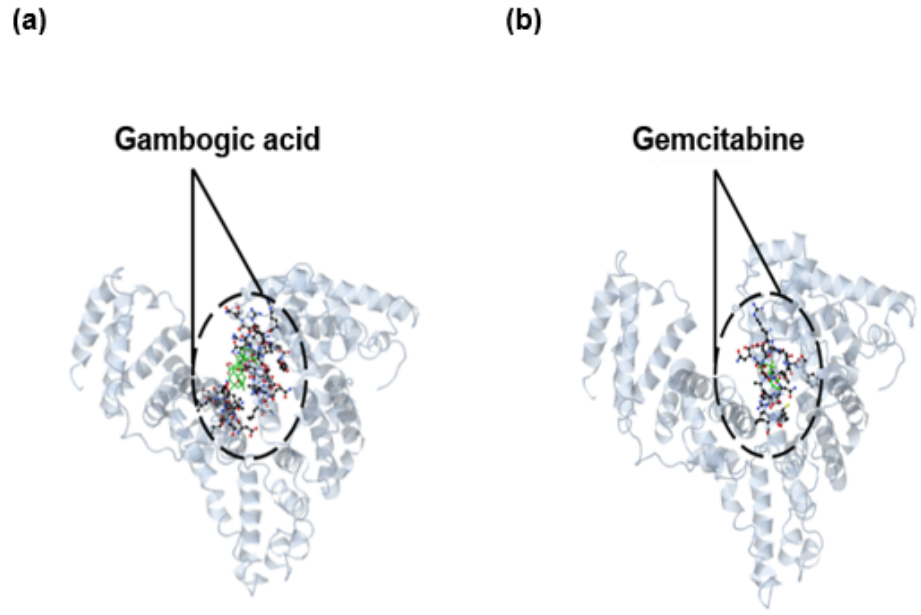

Figure 1-6. Docking gambogic acid and gemcitabine into HSA binding sites. GA and Gem (shown with green) was docked into the computational binding site of the human serum albumin (HSA) receptor (shown with blue).

Altogether, the central hypothesis of my project is that the internalization and permeability of self-assembled HTA NPs when loaded with combined anticancer agents (Gem and GA), will improve the therapeutic efficacy of Gem and GA in NSCLC tumor cells, while also reducing the off-target drug toxicities of conventional NSCLC therapies involving free drug combinations and single agents (**Figure 1-7**). Accordingly, with the objective to test this hypothesis, the following specific aims were proposed:

Aim 1. To Investigate the Interaction of Tannic Acid and Lung Fluid

The purpose of the first specific aim was to test the interaction of tannic acid with lung fluid proteins, to better understand the delivery aspect and binding affinity of the formed self-assemblies to NSCLC cells.

Aim 2. To Investigate the Synergistic Anticancer Potential of Gemcitabine and Gambogic Acid on NSCLC

The purpose of this specific aim was to investigate the elevated anticancer effect of Gem in combination with GA on NSCLC, as a potent apoptosis inducer and sensitizer. Furthermore, we examined the synergistic effect of GA with Gem in *in vitro* assays. We also studied the sensitization ability of GA on Gem therapy in NSCLC cell lines (A549 and H1299).

Aim 3. Construction and Investigation of the Synergistic Anticancer Ability of Self-Assembled Human Serum Albumin-Tannic Acid Nanoparticles (HTAs) Loaded with Combined Anticancer Agents (Gem and GA(G-G)) for NSCLC Therapy

The purpose of the last specific aim was to prepare and characterize HTA NPs and load them with Gem and GA referred as G-G@HTA. After the process of developing the G-G@HTA NPs, these NPs were characterized for mean size, polydispersity index (PDI), zeta potential, binding affinity, FTIR and morphology. Cellular uptake and elevated anticancer effects of G-G@HTA NPs were examined *via in vitro* assays. Finally, the targeting ability, biodistribution, and improved therapeutic efficacy of G-G@HTA NPs were tested using a xenograft mouse model.

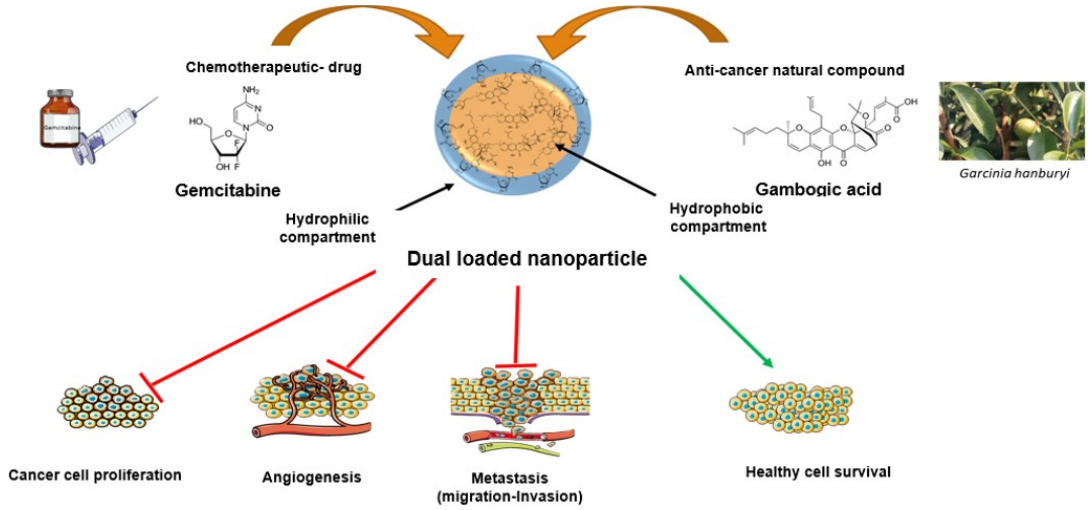

Figure 1-7. Schematic representation of overall project strategy for hypothesis.

CHAPTER 2. TANNIC ACID-LUNG FLUID ASSEMBLIES PROMOTE INTERACTION AND DELIVERY OF DRUGS TO LUNG CANCER CELLS[1]

Introduction

Lung or bronchial cancer is the most lethal cancer in the United States with 234,030 estimated new diagnoses and 154,050 deaths in 2018[5] [140].Chemotherapy is the most common treatment regimen for lung cancer (LC). Most common therapeutic drugs for LC treatments are carboplatin, cisplatin, gemcitabine, paclitaxel, and irinotecan. The efficacy of treatment mostly depends on the mechanism by which the drug is delivered and the optimum concentration of the drug available in the tumor cells. Conventional chemotherapy has poor distribution and results in only a limited amount of therapeutic agent(s) reaching tumor cells, due to lung fluid (LF), a biological barrier that restricts drug penetration to the lungs. There is a significant amount of research dedicated to the study of drug penetration to lung tumors. Often, the LF corona is a major determining factor on how these therapeutic agents/complexes behave in *in vivo* applications. This is a growing field of research aimed at understanding drug carrier stability and fate when the carriers encounter proteins in biofluids. These studies direct the research towards reducing uncertainties involved in the prediction of the behavior of therapeutic pharmaceutical nanoformulation in in situ and *in vivo*, and their application in clinical trials.

Tannic acid (TA) is a polyphenolic compound and an important form of water-soluble tannin. It is widely found and commercially extracted from plants such as tara (Caesalpinia spinosa), gallnuts (oak gall), and Sicilian sumac (Rhus coriaria). TA is a mixture of galloyl esters and their derivatives, and it is represented with the chemical formula C76H52O46. TA is a useful diagnostic tool as a dye that is used to stain plasma membranes, particularly binding most prominently to the margins of tumors. This suggests its binding and targeting efficiency to cancer cells. TA alone was able to protect against benzo(a)pyrene-induced LC in rats[141]. Considering these outcomes as patentable innovation, there was an invention allowed to develop tannin complexes or mixtures with TA and pharmaceutical compositions. There is substantial evidence that TA is an important biocompatible and biodegradable compound commonly used for biomedical and clinical applications[142] [143] [144] .The abundance of hydroxyl functional groups in TA can offer increased solubilization, complexation, entrapment, and encapsulation of therapeutic cargo for slow and sustained release applications. TA has been applied as a carrier for low molecular weight drugs (paclitaxel, docetaxel, amphotericin B, curcumin, and rapamycin)[145] and biomacromolecules (vaccines, peptides, antibodies, and DNA)[146] [147] [148] [149] .Additionally, TA has been known to crystalize various active pharmaceutical ingredients [150]. Pre-clinical evidence has shown that TA has significant anticancer and chemo-preventive profiles[151]. However, its application in LC has never been studied. All

[1] Reprinted from final submission with open access permission. Hatami, E. et al. Tannic acid-lung fluid assemblies promote interaction and delivery of drugs to lung cancer cells. Pharmaceutics **10**, (2018). http://dx.doi.org/10.3390/pharmaceutics10030111.

these events suggest that TA-based delivery would enhance delivery of therapeutics and would therefore have relevance in LC.

Drug carrier interaction with serum proteins, which results in a carrier-protein corona, is a predictor for *in vivo* stability and applicability[152 153]. This behavior is common in the case of intravenous and oral administration of nanotherapeutics. TA in wine is passively absorbed by serum proteins and has not shown side effects. Our ultimate objective is to develop TA as a therapeutic carrier to improve bioavailability and targetability of active pharmaceuticals applied to treatments for lung cancer. The intent of this formulation is to apply for nasal or pulmonary delivery. Therefore, in this study, we aimed to investigate the interaction of TA with LF. The interaction studies were investigated by fluorescence and Fourier Transform Infrared (FTIR), protein dot, SDS-PAGE, DLS, and transmission electron microscopy (TEM). The LF protein corona influence on cellular internalization was examined by fluorescence spectroscopy and flow cytometry. Improved pharmaceutical efficacy through TA-based assembly was confirmed by cell proliferation assay

Materials and Methods

Materials

All reagents and chemicals stated below were purchased from Fisher Scientific (Pittsburgh, PA, USA) or Sigma-Aldrich Co. (St. Louis, MO, USA), unless further information is presented. Bronchoalveolar lavage fluid of mice (simply termed as LF) was provided by Dr. Amali Samarasinghe (UTHSC, Memphis, TN, USA) collected under Institutional Animal Care and Use Committee (IACUC) approved protocol. For this, six week-old female C57BL/6 mice were purchased from Jackson Laboratories (Bar Harbor, ME, USA), and housed in microisolator cages with alpha-dri bedding and free access to mouse chow and autoclaved water in a climate-controlled room for acclimatization. At 12–15 weeks of age, mice were euthanized by CO_2 asphyxiation and the trachea surgically cannulated. The diaphragm was incised, and bronchoalveolar lavage performed with two 1 mL aliquots of sterile phosphate-buffered saline (PBS). Cells were separated by centrifugation at 600× *g* for 10 min at 4 °C, and the fluid was stored at −80°C until use.

TA-LF Complexation

TA and LF interaction leading to self-assembly/complexation was investigated by analysis of LF protein corona formation on TA molecules. For this, 30 μg of mouse LF was incubated with various concentrations of TA for 1 h in 2 mL Eppendorf tubes. According to our previous reports, protein corona formation takes place after 30 min[153 152] .The tubes were centrifuged in Sorvall ST 8 Centrifuge at 5000 rpm (Thermo Fisher Scientific, Suzhou, China) for 2 min to separate any large clumps. This fine TA-LF

complex suspension was used for all studies. Both TA alone and LF alone were used as controls, separately.

Fluorescence Spectroscopy

The binding ability of LF protein tryptophan residues with TA was evaluated by measuring fluorescence quenching using fluorescence spectrometry with a SpectraMax Plus plate reader (Molecular Devices, Sunnyvale, CA, USA). The fluorescence emission spectra were recorded between 250 and 400nm (slit at 5nm) at an excitation wavelength 295nm (slit at 2nm). Thirty micrograms of LF in 1 mL PBS buffer in a quartz cuvette was used for the fluorescence quenching experiment. After running this solution as a control sample, titration was performed with 5, 10, 15, 20, 25, 30, and 40μg of TA by successive addition of 1 μL of TA (5 mg/mL). This assay was performed in triplicate.

Fourier Transform Infrared Spectroscopy

Fourier transform infrared (FTIR) spectroscopy was employed to confirm the presence of LF proteins in TA-LF complexes. Ten microliters of TA-LF complex solutions were placed on a Diamond/ZnSe Attenuated Total Reflection crystal plate and air dried, then spectra were acquired using a PerkinElmer Spectrum 100 FTIR spectrometer (Waltham, MA, USA). The spectra were recorded for these samples and TA/LF samples (controls for peaks comparison) from 4000 to 650 cm^{-1} with a resolution of 4 cm^{-1}. FTIR spectra were presented as an average of 32 scans for all samples.

Protein Density and SDS-PAGE Gel of TA-LF Complexes

Following TA and LF complexation, the TA-LF complex solution was centrifuged at 1000 rpm (Sorvall ST 8 Centrifuge) to obtain stable TA-LF self-assemblies. Ten μL of these complex solutions, were transferred onto a nitrocellulose membrane (Bio Rad, Hercules, CA, USA) and the samples were allowed to diffuse protein into the membrane and dry at room temperature. Following a rinse with DI water, the membrane was incubated in 5 mL of 0.25% Coomassie Blue R-250 dye (#20278, Thermo Fisher Scientific) (50:10:40 v% methanol: glacial acetic acid:DI water). The nitrocellulose membrane in Coomassie Blue solution was heated in a 1200 W microwave for 30 s After cooling to room temperature, the dye solution was drained, and the membrane washed twice with DI water, then destained in 50:10:40 v% methanol: glacial acetic acid:DI water solution without dye until it displayed a clear background. After a final rinse with DI water, the blue spot protein-stained membrane was stored in DI water at room temperature and image captured using a camera. This assay was performed in triplicate. Similarly, these TA-LF complexes were used for generating SDS-PAGE gels according to our previous protocol [152].

Particle Size and Zeta Potential

The intensity-weighted average particle size (nm), particle distribution, and polydispersity index (PDI) of samples were measured with a dynamic light scattering method using a Zetasizer instrument (Nano ZS, Malvern Instruments Ltd., Worcestershire, UK). To acquire these measurements, 20μL of each sample solution was added to 1000μL of filtered Milli-Q water and probe sonicated (VirSonic Ultrasonic Cell Disrupter 100, VirTis, Woburn, MA, USA) for 30 s. Particle size measurements were performed at 25 °C for 3 min. An average of three readings for each solution was calculated and recorded. Zeta potential (ζ, mV) of the particles was quantified with laser Doppler velocimetry using the same instrument. Samples were diluted with PBS and measured for 30 runs each. Data were recorded as an average of three readings. These measurements were also acquired in solutions of different pH.

Particle Morphology

The particle size and morphology of TA-LF complexes were examined by using TEM (JEOL 200EX, JEOL Ltd., Tokyo, Japan). For this investigation, after probe sonication of the TA-LF complex solution for 30 s, 20 μL of solution was dropped carefully on the shiny side of the 200-mesh standard TEM grid (#FCF200-CU-SB, Electron Microscopy Sciences, Hatfield, PA, USA). UranyLess EM Stain solution (22409, Electron Microscopy Sciences) was used as a positive contrast agent to achieve a stronger contrast between the background and the nanoparticles. Morphology examination of TA-LF particles was performed on air-dried grids at 80 kV accelerating voltage under an advanced microscopy digital camera imaging system (Advanced Microscopy Techniques, Corp., Woburn, MA, USA).

Cell Culture, Growth, and Condition

The human LC cell lines A549 (carcinoma cell line derived from 58-year-old male Caucasian, #ATCC® CCL-185™) and H1299 (carcinoma non-small cell LC cell line derived at the metastatic lymph node from 43-year-old adult, #ATCC® CRL-5803™), were purchased from American type culture collection (Manassas, VA, USA). These cell lines were expanded, grown, and used at low passages for experiments. The expanded cell line aliquots (less than 5–6 passages) were stored frozen in liquid nitrogen for future usage. The cancer cell lines cultured under sterile condition in Dulbecco's Modified Eagle's medium (DMEM for A549) and Roswell Park Memorial Institute medium (RPMI for H1299) supplemented with 4.5 g/L of glucose, 10nM of nonessential amino acids (# 11140076, Gibco, Thermo Fisher Scientific, Grand Island, NY, USA), 100mM of sodium pyruvate (#11360070, Gibco), 1× antibiotic/antimycotic (#15240062, Gibco), and 10% heat-inactivated FBS (#10438026 Thermo Fisher). Cells were maintained in 100mm tissue culture dishes (#83.3902, Sarstedt, Inc., Newton, NC, USA) as 2D monolayers in a humidified incubator (5% CO2 and 95% air condition) at 37 °C (Thermo Fisher Scientific, Waltham, MA, USA).

Cellular Uptake

A semi-quantitative cellular uptake assay of TA-LF complexes was examined by flow cytometry and fluorescence microscopy methods. To allow cellular uptake quantification, TA-LF assemblies were labeled with coumarin-6 using our previously reported method [154 46 155]. The extent of dye internalized was used to track uptake of TA-LF self-assemblies into cells. 100 μg of coumarin-6 dye was loaded in 1 mg of TA-LF self-assembled. In this study, 2 mL of media containing 5×10^5 cancer cells per well were seeded in 6-well plates (#83.3920.005, Sarstedt, Inc.) and cells were allowed to attach to plates overnight, then were dosed with 5 μg coumarin-6 containing TA-LF particles with different densities of LF for 30 min to 6 h. After the incubation time, cells were washed twice with PBS and replaced with fresh phenol red-free media to each plate. The uptake of TA-LF particles was imaged using an EVOS® FL Imaging System (AMF4300, Life Technologies, Carlsbad, CA, USA) for visual comparison. For quantitative measurements, the cells were trypsinized, then centrifuged at 1000 rpm for 5 min and resuspended in 2 mL phenol red-free media. About 10,000 cells from these cell suspensions were used to acquire fluorescence levels using an Accuri C6 flow cytometer (Accuri Cytometer, Inc., Ann Arbor, MI, USA). The measurements were performed in triplicate using FL1 channel (488 excitations, Blue lase, 530 ± 15nm, FITC/GFP).

MTS Assay

The drugs (gemcitabine, carboplatin, irinotecan) encapsulated in TA-LF formulations were prepared following our established protocol [154]. Their anticancer efficacies were evaluated using a colorimetric cell titer 96 aqueous one solution cell proliferation assay (MTS assay, Promega, Madison, WI, USA). In this study, LC cell lines (A549 and H1299) were plated at 5×10^3 cells/well in 96-well flat bottom tissue culture plates (#83.3924.005, Sarstedt, Inc.) and incubated at 37 °C in a 5% CO2/95% air atmosphere overnight for attaching to plate. Cells were treated with free drugs (Gemcitabine, carboplatin, and irinotecan) and equivalent drug-containing TA-LF formulations. Respective cell lines with no treatment or TA alone were used as controls. After 48h treatment, 20 μL of MTS reagent solution was added to each well and incubated for 2 h at 37 °C. Absorbance was measured at 490nm by a Cytation 5 imaging microplate reader (BioTek, Winooski, VT, USA). Cell proliferation was normalized to that of cells cultured in medium with no treatment.

Statistical Analysis

All measurements and results generated in this study were presented as mean ± standard error of mean (SEM). The statistical analysis and significance of data were assessed using Student's t-test; significance was set at $p < 0.05$ with GraphPad 5.03 Prism program (La Jolla, CA, USA).

Results and Discussion

Efficient delivery of therapeutics remains the most desirable outcome for treating LC. However, successful delivery is always compromised by poor penetration, quick elimination, and poor bioavailability. This phenomenon is partly due to the abundance of LF, which determines the fate of the drug. Greater interaction with LF may lead to crosslinking with proteins, and thus a huge foreign particle can develop and be eliminated by the system. Therapeutic formulations with limited interaction with LF proteins and unique complexation/self-assembly formation may improve circulation and deep penetration into lungs. Considering this hypothesis, TA is proposed as a carrier for LC therapeutics, and thus this study aims to examine its specific interaction with LF. Further, this study will also explore the possible therapeutic role of drugs encapsulated within TA-LF self-assemblies.

Fluorescence Binding

First, we tried to delineate the TA-LF complexation process using the fluorescence (FL) quenching of proteins present in LF that would interact with tannic acid. The fluorescence of proteins arises from tryptophan residues in proteins[156 157]. TA exhibited a dose-dependent fluorescence decay (**Figure 2-1a**). This is primarily due to inter/intra-molecular interactions of the hydroxyl groups of TA with the amine groups of proteins. Such interaction occurs from a complex formation between protein and TA, which is responsible for quenching of the intrinsic fluorescence of the two tryptophan residues (Trp-134 and Trp-212).

These data suggest that TA interaction with LF proteins is caused by coating or protein corona formation. Further, at lower concentrations, TA exhibited a minor change in fluorescence decay, indicating little interactions, while significant quenching occurs when TA concentrations employed were 20µg/mL and above.

Fourier Transform Infrared Spectroscopy (FTIR) Spectral Analysis

FTIR spectral analysis allows for a quick and efficient confirmation of TA and LF proteins by their functional groups (**Figure 2-1b**). The spectra of TA and TA-LF complexes displayed characteristic peaks of TA at 3280 cm−1 due to phenolic O–H stretch of the hydroxyl groups, 1725 and 1697 cm−1 due to C–O stretch of the carboxyl groups, and 1082 cm−1 due to C–O–C vibrations. The additional absorption bands at 1016, 1066, and 1187 cm−1 are ascribed to the vibrations of substituted benzene rings in TA and TA-LF. The spectrum of LF alone shows characteristic peaks for the amide I band at 1655 cm−1 (mainly C–O stretch) and amide II band at 1525 cm−1 (C–N

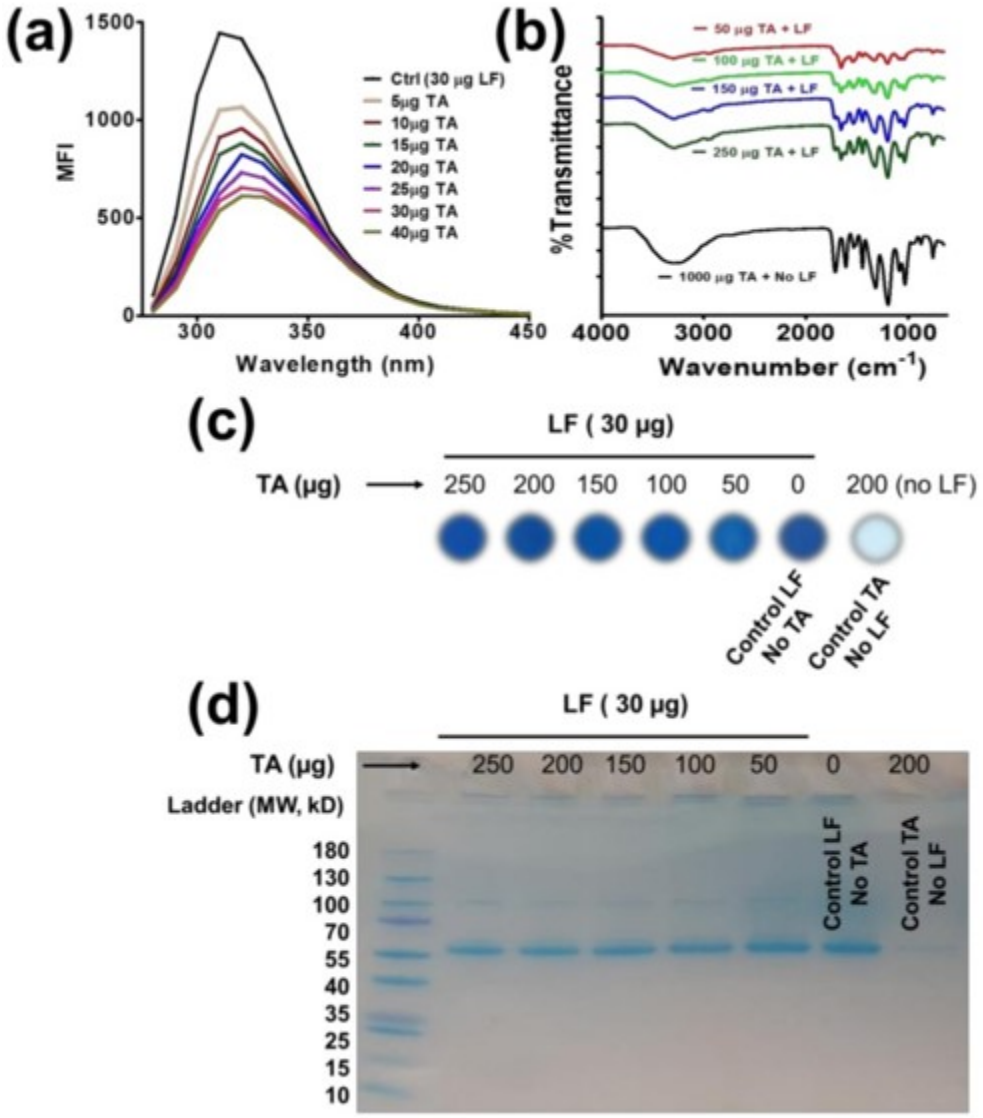

Figure 2-1. Spectral and biological confirmation of TA-LF complex formation. a) Instant binding and self-assembly/complex formation of LF and TA was measured by measuring fluorescence (FL) quenching. Representative FL quenching profiles of 30µg/mL LF with increased TA solution (5–40µg) at room temperature (λex = 295nm). (b) FTIR spectra of TA and TA-LF complexes. Characteristic peaks at 1653 and 1525 cm−1 represent the presence of LF in TA-LF complexes. (c,d) Protein dot and SDS-PAGE confirms presence of LF proteins in TA-LF complexes by visual evidence. Coomassie Blue stains lung fluid protein in TA-LF assemblies but not free tannic acid. (a,c,d) Data acquired from 3 sets of samples for confirmation. MFI=Mean fluorescence intensity.

Stretching and N–H bend) (**Figure 2-2**). The other peaks at 3290 and 1075 cm−1 correspond to N–H and C–N stretch of the aliphatic amine moiety (**Figure 2-2**). In the spectra of the TA-LF complexes, the specific peak at 1653 cm−1 belongs to the amide I band of LF, while other bands coincide with TA characteristic peaks (**Figure 2-1b**). The major amide I peak decreased relatively with increase of TA in TA-LF complexes.

LF Proteins in TA-LF Complexes

Control LF and the TA-LF complex samples show almost equivalent protein stain with Coomassie Blue on nitrocellulose membranes (**Figure 2-1b**). There is no strong signal observed for TA alone samples. To gain better insights of TA-LF complex formation, we separated supernatant and pellet of TA-LF complexes which are considered well-dispersed/perfect corona formation and loosely bound corona/aggregates of corona, respectively. Supernatant TA-LF complexes at TA:LF ratio(s), 30:250, 30:200, and 30:150 show more protein stain while 30:100 and 30:50 demonstrated almost nil. This indicates higher TA concentration helping to achieve a better protein corona (smaller TA-LF complex formation, **Figure 2-3**) TA-LF complex pellets indicate protein stain at 30:150, 30:100, and 30:50 reflect due to poor or random corona formation (**Figure 2-4**). Altogether, this indicates higher TA promotes smaller TA-LF complexes. The abundance of LF protein in TA-LF complex samples was observed in SDS-PAGE gel (**Figure 2-1d**) due to combination of smaller and bigger complex formation due to LF corona formation. A similar pattern of protein exists in these samples, which further confirmed the data shown in **Figure 2-1c**.

Protein Corona Formation

Protein corona formation is a biological phenomenon that occurs when nanoparticles incubated with proteins. To investigate such phenomena, DLS analysis method was employed. TA-LF complexes had particle size less than ~305nm (**Figure 2-5a**). TA and LF alone showed particle size of 340.8 ± 55.69nm and 338.2 ± 5.64nm, respectively (**Figure 2-3a**). A higher amount of TA (250 μg) leads to lower particle size (105 ± 11.83nm) due to hard protein corona on TA. Lower amounts of TA (50 μg) in TA-LF generated complexes with a particle size of 304.8 ± 43.64nm. This suggests that TA concentration plays a major role in determining the globular protein corona formation and determining particle sizes of complexes resulting from incubation with LF.

TA and LF alone exhibited low negative zeta potentials, −16.03 ± 0.17mV and −7.68 ± 0.91mV, respectively (**Figure 2-3b**). When TA content increased in TA-LF assemblies, their zeta potential values are similar, as seen for LF zeta potential, i.e., −8.55 ± 0.20 mV for assembly resulting from 250 μg TA in a TA-LF assembly (**Figure 2-5b**). This is evidence that LF proteins are perfectly aligned on the TA core. When TA concentration is lower in TA-LF assemblies, the resulting zeta potential values lie between those for TA and LF (**Figure 2-5b**). This provides support for the hypothesis that these assemblies might be complexes of irregular formation, depending upon the

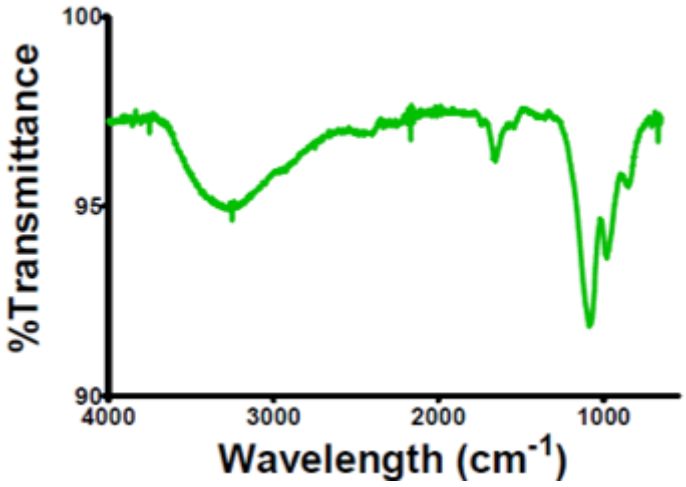

Figure 2-2. FTIR of lung fluid.
Protein characteristics peaks of the amide I band at 1655 cm−1 (mainly C–O stretch) and amide II band at 1525 cm−1 (C–N stretching and N–H bend) in LF. The other peaks at 3290 and 1075 cm−1 corroborates to N–H and C–N stretch of the aliphatic amine.

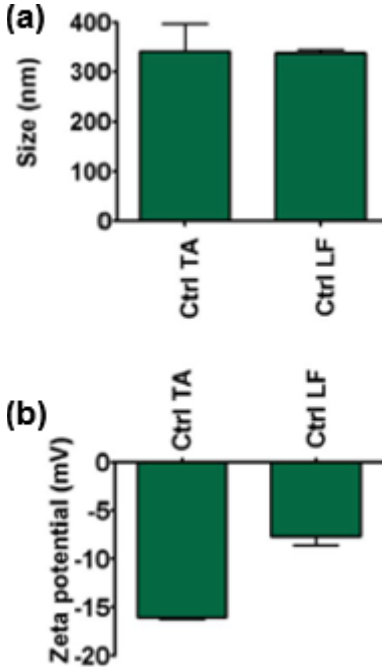

Figure 2-3. DLS data for (a) particle size and (b) zeta potential of TA and LF.
Measurements were performed using Zetasizer.

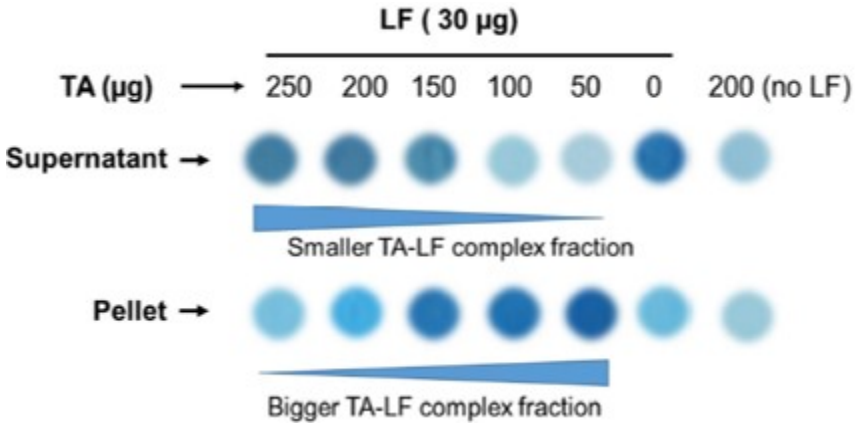

Figure 2-4. Protein dot assay of supernatant and pellet.
TA-LF complexes were separated by centrifugation at 5,000 rpm and supernatant and pellet TA-LF complexes were used for protein density probing on nitrocellulose membrane as mentioned in section above in the manuscript.

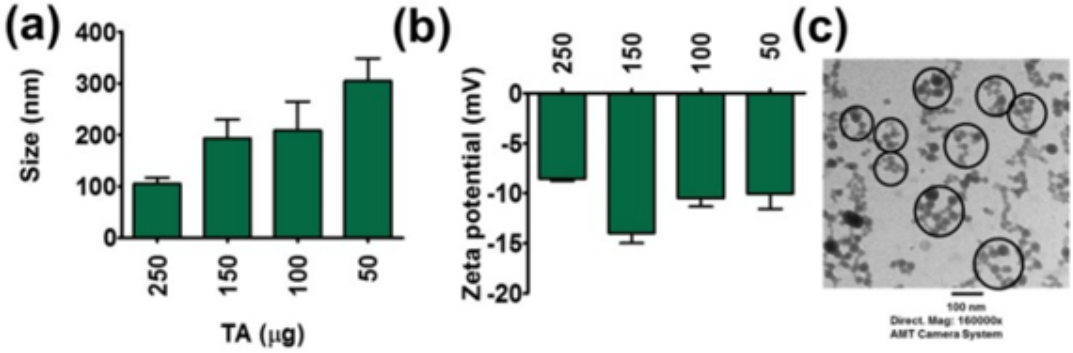

Figure 2-5. Physical characterization of TA-LF complexes.
(a) Particle size and (b) zeta potential of TA-LF complexes. Measurements were performed using Zetasizer. Increasing LF inclusion in TA-LF alters protein corona on TA and the change in their particle size and zeta potentials. Data presented as mean ± SEM (n = 3). (c) Representative transmission electron microscopic image of TA-LF self-assemblies. Image was acquired using advanced microscopy digital camera system Print magnification 160,000×.

amounts of TA employed. However, it is important to note that there is no positive zeta potential observed, which indicates that all TA-LF systems are stable, and complexation does not lead to huge aggregation or precipitation. Additionally, a negative zeta potential for nanosystem(s) or carrier(s) implies that these are safe for therapeutic applications, unlike a positive zeta potential for such materials, which induces systemic toxicity.

TEM analysis was conducted to investigate the visual evidence for TA-LF complex formation and to observe the morphological status of each complex. TA-LF complexes exhibited a self-assembled spherical shape, about <30nm with aggregations of <120nm (**Figure 2-5c**). Such well-defined morphology of TA-LF nanoparticles can be an indication of effective penetration ability in lungs. Further, this indicates that TA is not inducing larger aggregates, which often cause elimination from circulation.

The particle sizes of TA-LF assemblies were tested at different pH solutions (6.8, 7, and 7.4) (**Figure 2-6a**). Interestingly, a significant increase in particle size was noticed at pH 6.8 (751.33 ± 32.26nm) compared to all other pH measurements. This could be due to the loosening of proteins from the self-assemblies or protein corona on TA core. Such dissociation of self-assemblies may offer immediate release of therapeutics which is helpful in drug delivery. That means at tumor pH (around ~6.8) self-assemblies dissociate and release drugs for quick response or targeted delivery mechanism. It is also equally possible that TA is hydrolyzes more at this pH compared to other pH. However, zeta potentials were all negative for all pH tested (between −15.86 ± 0.76mV and −19.13 ± 0.92mV, **Figure 2-6b**).

LF Protein Corona Promotes Interaction with LC Cells

It is essential for cancer therapeutic applications that drug carriers be able to internalize into the cancer cells, and the release the drug in the cytosol, to achieve a relevant beneficial therapeutic effect.

First, we investigated the uptake of TA-LF complexes by A549 and H1299 LC cells using fluorescence microscopy. Abundant intracellular distribution of TA-LF complexes is observed in cells through coumarin-6 labeling (**Figure 2-7a**). To achieve a global pattern of uptake of TA-LF complexes, flow cytometry was employed. For this, an average of 1×10^4 cells were used to measure fluorescence intensities. An elevated intensity of green fluorescence was observed in both cell lines with increased amounts of LF protein in TA-LF self-assemblies used for the experiment (**Figure 2-7b**). Further, it was confirmed that this cellular interaction is time dependent (**Figure 2-7c**). With increased time of contact, the TA-LF complexes interact more with LC cells, due to the enhanced adherence of LF on the TA core.

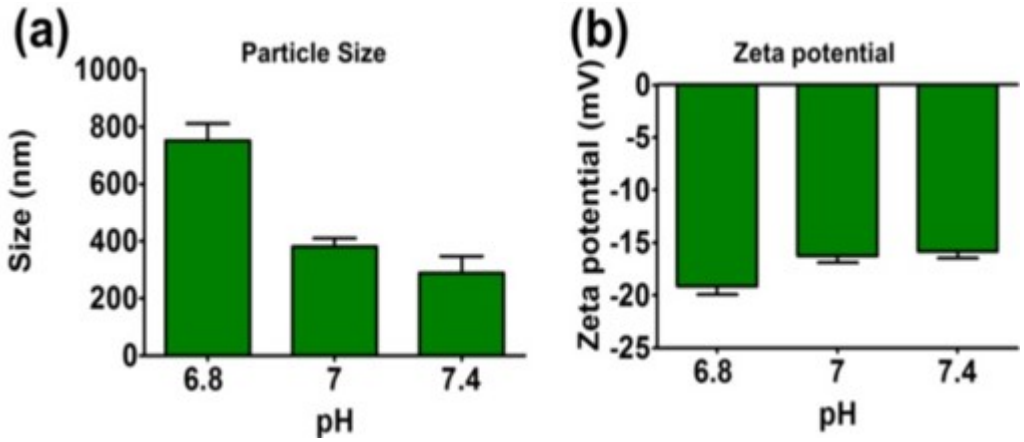

Figure 2-6. Influence of LF protein corona in TA-LF complexes with change in pH.

(a) Particle size and (b) zeta potential of TA-LF were measured in different pH of 4-(2-hydroxyethyl)-1-piperazineethanesulfonic acid (HEPES) buffer solutions. Data presented as mean ± SEM (n = 3).

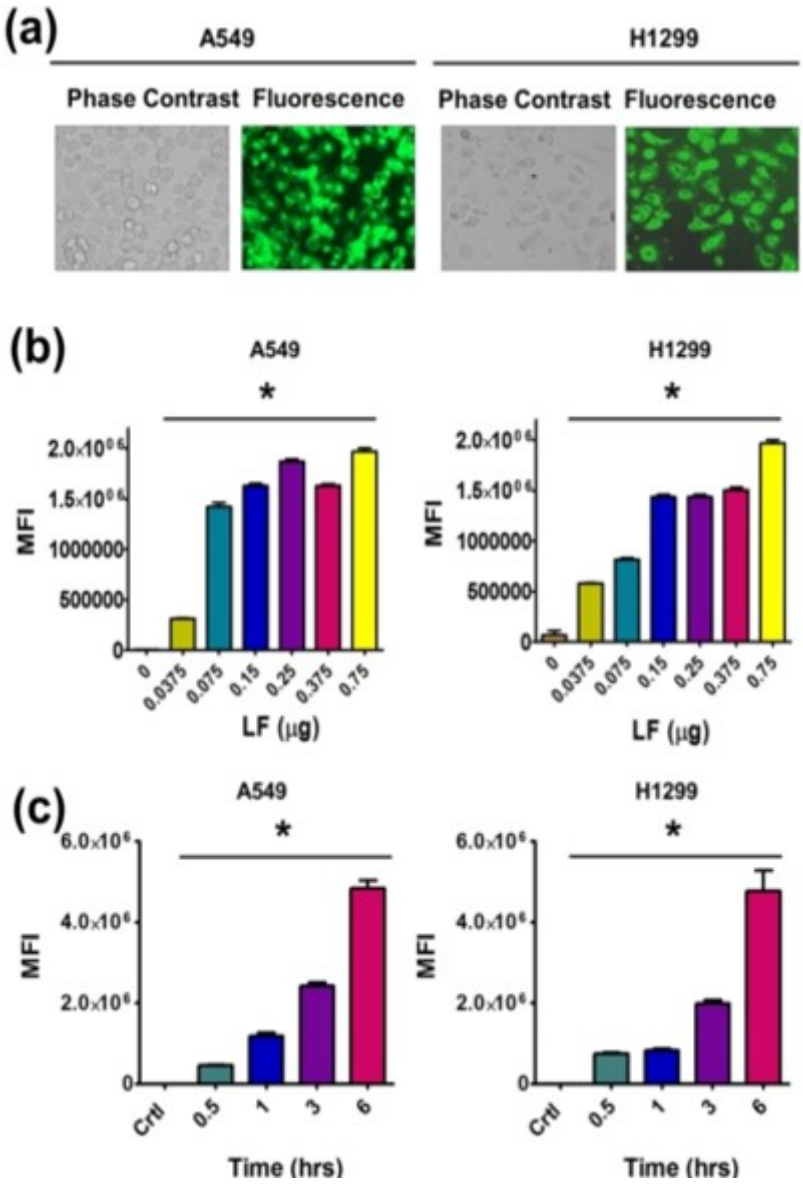

Figure 2-7. LF corona promotes cellular uptake of TA-LF complexes.
a) Cellular uptake of dye labeled TA-LF in A549 and H1299 cells. Cells were treated with coumarin-6 labeled TA-LF (5 μg coumarin-6 equivalent) for 3 h. Representative fluorescence image was presented. (b) LF corona on TA exhibited enhanced cellular uptake in A549 and H1299 cells. Coumarin-6 concentration in TA-LF was 5 μg/mL and incubation time was 3 h. (c) Time-dependent cellular uptake of coumarin-6 labeled TA-LF complexes. (b,c) FL levels of internalized coumarin-6 labeled TA-LF complexes were measured using an Accuri C6 Flow Cytometer in the FL1 channel. Data presented as mean ± SEM (n = 3). Uptake is significance compared to no LF or control cells (* $p < 0.05$).

TA-LF Improves Pharmaceutical Activity in LC Cells

To study the potential enhancement of anticancer activity when encapsulated in TA-LF assemblies, we employed an MTS assay against two LC cell lines. This assay measures viability of the cancer cells based on mitochondrial respiratory activity. There is no effect on A549 and H1299 cells when treated with free TA-LF complexes (without drug) (**Figure 2-8**), red color lines). A clear dose-dependent effect was observed with free pharmaceutical drugs (Gemcitabine, carboplatin, and irinotecan) against cancer cells (**Figure** 2-8), green color lines). TA-LF complexes showed more significant growth-inhibiting effects than free drugs (**Figure 2-8**), blue color lines). This indicates that TA-LF assemblies promote interaction and delivery of drug(s) to the cells tested. In all drug-encapsulated TA-LF assemblies, there was at least 2–2.5 fold reduction in their IC50 values compared to free drugs (**Figure 2-8c**).

An effective chemotherapy not only lowers systemic toxicity, but also lowers the therapeutic dose. This study supports the hypothesis that TA-LF can be implemented as an efficient drug carrier (**Figure 2-9**). The developed method may overcome conventional chemotherapy and its associated drawbacks such as modest benefit and drug resistance. Lately, nanomedicine (for example, AbraxaneTM, a paclitaxel self-assembled human serum albumin formulation) represents a universal drug delivery platform for the treatment of LC, which makes chemotherapeutic drugs more efficient in treatment regimens. Likewise, our TA-based drug formulations might serve as a better therapeutic modality for LC. Our future investigation on these formulations will include studies regarding superior molecular mechanisms and pre-clinical animal studies.

Conclusions

Overall, this investigation revealed a naturally occurring water-soluble polyphenolic drug carrier and its interaction with LF proteins. The study demonstrated that TA exhibits superior and well-defined protein corona formation. This was demonstrated by particle size, zeta potential, morphology, cellular internalization, and anticancer activity assays. Further, the results can be extrapolated to physiological relevance of the adsorption of LF and reduction of surface tension. Therefore, TA may be proposed as a promising carrier for future research into drug delivery application.

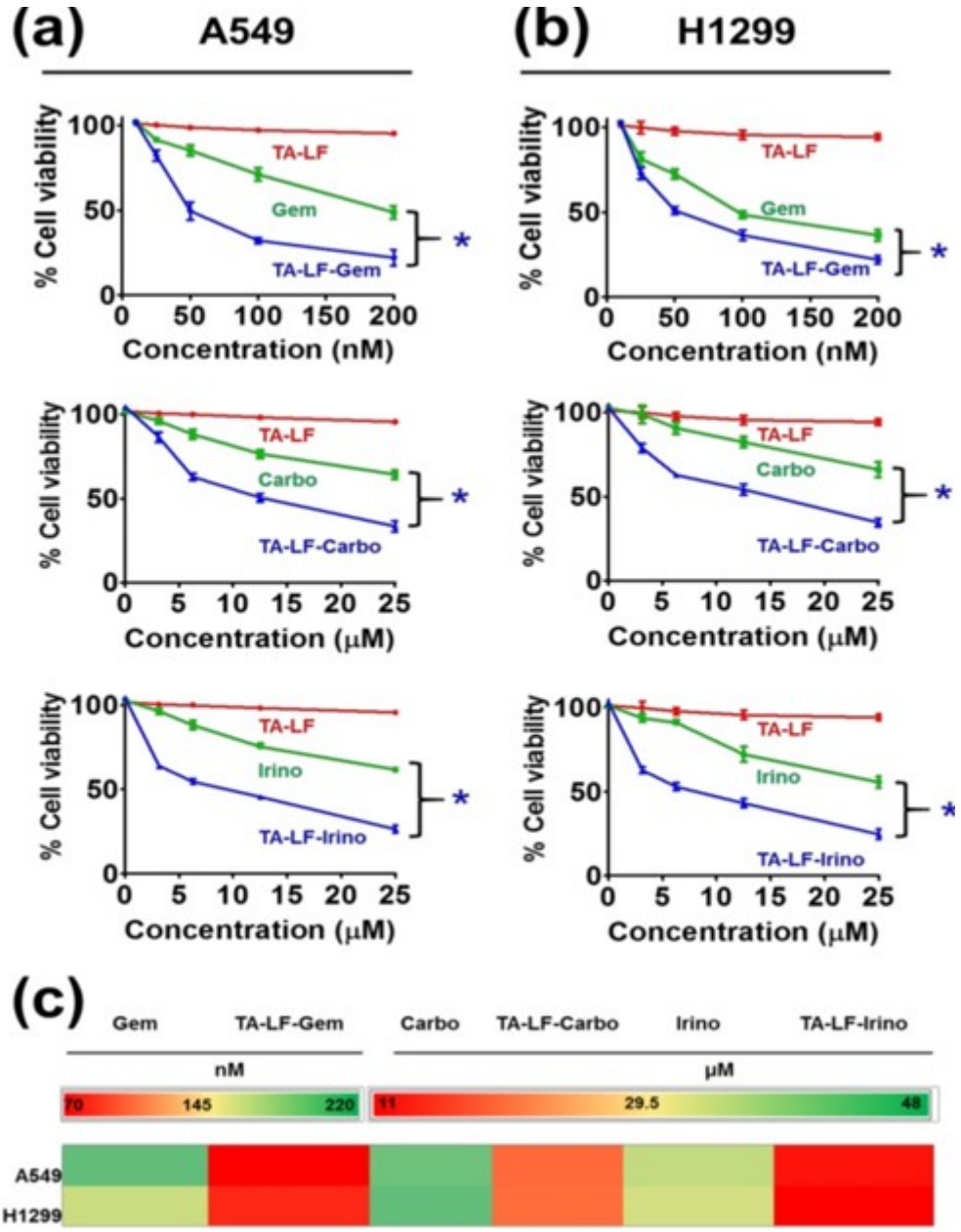

Figure 2-8. TA-LF complexes promote delivery of encapsulated therapeutic drugs to LC cells.

MTS assay of drug-encapsulated TA-LF complexes against a) A540 and (b) H1299 LC cells. Cells (5×10^3) were seeded in a 96-well plate and left overnight for cell attachment to the plate, the cells were treated with indicated concentrations of Gemcitabine, carboplatin, and irinotecan and their respective drug encapsulated TA-LF complexes for 48h. Cell viability was determined using MTS assay. The data were presented in the form of line graphs as percent viable cells compared to untreated cells in medium. Data presented as mean ± SEM (each treatment, n = 6). Cytotoxicity of TA-LF-drug formulations were significant compared to free drugs (* $p < 0.05$). (c) IC_{50} values of drug vs. drug-encapsulated TA-LF assemblies presented as heat map. IC_{50} values were calculated using GraphPad software (La Jolla, CA, USA).

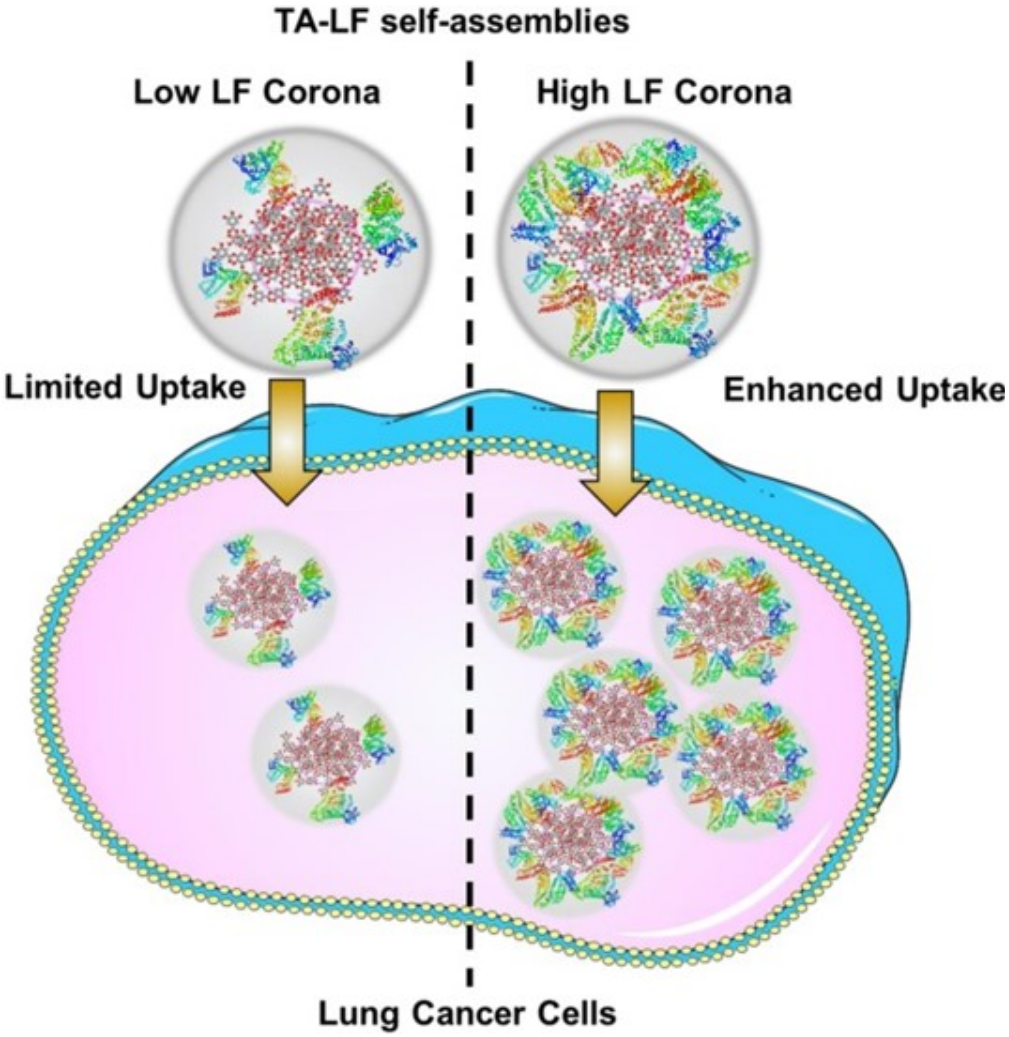

Figure 2-9. Schematic representation of LF corona influencing delivery of TA-LF assemblies to LC cells.

CHAPTER 3. GAMBOGIC ACID SENSITIZE NON-SMALL CELL LUNG CANCER CELLS TO GEMCITABINE THERAPY

Introduction

In spite of several currently approved therapies, lung cancer (LC) remains a leading cause of cancer-related mortality, the overall 5-year survival rate is as low as 15%, with approximately 142,670 estimated deaths in the United States in 2019 [4]. Based on histopathology[158], LC is categorized as either small cell lung cancer (SCLC) or non-small cell lung cancer (NSCLC).[2] Around 85-90% of the LC cases fall under the category of NSCLC.[5] Surgery, radiation, chemotherapy, targeted treatments and immunotherapy (alone or in combination) are the current therapeutic options for NSCLC. [159] By the time of the diagnosis most patients (~ 65%) already have advanced stage disease and have developed distant metastases[160].

The conventional chemotherapeutic agents such as Gem, carboplatin, cisplatin, paclitaxel and irinotecan offer the most effective and promising regimens[161 162]. Unfortunately, in most cases these chemotherapeutic agents only provide good initial responses, with patients eventually developing rapid drug resistance. The resulting modest survival improvements are due to issues such as recurring cancer relapse, intolerable toxicities as a result of increase in the drug dosage, and severe side effects [48 163]. Drug resistance is a major challenge for NSCLC therapy, and the main challenge is to improve the outcome of these group of chemotherapeutics, to preserve their potency in patients who developed acquired or innate chemoresistance, and to avoid cancer recurrence and relapse[164165]. Therefore, management of NSCLC demands a multimodal approach and there is an imminent need for optimization and validation of new therapeutic strategies to circumvent this problem.

Gem, a pyrimidine nucleoside antimetabolite, has been widely used for different types of cancer therapy. It is well known as the most commonly used chemotherapeutic agent in lung cancer for decades with favorable results[29 32]. Gem has a relatively low toxicity profile and is known to increase the median survival rate by 20-25% [166]. Therefore, Gem has improved the median overall survival rate by 4-9 months, but it is not exempted from chemoresistance which hinders the maximum capacity of Gem therapy. In a large study investigating 3,042 NSCLC patient tumors, the researchers found that 72% had extreme or intermediate resistance against Gem[167]. Intrinsic resistance is caused by metabolic regulation of Gem uptake and other anti- apoptotic pathways, and is mainly due to drug transporters and metabolic enzymes which lead to a decrease in its cellular uptake [34 168]. There are multiple ongoing clinical trials aimed to enhance outcomes of Gem therapy and conquer these pitfalls, by combining it with other therapeutic agents. For instance, combination of cisplatin (platinum-based antineoplastic) with Gem led to a 46% reduction in drug resistance[48]. However, combinatorial approaches of this type often encounter obstacles due to adverse side effects such as neutropenia, neuropathy, myelosuppression and nephrotoxicity. Despite several attempts at pursuing different drug combinations with Gem, there are still no convincing

results[169]. Hence, the combination of Gem with a chemo-sensitizer/anticancer natural compound that has distinct molecular mechanisms and a favorable safety profile could be considered a promising therapeutic strategy. Such a combination would strive to achieve higher efficacy of treatment, eliminating drug resistance development, and yet reducing the side effects and toxicity issues. In this regard, we selected Gambogic acid (GA, chemical formula; $C_{38}H_{44}O_8$), GA is a xanthonoid derived from the resin of *Garcinia hanburyi* tree[170 171]. Therefore, it has a plentiful and cost-efficient supply together. Previous reports have identified GA as a potent apoptosis inducer, an anticancer agent, and inhibitor of tumor growth. In addition, GA has a good safety profile and high therapeutic index in various diseases, including different type of cancers. Furthermore, unlike other natural anticancer agent which failed to gain favor due to lack of potency, GA has shown to be effective at lower concentrations (nM range)[64 62] . GA is known to have a chemo-sensitization effect on various cancer types ,for instance, it was shown that GA has sensitization effects on doxorubicin therapy for resistant breast cancer by inhibiting P-glycoprotein and suppressing survivin expression [70 172 173], Further studies showed that GA has apoptotic effects on cancer cells by modulating different signaling pathway such as MAPK/ERK, PI3K/AKT and NF-κB[174 175 176 177]. Therefore, GA has gain attention as an anticancer agent to be used for combination therapy. **Table 3-1** lists combination of GA with different chemotherapeutic agents in various cancer type. In addition to the number of studies about the anticancer inhibitory effect of GA on lung cancer, a phase IIa clinical trials conducted on GA administered as single agents for cancer therapy.[66] The results of a randomized and multicancer clinical study of GA therapy for advanced malignant NSCLC, colon and renal tumors demonstrated promising antitumor efficacy with a good safety profile. Taken together, GA has gained attention as a desirable candidate for combination therapy in recent decade (**Table 3-1**). For more details on GA mechanism of action please refer to introduction chapter.

Therefore, in this study we aimed to investigate the elevated anticancer effect of Gem in combination with GA on NSCLC as a potent apoptosis inducer and sensitizer. Furthermore, we examine the synergistic effect of GA with Gem in *in vitro* assays. We speculated that GA would sensitize NSCLC tumor cells to Gem therapy by inhibiting the expression of ribonucleotide reductase (RR) enzyme subunit 2(RRM2). We are confident that, this research findings, not only enhances the knowledge of NSCLC therapy, but also implements a theoretical base for the future clinical administration of GA for patients with NSCLC.

Methods

Chemicals and Reagents

Gambogic acid was purchased from Apex bio (Houston, TX, USA) and dissolved in in dimethyl sulfoxide (DMSO) and restored in -20ºC and diluted further for usage, where DMSO was less than 0.1% in the final dilutions. Gem was purchased from Fisher Scientific (Waltham, MA, USA), and dissolved in sterile PBS. All the other reagents,

Table 3-1. Classification of combination therapy with Gambogic acid (GA) and other anticancer agents tested in different cancer types.

Combined anticancer agent	Cancer type	Combination type	Mechanism of action	Ref.
Docetaxel	Breast Cancer	Sensitization	Inhibiting P-gp, post translational proteasome	178
	Gastric cancer	-	Survivin inhibition	179
	Gastrointestinal cancer	Synergistic	β-tubulin III, tau and Survivin	180
Chloroquine	Pancreatic cancer	Synergistic	Accumulation of reactive oxygen species	181
Heparin-quercetin	Breast cancer	Synergistic	Inhibiting P-gp	73
Cisplatin	NSCLC	Synergistic	Downregulating MRP2 and LRP expression	182
5-fluorouracil	Colorectal cancer	Synergistic	P53, Survivin and thymidylate synthase (TS)	183
Retinoic acid	Osteosarcoma	Synergistic	Increased apoptosis	184
chlorochalcone	Breast cancer	Synergistic		185
Vorinostat	Neuroblastoma	Synergistic	JNK-IRE1-mTORC1	186
Imatinib	Myeloid leukemia	Synergistic	Inducing Proteasome Inhibition and Caspase-Dependent Bcr-Abl Downregulation	187
Irinotecan	Liver cancer	Synergistic	ERK and p38 MAPK activation	188
Gefitinib	NSCLC	Synergistic	ERK and p38 MAPK activation	189
Tandutinib	Meningiomas	-	Suppressed the VEGFA-induced PDGFRβ tyrosine phosphorylation	174

Table 3-1. (Continued).

Combined anticancer agent	Cancer type	Combination type	Mechanism of action	Ref.
Doxorubicin	Breast	Sensitization	Inhibiting P-gp & Survivin	190
	Ovarian cancer	Sensitization	Accumulation of reactive oxygen species	191
Gemcitabine	Pancreatic cancer	Sensitization	Ribonucleotide reductase subunit-M2 (RRM2)	63
Methyl Jasmonate	Bladder cancer	Sensitization	Downregulation of enhancer of Zeste homologue 2 (EZH2) expression	192
Verapamil	Human epithelial cancer	Synergistic	Proteasome Inhibition and reactive oxygen species generation	193
Celastrol	Oral squamous cell carcinoma	Synergistic	NF-kappa B inhibition	194
Sunitinib	Renal cell carcinoma	Synergistic	NF-kappa B inhibition	195

solvents, chemicals, and cell culture plastics were obtained from Fisher Scientific (Pittsburgh, PA, USA) and Sigma–Aldrich Co. (St. Louis, MO, USA), unless otherwise stated.

Cell Lines and Culture Conditions

Human NSCLC lung adenocarcinoma (H1299 and A549), human lung bronchial epithelial (BEAS-2B), and human umbilical vein endothelial cells (HUVEC) cells were obtained from American Type Culture Collection, (ATCC, Manassas, VA, USA) and maintained as described earlier[196]. Briefly, A549 cells were cultured in Dulbecco's Modified Eagle's Medium (DMEM) and H1299 was cultured in Roswell Park Memorial Institute medium (RPMI-1640) Gibco, Thermo Fisher Scientific, Grand Island, NY, USA), Beas-2B was cultured in bronchial epithelial cell growth medium (BEGM), and HUVEC was cultured in endothelial cell growth medium-2 (EGM^{TM}-2) (Lonza, Morristown, NJ, USA), all medias contained 10% fetal bovine serum (FBS) and 1% (w/v) penicillin–streptomycin (Gibco, Thermo Fisher Scientific)) and they were incubated at 37 °C in a humidified atmosphere with 5 % CO2 (Thermo Fisher Scientific, Waltham, MA, USA). All cells were regularly monitored for their typical morphology and contamination under the microscope.

Cell Viability Assay

The MTT assay was performed to detect cell viability following treatment with free Gambogic acid (GA), Gem, and the combination of GA and Gem in NSCLC cells. While the effect of GA and Gem alone were also investigated in normal human lung bronchial epithelial cells (Beas-2B). Cells (0.5×10^3) were seeded into 96-well culture plates and left for overnight incubation (to attach to the plates) at 37 °C and 5% CO_2 treated with varying concentrations of GA alone (25, 50, 100, 200, 400nM) and (25, 50, 100, 200nM) of Gem alone as well as the combination of both GA+Gem for 48h. Every treatment was performed in triplicate per experiment, and each experiment performed in triplicates. Then, 20 µL MTT solution(5mg/ml) was added to 100 µL of the culture medium (per well), and incubated for 2-4 h at 37 °C. The culture medium containing MTT solution was discarded and 100 µL DMSO solution was added into the wells that were further incubated for 15 min at RT while shaking. After this step, the absorbance was measured using a microplate reader (Cytation™ 5, BioTek Instruments, Winooski, VT, USA) at 490nm according to the manufacturer's instructions[197 63]. The IC50 calculation was performed using GraphPad Prism 6.07 software. The combination index (CI) was calculated using the Chou–Talalay method[198]:

$$\boldsymbol{CI} = \left(\frac{\boldsymbol{Dc1}}{\boldsymbol{Ds1}}\right) + \left(\frac{\boldsymbol{dc2}}{\boldsymbol{Ds2}}\right) + \left(\frac{\boldsymbol{DC1Dc2}}{\boldsymbol{DS1Ds2}}\right)$$

Where Ds_1 and Ds_2 represent the IC50 of GA and Gem respectively, while, Dc_1 and Dc_2 are the IC50 values of the drugs applied in combination. (CI< 0.9, synergism, 0.9-1.1, additive effect, >1.1 antagonism).

Colony Formation Assay

Approximately 300-400 (per well) of A549 and H1299 cells were seeded into 12 well plates for 24h and then treated with/without 25 and 50nM of GA and 25 and 50nM of Gem as well as the combination of both drugs with respective concentrations for 15 days, and the drug-containing medium was renewed every 3 days. After 15 days of incubation, formed colonies were fixed with pure cold methanol and stained with 0.05% crystal violet at room temperature[186]. Images of the colonies were obtained using a ChemiDoc MP Imaging System (Bio-Rad, Hercules, CA, USA). All colonies were counted manually using the NIH ImageJ software freely available on the web (www.imagej.nih.gov/ij/).

Migration Assay

Cell migration assays were performed in Corning's 96-well Boyden chambers (8μm) plates containing polycarbonate membrane as per manufacturer's instructions. Briefly, cells were subjected to overnight starvation (by culturing in serum-free medium) then starved cells (0.5×10^5 cells/well) were seeded in upper chambers of the plate containing serum-free culture medium and treatments 100nM and 200nM of GA, and 100nM and 200nM of Gem (separately along with varying combination ratios equivalent to each single drug) for 18-24 h. Cells without treatment served as controls. Cells were allowed to migrate from upper chambers with serum free medium towards lower chambers with complete medium containing 10% FBS. The migrated cells were fixed with cold 4% paraformaldehyde in PBS for 30 min followed by rinsing with PBS and then stained with crystal violet for 45 min. Cells in the upper chamber were completely removed using cotton swabs[199 200]. The experiments were performed in triplicate and three random fields were imaged from replicate wells using a Keyence microscope BZ-X800(Itasca, IL, USA), and the number of cells that had migrated quantified using ImageJ software.

Cell Invasion Assay

The ability of cells to invade were evaluated using BioCoat Matrigel Invasion Chambers (BD Biosciences, Bedford, MA, USA) that were coated with matrix membrane. After starvation of mentioned NSCLC cell lines, 3.5×10^4 cells per well, were seeded in the upper chamber of the trans-well plate, containing serum free medium. Cells were left for adhesion. After 24h they were subjected to treatment with (100 and 200nM) GA and (100nM and 200nM) Gem alone and equivalent combinatorial doses of both drugs for 24-36h, cells without treatment served as controls[201 202]. NSCLC cells which invaded to the lower chamber were fixed, stained and subjected to the Keyence microscope, this experiment was done in triplicate.

Rhodamine-123 Efflux Assay

To study the effect of GA on Gem accumulation inside the cells and its sensitization activity, the Rhodamine-123 (RH123) accumulation assay was employed. For this purpose, 0.5×10^6 /well of A549 and H1299 cells were cultured in a 6-well plate and left overnight to adhere to the plate and grow. The next day, cells were treated with (100 and 200nm) of GA and 100nM of Gem and the equivalent combinatorial dosage. After 24h, 2.62mM of RH123 was added to each well and cells were placed back into the CO_2 incubator for 30 min following previously an established method [203] [130]. Cells were then rinsed twice with sterile PBS, in order to wash any undesirable RH123 dye adhering to the cell surface. Next, the medium was replaced by fresh phenol red-free medium and subjected to imaging using an EVOS® FL Imaging System (AMF4300, Life Technologies, Carlsbad, CA, USA) for qualitative observation. After that, cells were trypsinized and collected in phenol red-free medium and subjected to quantitative analysis by using the NovoCyte Flow Cytometer (ACEA NovoCyte® 1000, ACEA Biosciences, Inc. San Diego, Ca, USA) in FITC channel (fluorescence measurements at λex: 485nm and λem: 520nm) to measure the mean intensity fluorescence of RH123 dye that was internalized by the cells[204].

Cell Cycle Assay

Approximately 0.5×10^6 cells (A549 and H1299) were seeded into six-well plates for culture overnight, they were then treated with varying combinations of GA (100 and 200nM) and Gem (100 and 200nM), and the combination of both drugs for 24h. After which cells were washed with PBS and collected by centrifugation at 1400rpm for 5 min and fixed with 70% pure ethanol and kept at least for 48h at -20 °C. Cells were washed with PBS, and incubated with propidium iodide (PI) solution, FxCycle™PI/RNase Staining Solution at 37 °C for 1h in the dark following manufacturer's instructions, followed by analysis using a Flow cytometer on BL4 channel[205]. Cell cycle distribution and the different cell cycle phase data were analyzed by the ModFit software (Verity Software House, USA).

Apoptosis Detection

The dead cell apoptosis kit with Annexin V Alexa Fluor™ 488 & Propidium Iodide (PI) Kit (Thermo Fisher Scientific, Pittsburgh, PA, USA) were used to detect apoptosis by following manufactures instruction and using fluorescence-activated cell sorting (FACS) machine for analysis. A549 and H1299 cells (5×10^5 cells) were plated onto 6 well plate and cultured overnight, followed by incubation with GA (200nM) and Gem (200nM) simultaneously and also separately for 48h. The cells were harvested and washed twice in cold PBS, and pelleted by centrifugation at 500 g for 10 min. They were then resuspended at 10^6 cells/100 µL in 1X annexin-binding buffer. Stained with 5 µL Alexa Fluor® 488 annexin V reagent and 1 µL 100 µg/mL PI, for each 100 µL of cell suspension and incubated in the dark for 15 min at room temperature[190] [199]. They were

then mixed gently with 400 µL of binding buffer and kept on ice while immediately processing them with a Bio-Rad ZE5 FACS flow cytometer (Bio-Rad Laboratories, Hercules, CA, USA**).**

Western Blotting

Protein extractions from A549 cells treated with different concentrations of 400nM GA and 200nM Gem, and equivalent combination of these two agents, were performed using standard protocols as previously reported [206] [175]. For the western blotting assay, equal amounts of total cellular protein (40µg) were denatured in sample lysis buffer and subjected to (4-20%) SDS–PAGE. Proteins were transferred from gel to a nitrocellulose membrane using the trans-blot electrophoretic transfer cell containing Tris glycine buffer, pH 8.3, and methanol, the transfer procedure was performed 0–4 ◦C for 150 min at 55 V (400 mA). For blocking purposes 3% BSA was used for 1h at RT. Membranes were incubated with primary antibody with 2%BSA in PBST. Treated cell lysates were probed by overnight incubation at 4 ◦C on a rocker with the following primary antibodies:- cleaved caspase 3(#9665), Bcl-2 (#2872), Bak (#3814), Bax (#2772), RRM2(#65939) and β-Actin (#4970) (Cell Signaling Technologies, Danvers, MA, USA). Next, membranes were washed three times with PBST (each time for 5min) and incubated with respective secondary antibodies for 45min. Finally, the blots were subjected to immunoreactive proteins on nitrocellulose membrane using Bio-Rad ECL Western Blotting Substrate Solution (Bio-Rad Laboratories, Hercules, CA, USA) [203] [129].

Blots were imaged using a Bio-Rad computer-based gel imaging instrument and analyzed using ImageLabTM software (Bio-Rad Laboratories, Hercules, CA, USA).

Angiogenesis Assay

For examining *in vitro* angiogenesis, the tube formation ability of HUVEC cells were assessed in presence and absence of the treatments. HUVECs with passages number less than five, were seeded in pre-coated flat-bottomed 96-well plates with Matrigel (Corning, NY, USA) at 1×10^4 cells/well. After incubation for 4 h with the medium containing different concentrations of treatment (200nM GA and 200nM Gem, and equivalent combination of these two agent), HUVEC tube formation were evaluated by phase-contrast at 10X magnification and photographed by using the EVOS® FL Imaging System. The length of tubules was assayed inside 2 × 2 square area at the center of each well[207] [128]. Each experiment was repeated in triplicate.

Statistical Analysis

The GraphPad Prism (GraphPad Software, Inc, La Jolla, CA, USA) software was used for statistical analysis. Data was presented as means ± SD, and the Student's t- test was used to calculate P-values. A p value ≤ 0.05 was considered statistically significant.

Results

GA and Gem Synergistically Reduce the Growth of NSCLC

The inhibitory effect of GA and Gem on NSCLC cells proliferation was examined by MTT assay. The MTT assay results, showed that low doses (100-400nM) of GA had no significant effect on the viability of A549, H1299 and BEAS-2B (**Figure 3-1**) cell lines, while cell viability was dose-dependently inhibited at combinatorial doses of GA with Gem. (**Figure 3-2**).

We further calculated the combination index (CI) using the Chou–Talalay method. As displayed in **Figure 3-3**. the combination of GA and Gem showed a synergetic effect (CI< 1) in both A549 and H1299 cells. Moreover, as shown in the heatmap (**Figure 3-3**), CI values obtained at higher concentration were lower, indicating more of a synergistic effect on cells. Accordingly, the half maximal inhibitory concentration (IC50) values after treatment with Ga and Gem in combination were substantially lower than those obtained after treatment with each single agent.

Furthermore, the ability of NSCLC to form colonies in presence of the Gem and Ga treatments were examined via colony formation assay. The number of colonies formed were larger and more prevalent in control wells, while opposite results were observed in the drug-treated groups (**Figure 3-4**) indicated that the colony formation ability of NSCLC cells was significantly reduced by GA and Gem and had a more pronounced effect when treated with higher combinatorial doses compared with the single drugs ($p < 0.01$).

GA and Gem Combination Reduced Permeability P-gp Activity in NSCLC

Rhodamin123 is a fluorescent dye and also a P-gp substrate[208]. Therefore, it is a common indicator to evaluate the ability of drug efflux by P-gp transporters. To determine the effect of GA on P-gp efflux activity and its capability to act as a P-gp inhibitor and act as a chemo-sensitization agent, A549 and H1299 cells were exposed to different concentrations of GA and Gem (alone and in combination). In this case the higher accumulation of RH123 indicates lower P-gp expression. As shown in (**Figure 3-5**), cells pretreated with GA showed higher RH123 accumulation in comparison with cells without GA treatment. Intracellular RH123 accumulation in NSCLC cells was dose-dependent, as higher GA concentrations showed higher RH123 accumulation, while lower accumulation was observed with Gem treatment. This may be due to the higher expression of P-gp, which suggest that GA has an inhibitory effect on P-gp efflux activity that resulted in the higher fluoresce inside cells. This result signifies the chemo-sensitization ability of GA on NSCLC and shows that GA prevents the RH123/ Gem efflux from cancer cells, and potentially contributing to a lower probability of drug resistance occurrence.

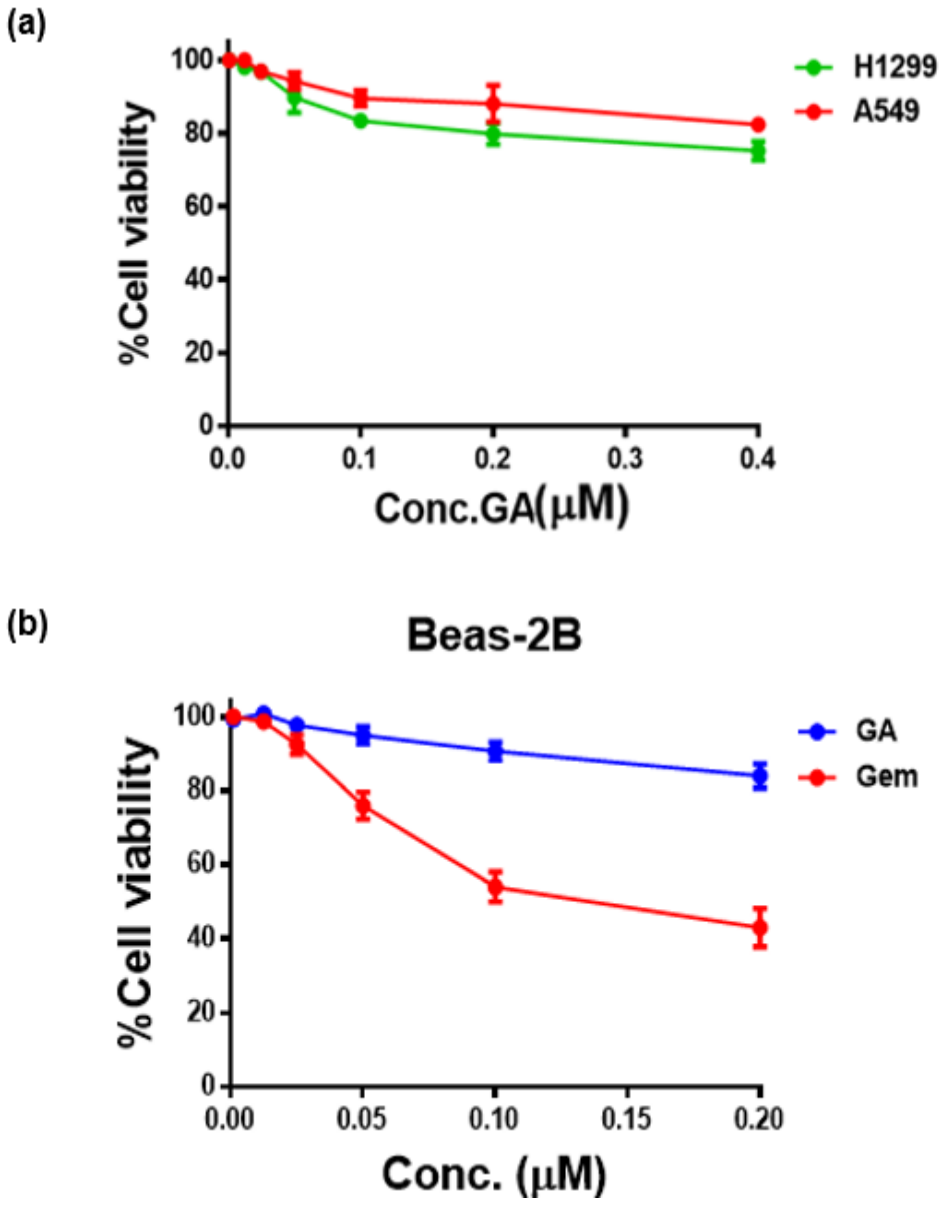

Figure 3-1. Inhibitory effect of GA and Gem on cell viability of NSCLC cells (A549 and H1299) and on normal bronchial epithelium (BEAS-2B).
(a) GA alone was also tested on A549 and H1299 NSCLC. (b) Gem and GA alone was tested on normal bronchial epithelium BEAS-2B cells.

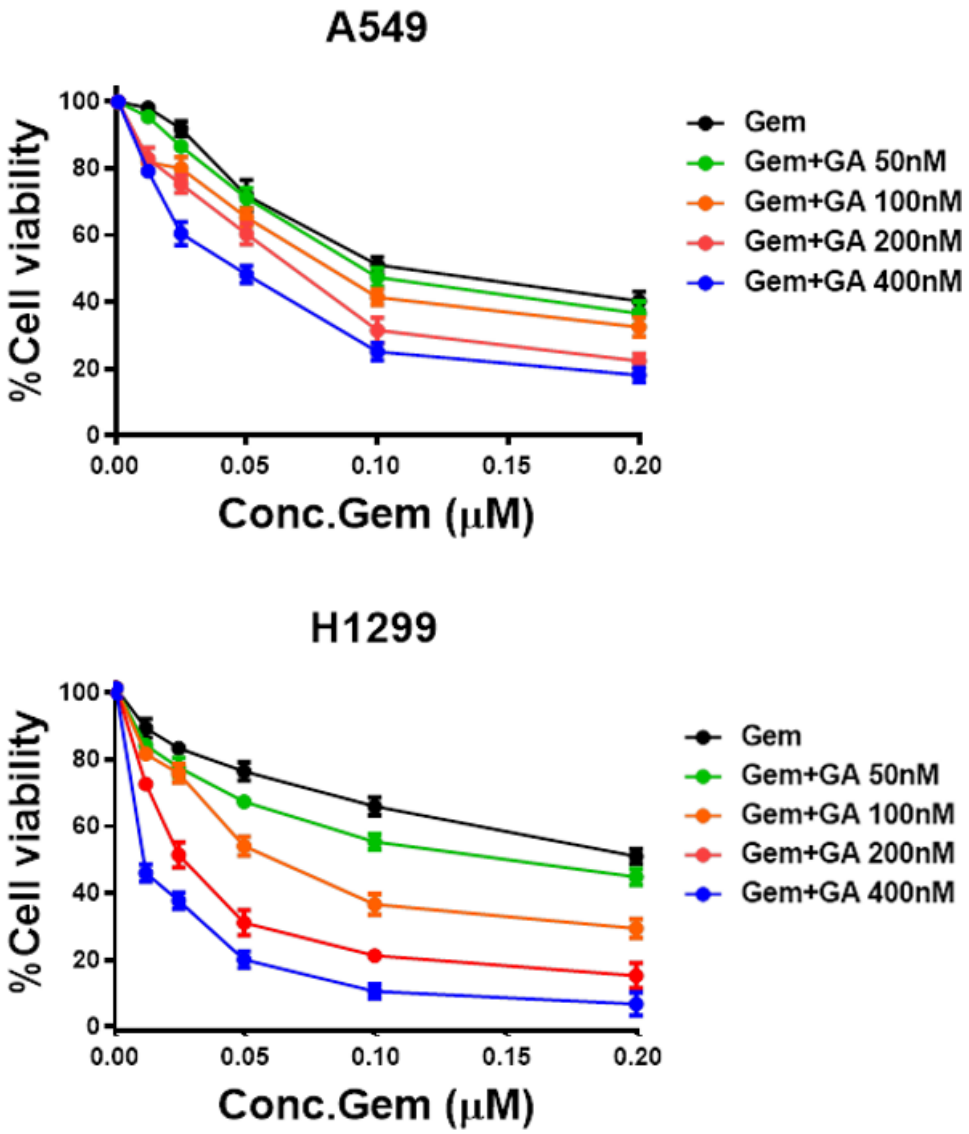

Figure 3-2. Inhibitory effect of GA and Gem combination on the cell viability of NSCLC cells.

Cell viability was assessed by MTT assay. Cells were incubated with different concentration of GA and Gem as single drugs and in combination for 48h. on two NSCLC cell lines (A549 and H1299).

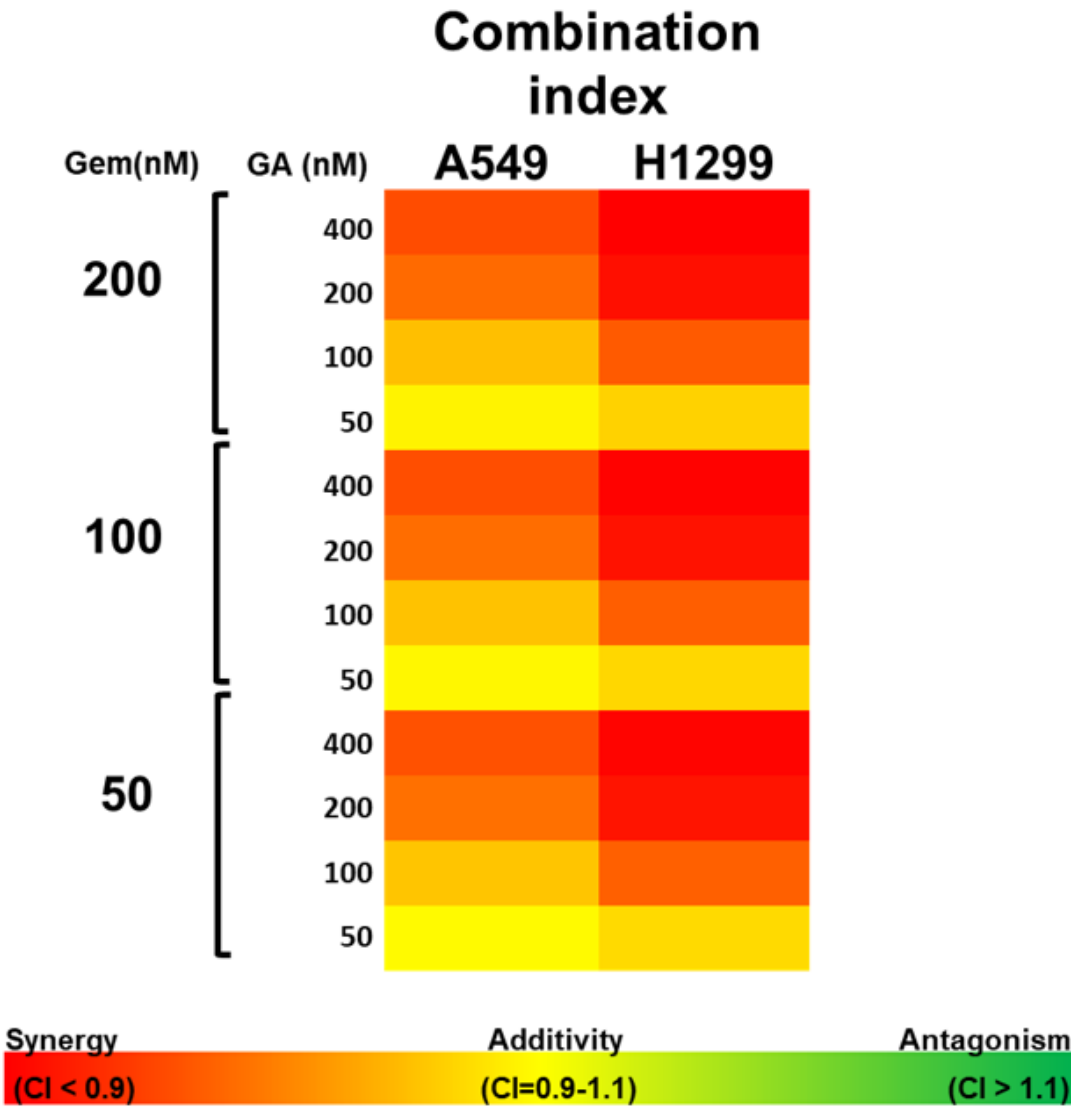

Figure 3-3. Heat map of combination index.
CI values calculated using Chou and Talalay method for different concentration ratio of Gem and GA on A549 and H1299 NSCLC. Values represent the mean ± SEM from three independent experiments.

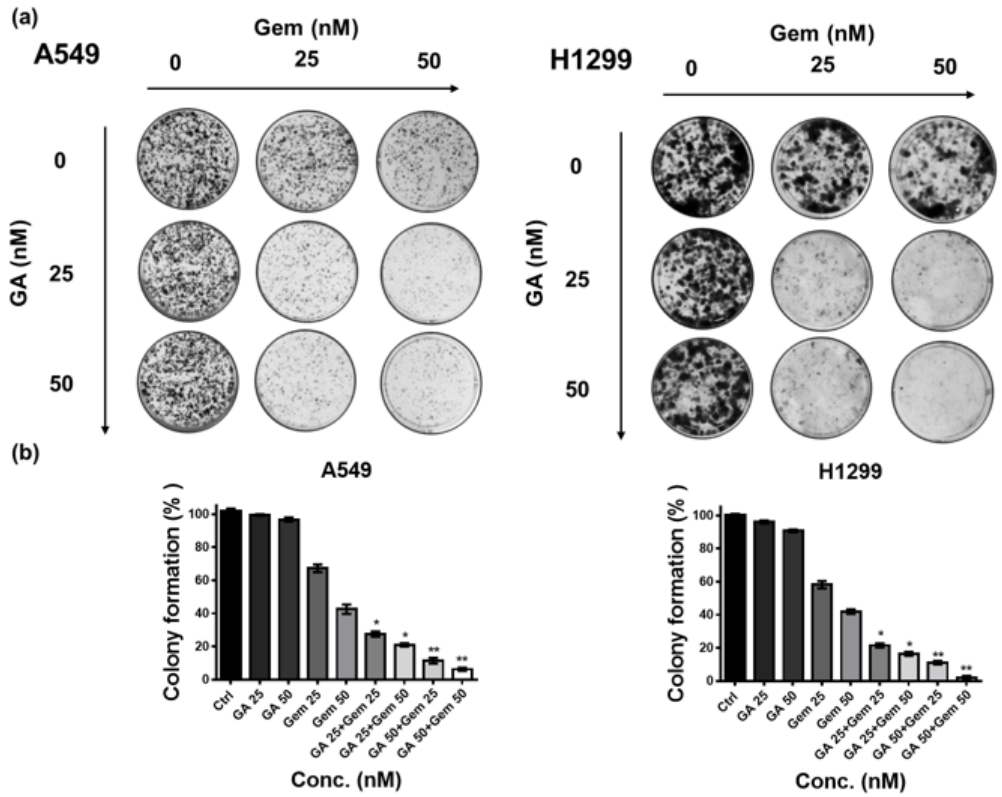

Figure 3-4. Inhibitory effect of GA and Gem combination on the colony formation of NSCLC cells.

Colony Formation capability of NSCLC were analyzed for the above-mentioned concentration for 14 days. (a) representative images and (b) graphical representation of quantitative data analyzed with ImageJ; untreated cells were taken as control (100%). Values represent the mean ± SEM from three independent experiments; The significance level was * $p < 0.05$.

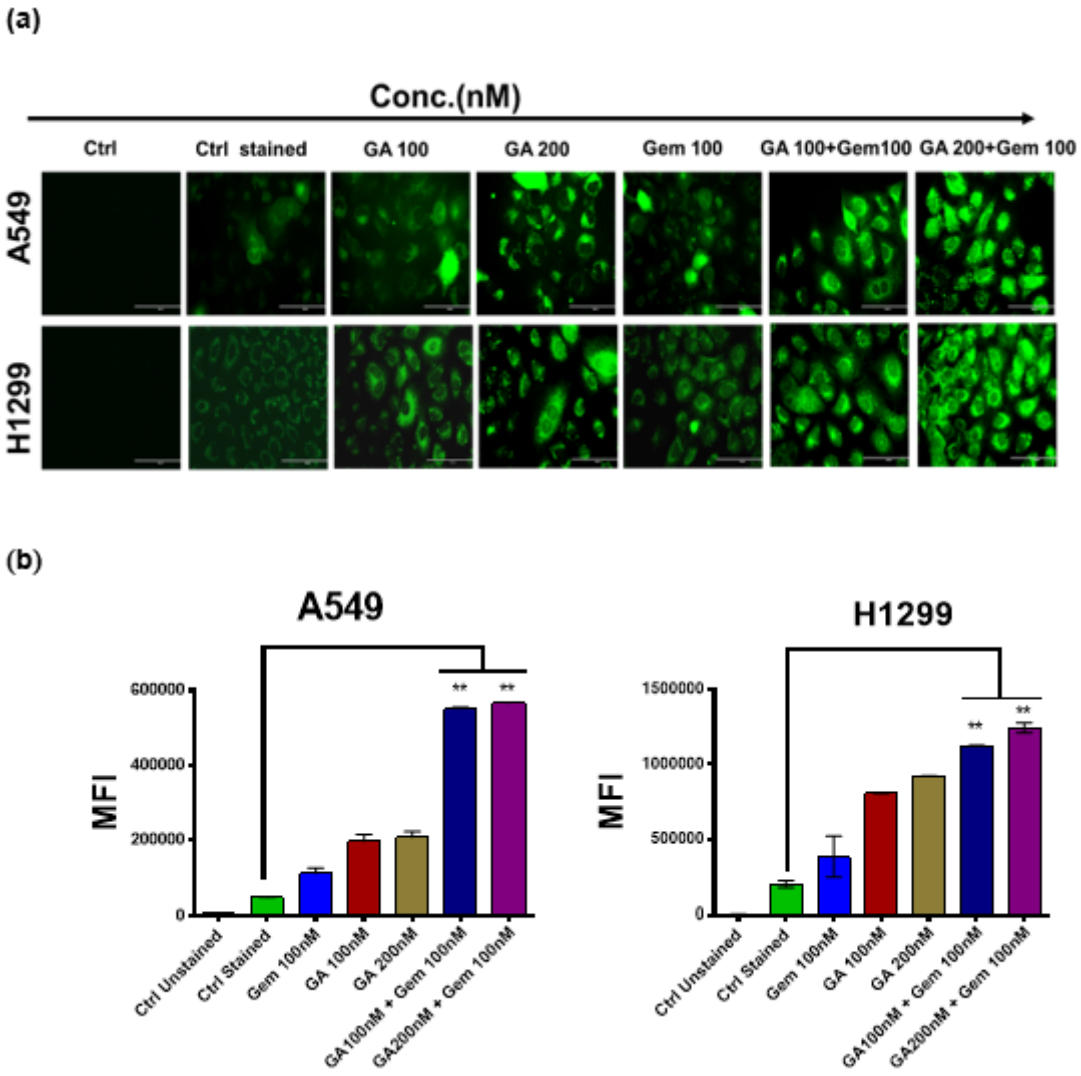

Figure 3-5. Effect of GA on intracellular Rho123 accumulation in A549 and H1299 NSCLC cells.

Cells were incubated with medium containing 2.62mM Rho123 pretreated with GA and Gem with the respective combination dosage for 48h and without pretreatment. After 30min, mean fluorescent intensity (MFI) associated with intracellular Rho123 accumulation was assessed. (a) representative image, (b) A graphical representation of quantitative data analyzed by flow cytometry. Each point represents the mean ± SD from four experiments. Values represent the mean ± SEM from three independent experiments; *$p < 0.05$, **$p < 0.01$.

Combination of GA and Gem Promotes the Suppression of the Migration and Invasive Ability of NSCLC Cells

The migration and invasion of NSCLC cells plays a crucial role in metastasis. To evaluate the effect of our drugs on the migration/invasion of H1299 and A549, Boyden chamber and Matrigel coated plates were used respectively. The number of cells that migrated (**Figure 3-6**) and invaded (**Figure 3-7**) when treated with a combination of GA and Gem was markedly lower than that of control, as well as the GA and Gem alone. These results indicated that the combination of GA and Gem significantly inhibited the migration and invasion of the H1299 and A549 cells.

Combined GA and Gem Treatment Induces Significant Apoptosis in NSCLC

Cell cycle assay was employed to investigate the GA and gem ability to arrest the NSCLC cells which would lead to apoptosis induction, as well. The cell cycle analysis revealed that GA arrest cells and promotes S/G2 progression, Gem treatment also arrest cells in S phase. Next, we investigated whether the synergism between GA and Gem was related to their combined effect on cell cycle distribution. As shown in (**Figure 3-8**), combined treatment significantly increased the apoptotic cell population in the cell cycle process compared to treatment with either single agent, in both A549 and H1299 cells. Albeit, the contributions of cell cycle checkpoints and their regulatory effects in a synergistic manner are mainly unknown. On the other hand, it is well documented that apoptosis, or the process of programmed cell death is a very important aspect for maintaining tissue homeostasis. Therefore, further dissection of the cell cycle results was necessary. Apoptosis is truly differentiated from necrosis, or accidental cell death, by distinctive morphological changes in conjunction with biochemical changes, as illustrated by specific nuclear and cytoplasmic properties, and loss of membrane alignments and asymmetry. Since transference of phosphatidylserine protein (PS) to the outer surface of the cell membrane is one of the primary features of apoptosis, thus in order to distinguish the early or late apoptotic cells, the Annexin-V/ PI double staining assay was employed.

Additionally, dual staining with PI allows differentiation of early apoptotic cells with undisturbed membranes (positive Annexin V and negative PI) from late apoptotic/necrotic cells with permeable membranes (positive Annexin V and positive PI) and normal cells (negative Annexin V and negative PI). The Annexin-V- Alexa Fluor /PI dual staining assay indicated that GA induced a decrease in the percentage of live cells (bottom left) with a concomitant increase in the percentage of early apoptotic cells (upper left) and late apoptotic cells (upper right) as compared to untreated cells, in a dose-dependent manner (**Figure 3-9**). GA+Gem cotreatment significantly induced approximately 6% and 18 % of early and late apoptotic cells respectively). Our result showed that the expression level of the pro-survival and anti-apoptotic protein (BCL-2) was significantly reduced with the combination treatment compared to single GA and the control, and lower than Gem treatment alone. Correspondingly, the expression level of pro-apoptosis and anti-survival protein (BAK), cleaved PARP, and cleaved caspase 3 was

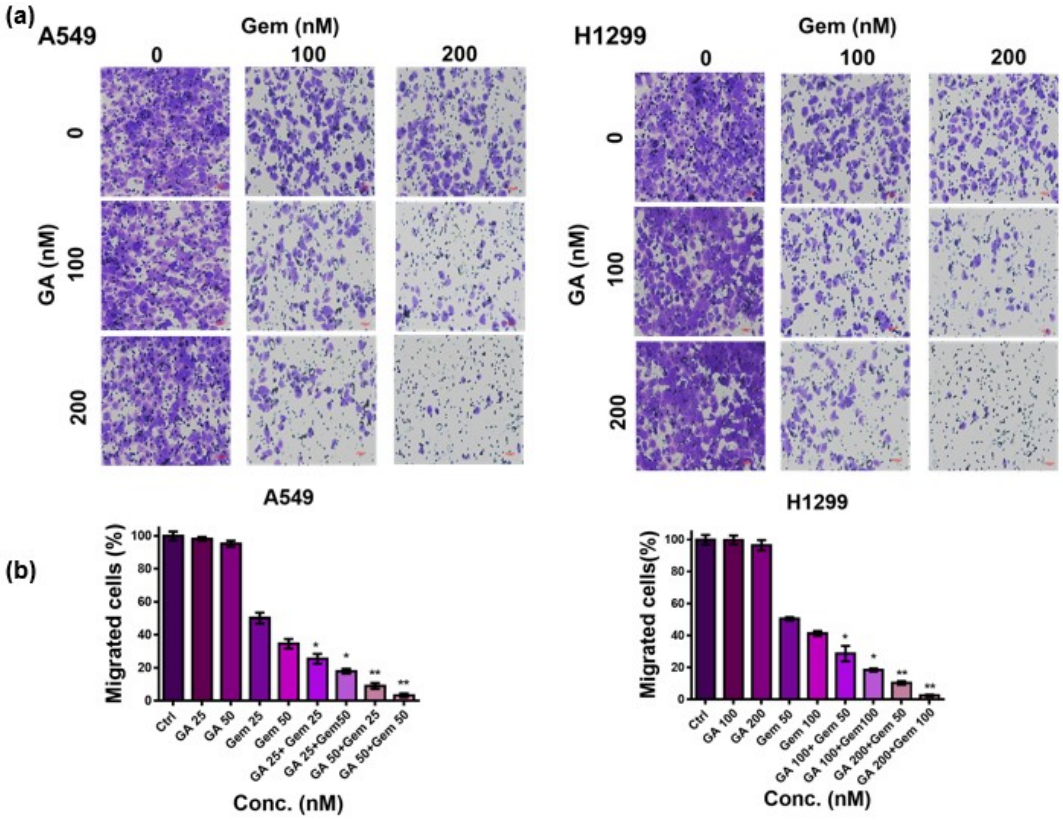

Figure 3-6. GA and Gem inhibited cell migration abilities *in vitro*.
A549 and H1299 cells were incubated with either GA and gem or in combination. Migration ability was analyzed using a Transwell assay (a) A549, H1299 migration images, (b) A graphical representation of quantitative data showing the number of migrated cells. The data were analyzed by ImageJ software. Values represent the mean ± SEM from three independent experiments; *$p < 0.05$, **$p < 0.01$.

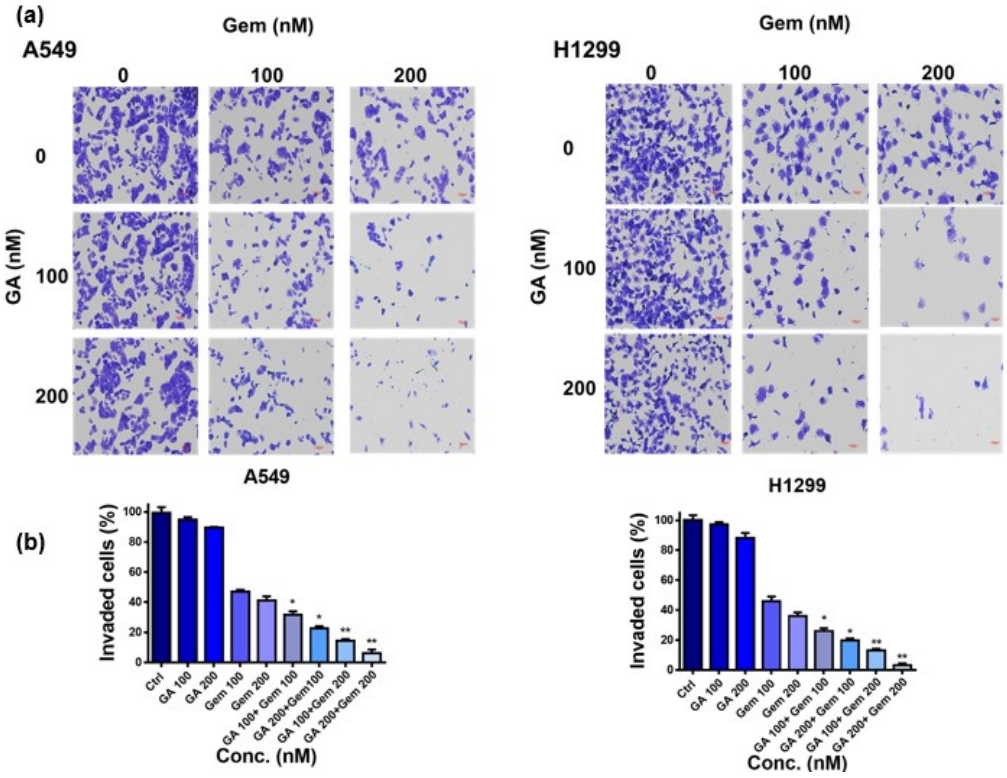

Figure 3-7. GA and Gem inhibited cell invasion and adhesion abilities *in vitro*. A549 and H1299 cells were incubated with either GA and gem or in combination. The cell invasion abilities were analyzed using a Boyden chamber assay (a) A549 and H1299 invasion images. (b) A graphical representation of quantitative data showing the number of invaded cells. The data were analyzed by ImageJ software. Values represent the mean ± SEM from three independent experiments; *$p < 0.05$, **$p < 0.01$.

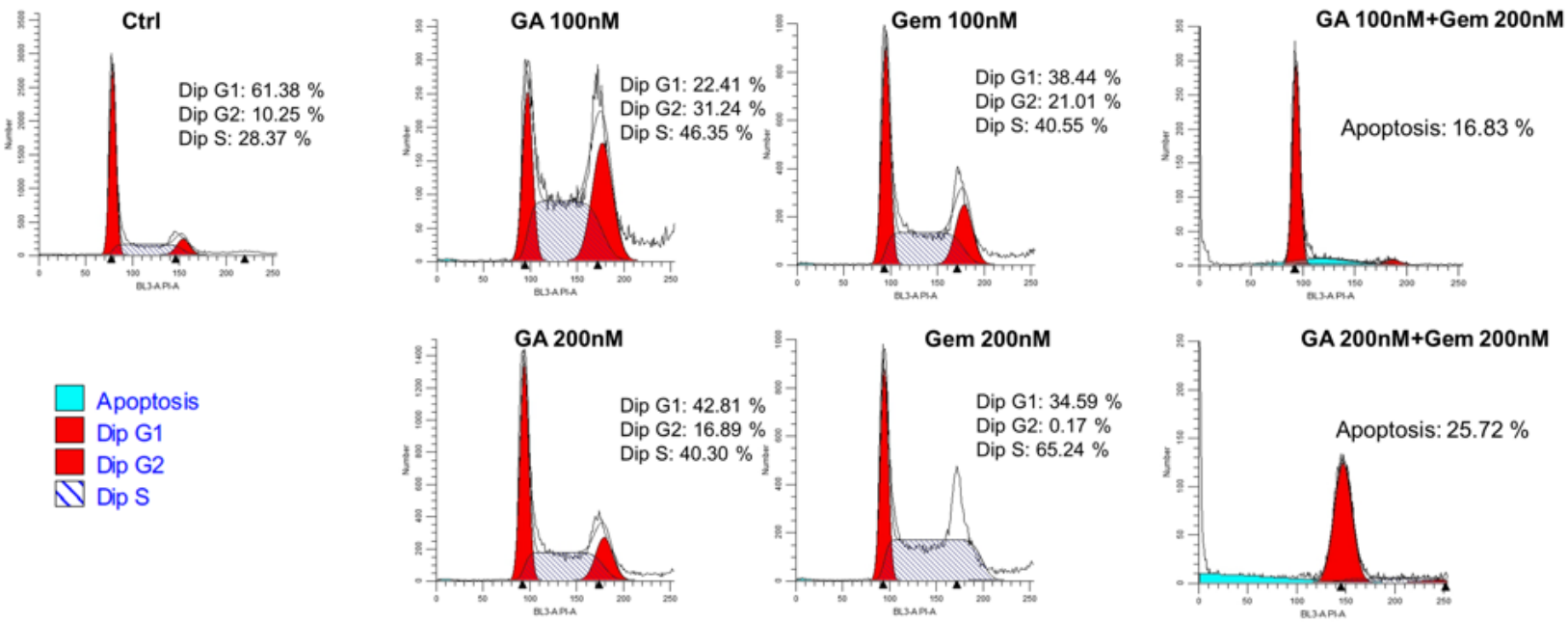

Figure 3-8. Effect of GA and Gem on cell cycle induction in NSCLC analyzed by flow cytometry.
GA and Gem combination increased the apoptosis population on A549 cells, after 24hr treatment incubation for cell cycle analysis.

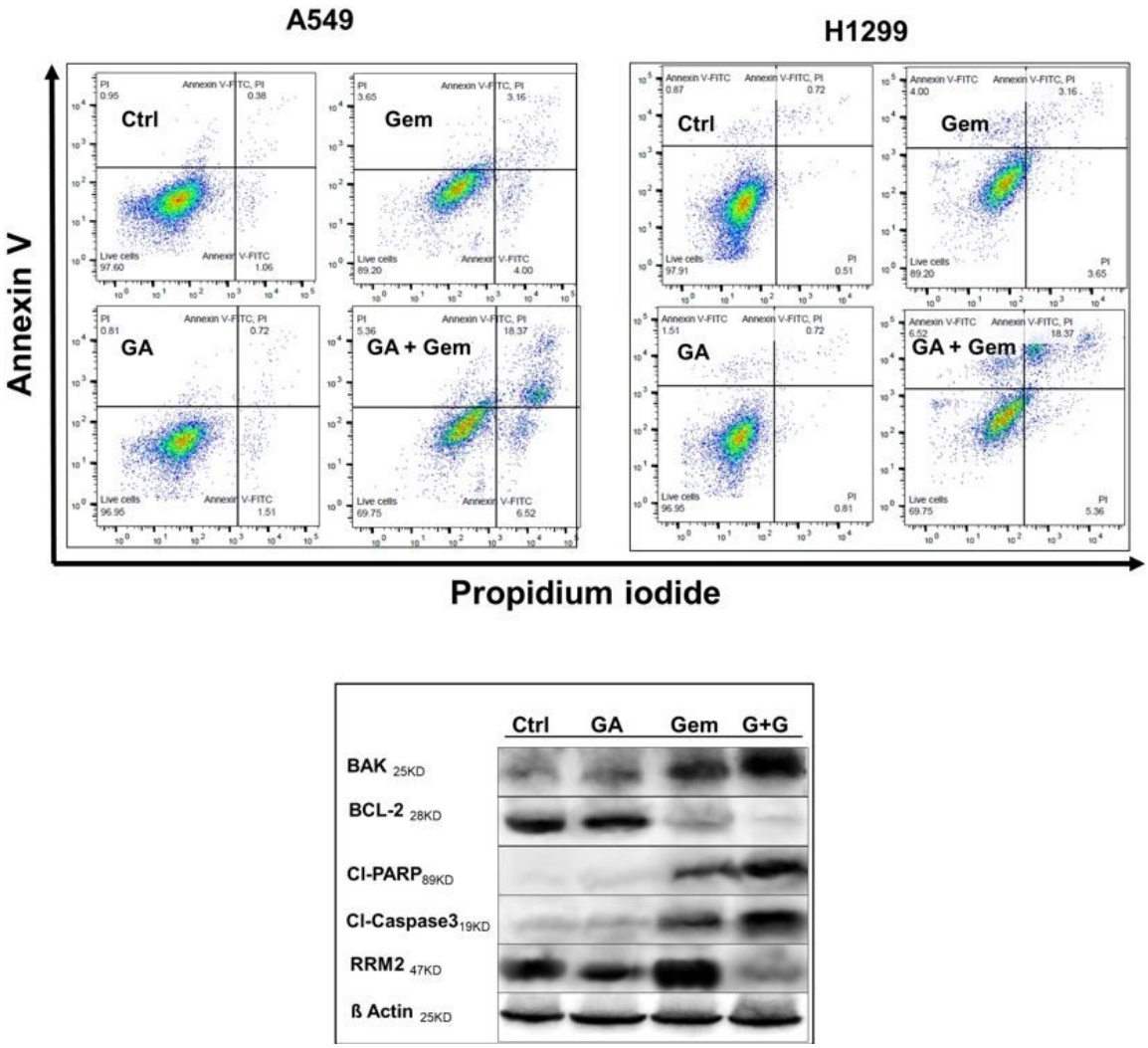

Figure 3-9. Effect of GA and Gem on apoptosis induction in NSCLC analyzed by flow cytometry and western blotting.

A549 and H1299 cells were incubated with GA and Gem and respective combination concentrations of GA+ Gem for 48h. The x-axis shows Annexin V-FITC staining and y-axis indicates Propidium iodide staining; Lower left (LL) quadrant: viable cells; lower right (LR) quadrant: early apoptotic cells; upper left (UL) quadrant: necrotic cells, upper right (UR) quadrant: late apoptotic cells. (b) Western blotting was performed on protein extractions from A549 cells treated with GA and gem and their combination, using standard protocols as previously reported. G+G= Combination of Ga and Gem, Cl-PARP= cleaved PARP and Cl- cleaved= cleaved caspase 3, β-actin was probed for as internal loading control.

effectively increased following Gem treatment and GA+GEM cotreatment. The changes in expression levels were more dramatic for the combination group suggesting that the induced levels of apoptosis were more prominent compared to single drug treatment. Next, in order to investigate the effect of these treatments on ribonucleotide reductase enzyme at the cellular level, we probed the specific RRM2 antibody on the immunoblots. Interestingly, the expression level of the RRM2 in the presence of Gem alone increases, but when combined with GA the expression of this protein is downregulated. Suggesting that GA synergistically inhibits the expression of RRM2 when combined with Gem, and therefore contributing to Gem resistance reversal. All these considered, the superior anticancer activity of GA combined with Gem can be confirmed (**Figure 3-9**).

Combination of GA and Gem Inhibit Tube Formation in HUVEC Cells

The effect of GA and Gem, either as monotherapy or in combination, was assessed for their ability to inhibit tube formation assays using a HUVEC line[209] . Suppressing the angiogenesis and causing damage to the tumor vascular network, leads to the inhibition of tumor growth by abducting e supply of oxygen and nutrients. Herein, with treatment of 200nm GA, 200nm Gem, and their respective combination (GA + Gem), total master segments length was reduced by 33%,71% and 97% ($p < 0.0001$) respectively, compared to the vehicle control (**Figure 3-10**). Combining these two compounds achieved the highest inhibition (97%) compared to single drug and the difference was statistically significant ($p < 0.0001$).

Discussion

Lung cancer in general including NSCLC has a very poor prognosis and a record of low therapeutic achievements in recent years. Hence, there is an ongoing, intensive search for better treatment approaches to minimize the development of chemo-resistance and its deleterious consequences. GA, a caged xanthone natural compound, is known for its potent anticancer properties, and to date a couple of studies have already shown the anticancer effect of GA on NSCLC [176 182 177]. However, GA's chemo-sensitization effect on Gem therapy in NSCLC has not been examined, therefore in this present study we further investigated this aspect in order to provide a potential opportunity to overcome Gem resistance limitations.

In this study, we observed an enhanced anticancer effect of GA+Gem combination on NSCLC. We demonstrated that the combination of GA and Gem resulted in synergistic growth inhibition of A549 and H1299 cells, suggesting that GA could serve as a chemo-sensitizer for Gem therapy on NSCLC, chemo-sensitization effect of GA observed in our studies concurs with findings from previous investigation with GA and other chemotherapeutic agents such as doxorubicin and 5- fluorouracil on ovarian cancer and colorectal respectively [191 183]. Many more that reported synergistic anticancer effect of GA with other chemotherapeutic agents[210 211] . Furthermore, we found that this

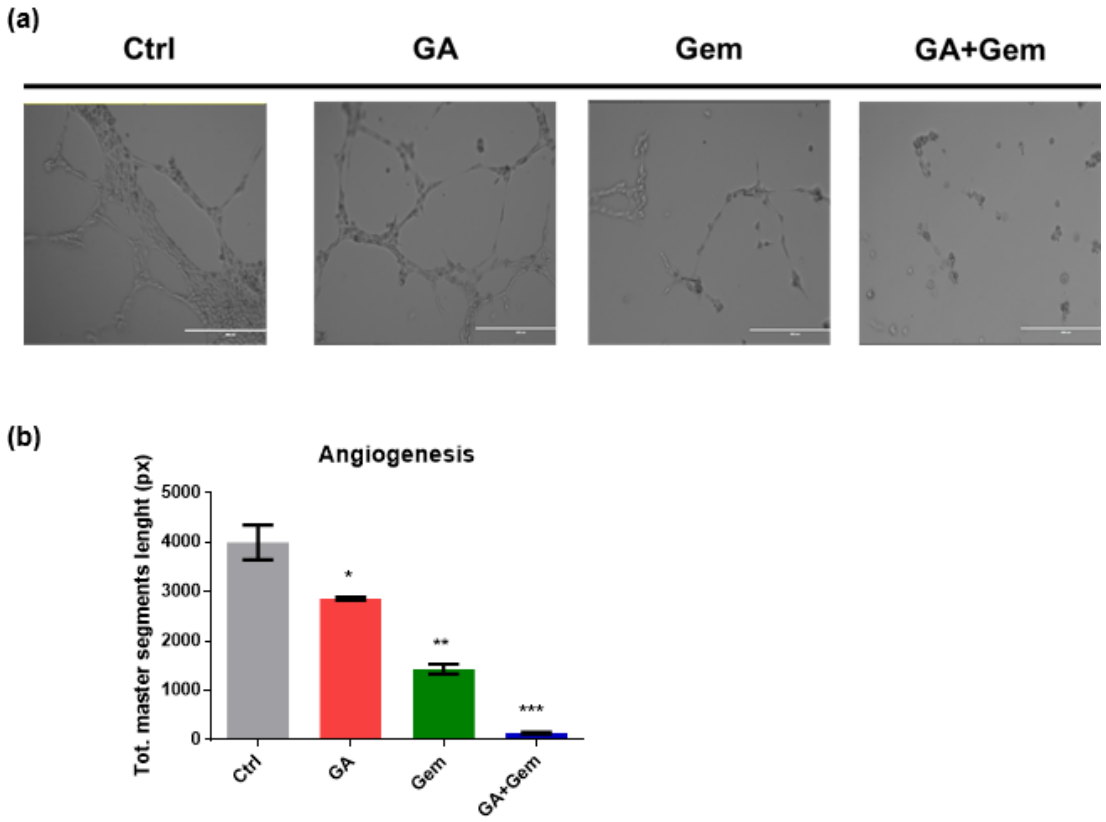

Figure 3-10. Inhibition of tube formation by GA and Gem.
HUVEC cells were treated with GA and/or Gem for 4 h and total master segments lengths were measured with ImageJ. a) Results of three replicates are shown as the mean master segments length (Unit: Pixels) compared to the control. (b) Representative images of HUVEC cell line treated and untreated(control). Magnification = 10X (scale bar = 0.5mm). Values represent the mean ± SEM from three independent experiments; **p < 0.05, ****p < 0.01.

inhibitory effect operates *via* the downregulation of ribonucleotide reductase enzyme subunit 2 (RRM2) expression, this data is also in line with the findings of Xia g et al. (2017) they reported that GA and Gem showed a synergistic therapeutic effect on pancreatic cancer[63].

Based on results from the cell viability assay, we selected the most effective concentration ratio of GA and Gem for NSCLC cells. The results of the MTT assay reveled that cotreatment of GA and Gem on A549 and H1299 significantly inhibited proliferation in a dose-dependent manner, and accordingly caused a reduction in IC50 values. This effect, validated with the Chou–Talalay method, exhibited combination indexes that were lower than 0.9 (CI<0.9) indicating that the combination of GA and Gem had a synergistic effect (**Figure 3-3**)[198]. Indeed, it is noteworthy to mention that the GA concentrations used in the present study were remarkably lower than the IC50 of GA as a single drug on both cell lines. Furthermore, we observed the similar dose-dependent inhibitory effect on the number of colonies formed, the invasion, and migration properties of both cell lines in the presence of the combination treatments .These studies provided further evidence that GA+Gem were highly effective and had a synergistic anticancer effect on NSCLC cells. Altogether, our findings on the inhibitory effect GA+Gem on cell proliferation, colony formation, invasiveness, and migration was in accordance with the GA inhibitory effect reported in various cancer studies [212] [213] [214], as well as in NSCLC[215] [177] [176] and certainly for Gem.

The main mechanism of action for Gem is inhibiting DNA synthesis[29], this process is achieved indirectly by suppressing the ribonucleotide reductase (RR) enzyme activity[216]. This enzyme converts ribonucleotide 5'-diphosphates to deoxyribonucleotide 5'-diphosphates, one of the essential steps for DNA replication[168]. It is also known that the expression level of RR is inversely related to the Gem resistance [217] [34]. Previous studies have shown that the expression of two subunits of the RR enzyme is related to the sensitivity of NSCLC to Gem [36]. Moreover, the RR enzyme is responsible for cell cycle process regulation[218] . Notably, our western blot results showed a significant decrease in the expression level of RRM2 (the catalytic subunit of the RR enzyme). Furthermore, clinical trials have shown that the poor prognosis in lung cancer correlates with high expression levels of the subunits of RR [39] . We can suggest that this synergistical effect cause intrinsic differences in molecular mechanism and leads to apoptosis induction and reverse the multi drug resistance.

It is well documented that a common mechanism for chemoresistance is the overexpression of ATP-binding cassette (ABC) efflux transporters in cancer cells such as the P-glycoprotein efflux transporters (P-gp/ABCBl) [203]. Notably, previous studies showed the dependency of reducing P-glycoprotein transport expression (i.e., decreased expression of the P-gp transporters) for reversing the Gem resistance in cholangiocarcinoma [133]. In addition, Gem resistance is usually reported to be a consequence of the reduction in drug concentration within the cells due to either drug efflux or decrease in drug influx.[130] [129] [167] As shown, the free GA could not demonstrate cytotoxicity with our tested concentration (highest 400μM) but when combined with Gem shows elevated level of cytotoxicity compare to native GA and Gem. This lower

cytotoxicity of the Gem could be related to the MDR effect, the free drug efflux through P-glycoprotein transporter available on the cell membrane which results to the decline in the intracellular concentration of the drugs, our RH123 assay result (**Figure 3-5)**. Our results on GA sensitization on cancer cell lines *via* inhibition of P-gp and MDR1 are in accordance with findings of previous investigation conducted by Wang H et al. (2015) which showed that GA increases the accumulation of doxorubicin through reversing MDR and suppressing P-gp efflux activity[70].

Furthermore, the ability to stimulate apoptosis in different cancer cells was proposed as one of the fundamental mechanisms for the anticancer properties of GA. Cell cycle analysis revealed that the G2 cell population increased in response to an increase in the dose of GA in H1299 cells. Impressively, these findings were consistent with the previous finding that agents modulating and promoting G2 phase arrest strengthen the cytotoxicity effect of agents that influence the DNA directly, [219] while as expected Gem induces S phase arrest and acts on DNA (the main mechanism by which Gem causes cell death is *via* apoptosis). Not surprisingly, co-treatment of Gem with GA increases the apoptotic cell population to a greater extent than single-agent treatment.

Thus, our results suggest that combined treatment of GA and Gem inhibited the growth and proliferation of NSCLC cells by inducing apoptosis *via* promoting cell cycle arrest. This data strengthens our hypothesis, and further proves the importance of cell-cycle arrest to Gem cytotoxicity. The extent of apoptosis was determined by Annexin-V/propidium iodide staining to identify and quantify the population of the cells undergoing apoptosis. Upon exposure of cells with cotreatments of GA+Gem, an increase in the apoptotic population was observed in A549 and H1299 cell lines, demonstrating that GA can induce cell death *via* inducing apoptosis for cells treated with Gem. This result explains the ability of GA when combined with Gem to increase the apoptotic population.

We were able to show that elevated levels of apoptosis in cells subjected to simultaneous treatment with both drugs was associated with downregulation of an antiapoptotic protein, B-cell lymphoma 2 (Bcl-2), with concomitant upregulation of pro-apoptotic proteins such as Bax, cleaved PARP and cleaved caspase-3 (known key markers for apoptosis regulation). Similar, previous study done on GA a potent apoptotic inducer, demonstrated downregulation of Bcl-2 and Bax expression on platinum resistance NSCLC[220].

These results provide further validation for synergetic effect of GA and Gem when compared to Gem treatment alone as shown in previous findings.[207] However, further studies are needed to determine regulatory proteins and markers involved in modulation of this combination of cell cycle arrest and apoptosis population at a molecular level.

The tube formation study on endothelial HUVEC cells revealed that GA and Gem combination showed an elevated inhibitory effect on tube formation (**Figure 3-10**) similar angiogenesis inhibition effect was reported previously by Wen L et al.(2014)[221].

Hence, future investigation necessary to explore the effect of this drug combination on the regulation of angiogenesis, and formation of blood vessels which counts as a critical step in tumor growth. Overall our result demonstrated a superior effect of Gem treatment on NSCLC due to GA sensitization effects.

Conclusion

This study demonstrated that GA increases the antitumor effect of Gem in NSCLC *in vitro*, and that the combination of these two drugs could effectively inhibit NSCLC growth and induce apoptosis. Moreover, our study demonstrated that GA could suppress the expression of RRM2. Overall, these data suggest the potential effectiveness of combination treatment with GA and Gem in patients with NSCLC. However, in order to validate this effect, further *in vivo* studies followed by controlled clinical trials are mandatory.

CHAPTER 4. SELF-ASSEMBLED HUMAN SERUM ALBUMIN-TANNIC ACID NANOPARTICLES FOR COMBINATION THERAPY IN NON-SMALL CELL LUNG CANCER

Introduction

Lung cancer is a predominant cause of morbidity and mortality across the world. Moreover, among all types of cancers, lung cancer is the leading cause of cancer mortalities[11]. Non-small cell lung cancer is one of the dominant division of lung cancer that solely represents 85-90% of all lung cancer cases [2 89]. Up to the present time, primary treatment regimens for cancer include radiation therapy, chemotherapy and surgery, with chemotherapy being the best option thus far. Despite the eminent benefits of chemotherapy, its value is offset by severe side effects such as renal and/or hepatic toxicity or insufficient amounts of drug available at the target site. Such pitfalls can be handled by employing a target-specific, biodegradable and biocompatible drug delivery carrier. In present study, we propose a human serum albumin (HSA)-based nanoplatform for dual loading drug delivery. Produced by the liver, HSA is the most abundant protein in the human body, with a molecular weight of 66.5 kDa and a half-life of approximately 20 days.

The X-ray analysis shows that HSA consists of three domains (I, II and III), and each domain has two subunits (a and b) that are considered the binding sites of the HSA molecule[121]. In general, HSA is a vehicle for various substrates such as hormones, bile acids, amino acids, metals and toxic metabolites. In recent decades, scientists have taken advantage of this extraordinary feature by using this protein as a biodegradable and biocompatible carrier to load therapeutic agents. HSA not only delivers drugs to their target, but also preserves bound drugs from oxidation[138]. In addition, a biodegradable carrier such as HSA can effectively influence the pharmacokinetic and pharmacodynamic properties of anticancer agents. Furthermore, it can also modify the *in vivo* distribution to be more advantageous. Due to hydrophobic pockets and hydrophilic regions in the molecule, HSA can bind to both categories of drugs with different physical properties[85]. Nanoparticles designed using an HSA basis are more favorable due to beneficial features such as biocompatibility, biodegradability and non-immunogenicity. In addition, passive targeting with HSA can also be considered somewhat facilitated targeting due to the presence of the glycoprotein60 (gp60) receptor on cancer cells, which is an HSA- specific receptor[138]. Abraxane® is an HSA-loaded Paclitaxel (Pxtl) nanoformulation that has successfully been utilized to treat a number of cancers in recent years[222]. With this approach, the chemotherapeutic capacity of paclitaxel—commercially available as Taxol— reached another level, as this nanoformulation efficiently lowered the toxic effects of Pxtl and its off-target side effects.

Nano-drug delivery systems have been employed to conquer the disadvantages of conventional drugs. The rationale of using nanoparticles is based on their ability to accumulate at the tumor site *via* the Enhanced Permeation and Retention (EPR) effect[83]. Additionally, nanoparticles prolong circulation time and improve toxicity and tolerability

issues. We selected HSA as a nanoparticle matrix because albumin is commonly used for both lipophilic and hydrophobic drug delivery. Therefore, we developed simple, multifunctional nanoparticles (NPs) using a human serum albumin nanoplatform base and tannic acid as a low-toxicity stabilizer, for targeted drug delivery in the treatment of NSCLC[223-224]. In our previous studies, we have shown that tannic acid has a very good binding affinity to lung fluid, making it a suitable excipient for adding stability to our HSA nanoparticle[196]. Our human serum albumin-tannic acid (HTA)-based nanoparticle is a biocompatible nanocarrier that has a dual loading capacity for both lipophilic and hydrophobic drug delivery.

We previously revealed that Gambogic acid (GA) and Gemcitabine (Gem) combination therapy has a synergistic anticancer effect on NSCLC. Gem is a unique nucleoside analog with a mild safety profile that mimics deoxycytidine and interferes with DNA synthesis. Although Gem is water soluble agent, GA is a hydrophobic compound. Administration of hydrophobic drugs with their organic solvents promotes *in vivo* toxicity, thereby limiting clinical use. Therefore, there is an emerging interest in encapsulating GA in nano carriers[225]. Utilizing HSA, hydrophobicity can become an advantageous characteristic, as hydrophobic drugs can induce the self-assembly of HSA proteins when mixed[136]. Furthermore, loading a chemotherapeutic agent, e.g. Gem, on a nanocarrier, promotes sufficient drug delivery to the tumor environment and lowers undesired effects[226].

Using HSA as a platform for NDDS has been used widely in cancer therapy[227 121]. Generally, there are three different process for the development and preparation of HSA NPs: 1) emulsion formation, 2) solvent evaporation method), and 3) coacervation method. The limitation of the emulation method due to adding organic solvent can be overcome by solvent evaporation method evolved from microencapsulation by the coacervation process[228]. Where particles are usually formed by drowse addition of the acetone into the aqueous solution of HSA. This process can be further improved and lead to the production of more stable NPs with adding a crosslinker [229 228].

Moreover, tannic acid is a hydrolysable polyphenol. This natural compound is abundant in various plants such as fruits and tea leaves. Recently, TA gained attention as a pharmaceutical excipient. This unique, safe molecule is not only able to increase the water solubility of hydrophobic drugs but can also improve the stability of self-assemblies by forming hydrophobic interactions with hydrophobic molecules[230 80]. Further, TA acts as a crosslinker due to the presence of hydroxyl groups that act as hydrogen bond donors[231 201].

Therefore, in this study, we designed biodegradable and biocompatible human serum albumin-tannic acid (HTA)-based nanoparticles loaded with a combined dosage of GA and Gem (G-G@HTA). We further investigated the efficient internalization of these NPs into cancer cells and determined the synergistic effect of Gem and GA on NSCLC using *in vitro* and *in vivo* studies, with the purpose of establishing a strong and predictable platform for use in clinical settings.

Methods

Cancer Cell Lines and Animals

Non- small cell lung cancer cell lines, A549 (a carcinoma cell line derived from 58-year-old male Caucasian, #ATCC® CCL-185™) and H1299 (carcinoma non-small cell LC cell line derived at the metastatic lymph node from 43-year-old adult, #ATCC® CRL-5803™), were purchased from ATCC (American Type Cell Culture) and cultured using Dulbecco's Modified Eagle Medium (DMEM)-F12/ Roswell Park Memorial Institute medium (RPMI-1640, which was supplemented with 10% FBS and 1% antibiotic/antimycotic (Gibco, Thermo Fisher Scientific, Grand Island, NY, USA) solution at 37 °C in a humidified atmosphere (5% CO2 - 95% air atmosphere)). A new frozen stock prepared from original stock was used every six to seven months, to maintain the cell lines' morphology and validity for experimentation. Animal experiments were carried out using 6 to 8-week-old male athymic nude/nude mice purchased from Jackson Laboratories for antitumor efficacy studies. All procedures were in accordance with approved protocols from the University of Tennessee Health Science Center Institutional Animal Care and Use Committee.

Chemicals, Reagents, and Antibodies

The chemicals and reagents for experimentation purposes were purchased from Sigma Aldrich and Fisher Scientific, unless otherwise stated. Cell culture consumables were purchased from Gibco, Thermo Fisher Scientific. Monoclonal antibodies were purchased from Abcam or Fisher Scientific. For all cell culture studies, cell lines were subjected to trypsin and monodispersed into appropriate plates according to the assay and allowed to adhere overnight and reach 70-80% confluency before initialization of treatments.

Preparation of Dual Loaded HSA Self-Assembly Nanoparticle (G-G@HTA)

The self-assembly formation was conducted using the solvent evaporation technique[232 233]. Briefly, to the 500µl of human serum albumin (HSA) dissolved in an aqueous medium (1mg/ml in Milli q filtered water),700µl of Tannic acid (1mg/ml in Milli q filtered water) was added, formulation was in 8mL glass vial with continuous stirring at 500 rpm on a stir plate (Benchmark stirrer, ABC Scientific, Glendale, CA, USA) . Next, the concentration of the solution was adjusted to 1mg/ml. Then the drug loading process occurred in two steps. Firstly, 100µL of Gem (1 mg/mL) dissolved in water was added slowly (dropwise) to the described solution and left stirring for 30-45 min. After the solution thoroughly mixed, 100µL of GA dissolved in acetone (1 mg/mL) was again added slowly (dropwise) to this solution and the speed increased to 900 rpm. The resulting solution stirred overnight to evaporate the acetone, allowing the formation of dual-loaded self-assembled nanoparticles composed of assembled HSA/TA loaded

with GA and Gem, referred to as a GA and Gem-loaded human serum albumin-tannic acid (G-G@HTA) self-assemblies. The solution was centrifuged at 1000 rpm for 5 min to eliminate any unbonded and aggregated clumps. The developed G-G@HTA solution was kept in 4˚C and used within a week. For all *in vitro* cell culture experiments, a freshly made stock of G-G@HTA was used in order to protect GA and Gem activity in the formulations.

Particle Size and Zeta Potential

The particle size of G-G@HTA nanoparticles was measured through the dynamic light scattering (DLS) analyzer using the Zetasizer (Nano ZS, Malvern Instruments, Malvern, UK)[223]. For this purpose, 20µl of developed nanoparticles was thoroughly dispersed in 1ml of filtered Milli q water and subjected to quick probe sonication (VirSonic Ultrasonic Cell Disrupter 100, VirTis) for 30 s in order to destroy any aggregates formed and produce a homogeneous solution of nanoparticles[234]. Particle size measurements were conducted for 3min at 25˚C, unless otherwise mentioned. The experiments were performed in triplicates.

The average zeta potential was determined using 20µl of the described solutions in 1× phosphate-buffered saline (PBS) solution, using the Zetasizer for 30 runs in each reading, and data is presented as an average of three readings.

Size and Zeta Potential Stability Testing

The GA and Gem-encapsulated HTA nanoparticles were subjected to storage in refrigerated (4 ˚C) conditions over 14 days. Every 3 days, these dual-loaded nanoparticles were analyzed for particle size and zeta potential and were compared against 0-time point samples.

Particle Morphology by Transmission Electron Microscope (TEM)

To analyze size and morphology, G-G@HTAs were examined by JEOL 200EX transmission electron microscopy (TEM, JEOL Ltd, Tokyo, Japan) operating at the voltage of 80 kV, and the grids were prepared by placing a drop of a probe sonicated (30 sec) G-G@HTA solution on the shiny side of 150 mesh TEM grid (Electron Microscopy Sciences, PA, USA), followed by a two time phosphate-buffered saline (PBS) wash, and left for drying[235 85]. Afterward, grids were stained using a 2% (w/v) uranyl acetate solution. Different regions of these grids were imaged with the above mentioned TEM system using an AMT camera[203 230] (Magnification =100 000X).

Fourier Transform Infrared Spectroscopy (FTIR) Analysis

Formation of G-G@HTA nanoparticles was confirmed by FTIR analysis. The actual lyophilized samples of G-G@HTA with their respective individual compositions (TA, HSA, GA and Gem) were prepared and placed on ATR sampling Accessory plate and recorded using the Spectrum 100 FTIR spectrophotometer (Perkin Elmer, Waltham, MA) instrument. Relevant spectra were obtained between 4000 and 650 cm−1[80 236 230].

Fluorescence Quenching

For further validation of G-G@HTA nanoparticle formation, the fluorescence binding assay was performed on the SpectraMax Plus plate reader (Molecular Devices, Sunnyvale, CA, USA). In order to achieve that objective, the spectra were documented in the wavelength range of 250 ~ 400nm upon excitation at 295nm, using 5nm/2nm slit widths, and each spectrum was the average of three scans[236,237] . The stock solution of 100 mg of HSA solution in 1ml of PBS was titrated *via* successive addition of the stock solution of TA (1mg/ml Water) in a quartz cuvette, to give final concentrations in the range 0 ~ 100µg TA in the whole solution[196].

Cellular Uptake Assay

Cumarin6 (C6)-loaded G-G@HTA NPs were developed following the previously described procedure[80 196] to assess the HTA NPs delivery capability. To investigate the enhanced uptake of drugs in NSCLC cells, A549 and H1299 cells (0.5×10^6 cells/well) were cultured in a six-well plate in their respective fresh media, left for overnight adhesion to the plate surfaces, and incubated in a CO_2 incubator at 37 °C. The next day, the cells were treated with 2.5, 5 and 10µg of C6-labeled G-G@HTA, for 3 h for the dose dependency study. Cells were treated with 5µg of C6-labeled G-G@HTA for 1,3 and 6 h for the time dependency study [203 238]. The cells were washed thrice with PBS to wash out any superficially bound formulation or dye. After their respective incubation duration, the media was changed to fresh phenol red-free media, and cells were analyzed for internalization using the NovoCyte FACS machine (ACEA NovoCyte 1000, ACEA Biosciences, Inc. San Diego, Ca, USA) in a FITC channel (fluorescence measurements at λex: 485nm and λem: 520nm). The mean fluorescence intensity (MFI) was documented from three independent measurements. For visualization support, cells were subjected to EVOS 214 FL Imaging System in a GFP channel (AMF4300, Life Technologies, Carlsbad, CA, USA)[203 239].

Cell Viability Assay

A549 and H1299 Cells were seeded into 96-well plates at 0.5×10^4 cells/well, 48h after the indicated treatments ((0.01-0.2nM of GA, 0.01-0.2nM of Gem, and equivalent concentration of Ga+ Gem, G-G@HTA, and HTA NP), and cell viability was

determined using the MTT reagent (Promega, Madison, WI, USA). Absorbance was measured at 570nm after 2-4 h incubation with the MTT reagent, using a Microplate Reader (BioTeK Cytation 3, Winooski, VT, USA)[195]. Each treatment concentration was studied in triplicate. Viability of the treated cells was examined with respect to the untreated cells (control). In addition, the cell morphology upon incubation with treatment and without treatment was imaged using EVOS® FL Imaging System at 20X magnification[176 179].

Colony Formation Assay

Using 12-well plates, approximately 300-400 cells were seeded per well. After overnight incubation to allow cells to adhere to plate surfaces, cells were subjected to incubation with the indicated treatments (25nM Ga+25nM Gem and equivalent concentration of G-G@HTA and HTA NP). After 14 days of culture, cells were washed with PBS, fixed with cold methanol and stained with 0.5% crystal violet. Representative images from each well were used for counting the number of colonies formed, and the mean of three independent treated wells was reported[236].

Migration Assay

To examine the ability of the treated cells to migrate, A549 and H1299 cells were seeded into the upper chamber of a 24-well transwell insert (8-μm pores, BD Biosciences, San Jose, CA) after 24h starvation in FBS free media. 5×10^4 cells were seeded per well, with FBS free medium plus the indicated treatments (50nM Ga+50nM Gem and equivalent concentration of G-G@HTA and HTA NP)[76]. The respective complete medium was added into the lower chamber and incubated for 18 h. After end of the time point, any cells that migrated through the pores from the bottom of the upper chamber's membrane to the lower surface of the chamber, were fixed with cold 4% paraformaldehyde for 30 min and stained with 0.1% crystal violet. The remaining cells on the surface of the upper chamber were gently wiped off with a cotton swab. Three randomly selected regions on each well were imaged using a Keyence microscope BZ-X800(Itasca, IL, USA), and the number of cells in each field was counted with help of ImageJ software[240].

Invasion Assay

To test the NSCLC cells' ability to invade, cells were subjected to 24h starvation, and an invasion assay was performed using BioCoat Matrigel Invasion Chambers (BD Biosciences, Bedford, MA, USA). The upper chambers of the trans-well plate were pre-coated with Matrigel and seeded with 3.5×10^4 A549 and H1299 cells per well, using serum-free media. The same media was placed in the lower chambers. After 24h incubation to allow cells to adhere to the plate surface, the media was replaced with fresh FBS-free media, containing the indicated treatment concentration. Cells without

treatment served as the control group. After 24h, any NSCLC cells that invaded the lower chamber were fixed with cold 4% paraformaldehyde, stained with crystal violet and subjected to imaging with the Keyence microscope[241 201]. This experiment was repeated three times, and quantification was performed using ImageJ software.

Xenograft Tumor Model

Six-week-old male athymic nude (nu/nu) mice, purchased from Jackson laboratory, were housed and maintained in a pathogen-free environment for two weeks before the study began. Each mouse was injected subcutaneously into the right flank with 1×10^7 A549 cells suspended in 100µl PBS, containing 1% (v/v) Matrigel. Once the average tumor volume reached 100mm^3, mice were randomly divided into four treatment groups, including a PBS only control group (n=4): nanoparticle control (HTA only), GA (2 mg kg^{-1}), Gem (20 mg kg^{-1}) and a combination equivalent (GA +Gem). Respective dual-loaded nanoparticles (G+G@HTA) were administered biweekly *via* the intraperitoneal route, for four subsequent weeks. Mouse weights and tumor growth rates were monitored twice, and overall health was simultaneously observed closely. Tumor volume (V) was estimated by measuring the length (L), width (W), and height (H) of the tumor, using this formula: V =0.5236 (L x W x H). Four weeks after the first drug injection, mice were euthanized, and tumor burden (wet weight) and metastases were measured. Pictures were taken for visual representation, and organs, blood and tumors were excised and stored at -80 ˚C until further analysis[242 175]. For this study, animal care and handling were performed in accordance with institutional guidelines, and all animal experiments were done using protocols approved by the Institutional Animal Care and Use Committee (IACUC).

Blood Analysis

At the end of the treatment, mice were sacrificed with CO2 exposure and cervical dislocation. Blood samples were collected (cardiac stick post-euthanasia) from each mouse, and serum samples were isolated for further clinical chemistry. To test Kidney and hepatic function in treated groups compared to the control (no treatment) group, Aspartate aminotransferase (AST), Alanine aminotransferase (ALT), Alkaline phosphatase (ALP), Total protein (TP), Total bilirubin (TBili), Albumin (Alb), Creatinine (create), Blood urea nitrogen (BUN), Glucose (Glu) were measured from serum samples utilizing a DiaSys Response 910 Vet Chemistry Analyzer (DiaSys Diagnostic Systems, USA, LLC, Wixom, MI)[243 231].

Immunohistochemistry and Histopathologic Examination

Immunohistochemical studies (IHC) of tumor tissue slides were investigated by probing with apoptotic, antiapoptotic and regulatory proteins and their respective antibodies. Immunohistochemical analyses were conducted following a previously

developed protocol in our lab[205]. Briefly, slides were dewaxed at 65 °C for 30 min followed by two 10 min washes with xylene and then rehydrated with different concentrations of ethanol, including 100%, 90%, 70%, 60%, 50%, in sequence and finally with distilled water for 5 min each. Next, the slides were put into triton x-100 and were kept for 5 min. Then, the endogenous peroxidase activity was inhibited by hydrogen peroxide for 5min, following incubation with antigen retrieval to unmasked epitopes for 45min. After blocking with background sniper (BioCare Medical, CA, USA) for 30 min, the slides were incubated with Bcl2 (1:1200 dilution), Bak (1:400 dilution), MDR1 (1:800 dilution), and RRM2(1:100 dilution) overnight at 4 °C. The sections were then incubated for 1 h with a respective secondary antibody. After hematoxylin counterstain and dehydration, the sections were sealed with cover slips. The images were taken by using Keyence microscope. In addition, the major organs (heart, liver, spleen, lung, and kidney) which were harvested at the end of the study were kept in 10% neutral formalin. Formalin-fixed tissues were sectioned and further stained with H& E and observed under an optical microscope[244 245].

In Vivo and *ex Vivo* Tumor Targeting HTA NP Imaging

To conduct an investigation on biodistribution and the tumor targeting ability of HTAs, *in vivo* imaging was employed on mice bearing an A549 xenograft tumor. For the purpose of this study, mice were on special Teklad Global Rodent Diets (Envigo, Huntingdon, United Kingdom) to prevent and halt any possible background fluorescence as a consequence of a normal diet. Once the tumor volume reached ~300-500mm^3, mice were randomly segregated to two individual groups (3 mice/group). A one-time the intraperitoneal (IP) injection of free-Indocyanine green (ICG) dye (100µg/mice in 100µL PBS) was used for the control group. The second group was injected with ICG-tagged HTA (100µg ICG-equivalent HTAs/mice in 100µL PBS,) *via* IP route. For preparation, the same encapsulating method of the C6-HTA was followed according to previously developed, where C6 was substituted with ICG. Briefly, 100µl of freshly made HTA stock solution and ICG solution (1 mg/ml in water) were thoroughly mixed and incubated at room temperature, while stirring for 20 min. In each mouse, distribution and tumor accumulation of ICG dye and ICG-tagged HTA were monitored at different time points (3, 6, 24, 48, and 72h) using an IVIS XRMS Imaging System (Caliper Life Sciences, Waltham, MA) armed with a coupled device camera (CCD) at Ex: 785nm, Em: 820nm. After 72h, mice were sacrificed. Tumors and major organs, e.g. heart, lung, liver, kidney, and spleen, were collected for ex vivo imaging[246 247].

Statistical Analysis

All acquired data were analyzed *via* Graph pad Prism 5.03 Software (GraphPad Software, San Diego, CA), and results were displayed as a mean of three individual readings ± standard error of mean (SEM). All statistical analysis was performed using student's t test. A p value ≤ 0.05 was considered statistically significant.

Results

Size and Morphology Characterization

The common solvent evaporation method was followed for the preparation of HTA self-assemblies demonstrating reproducible and scalable results. Tannic acid was added to the self-assemblies as a stabilizer due to TA's ability to form hydrogen bonds and/or crosslink with HSA, which occurs due to noncovalent interactions (π–π stacking), making a firm and secure network in the solution. Moreover, the presence of TA promotes a stable matrix that allows GA and Gem molecules to be encapsulated efficiently.

As measured by DLS in water, the average particle size of G-G@HTA NPs was 205.4±7.6nm, the average zeta potential was -22±3.12 mV, and the polydispersity index was 0.22±0.009 (**Figure 4-1a**). Measurements illustrate that the developed nanoparticles were evenly dispersed, with minor size alterations. The G-G@HTA NPs average size is in the approved size range of nanoparticles for preclinical and clinical studies of cancer therapy[78]. Furthermore, it is well-documented that nanoparticles with zeta potential (surface charge) values between +30 mV to -30mV typically have high degrees of stability[248]. It is noteworthy that a negative charge is favorable for greater cellular uptake and lower systemic toxicity[76 135](**Figure 4-1b**).

Transmission electron microscopy (TEM) images provided additional evidence that the G-G@HTA nanoparticles have a uniform, spherical shape and confirm their average size of ~ 185nm (**Figure 4-1d**)). This size reduction is excepted, as the dehydrated form of the nanoparticle has a smaller size versus the hydrated form measured by the DLS machine.

Moreover, based on our stability test over 14 days, the size and zeta potential had a narrow variation range (164.167±21.1 to 209.667±30.74nm and -18.9±0.77 to -21.77 ±0.98 mV), demonstrating a stable size (**Figure 4-1e**) and zeta potential of G-G@HTA NPs over time, (**Figure 4-1f**)[206].

Fourier Transform Infrared Spectroscopy (FTIR)

To confirm the presence of each individual component of G-G@HTA NPs (HSA, TA, GA and Gem), the molecular composition was examined by FTIR spectroscopy with demonstrating the characteristic peaks of TA, GA, Gem, HSA(**Figure 4-2a**). Peaks at ~1700 c cm^{-1}, ~1603 cm^{-1}, and ~1198 cm^{-1} are associated with the characteristic peaks of CO stretching, aromatic CC stretching, and phenolic CO stretching, respectively, that are present in TA. Spectroscopy shows that these characteristic peaks are also present in HTA NPs and the G-G loaded HTA NPs. Furthermore, characteristic vibrational peaks of Gem include ~2920, ~2850 cm^{-1} (CH2 stretching) ~1689 cm^{-1} (C=O stretching) and ~1053 cm^{-1} (C-O stretching).in addition the characteristic peak of GA (=-C-H stretching)

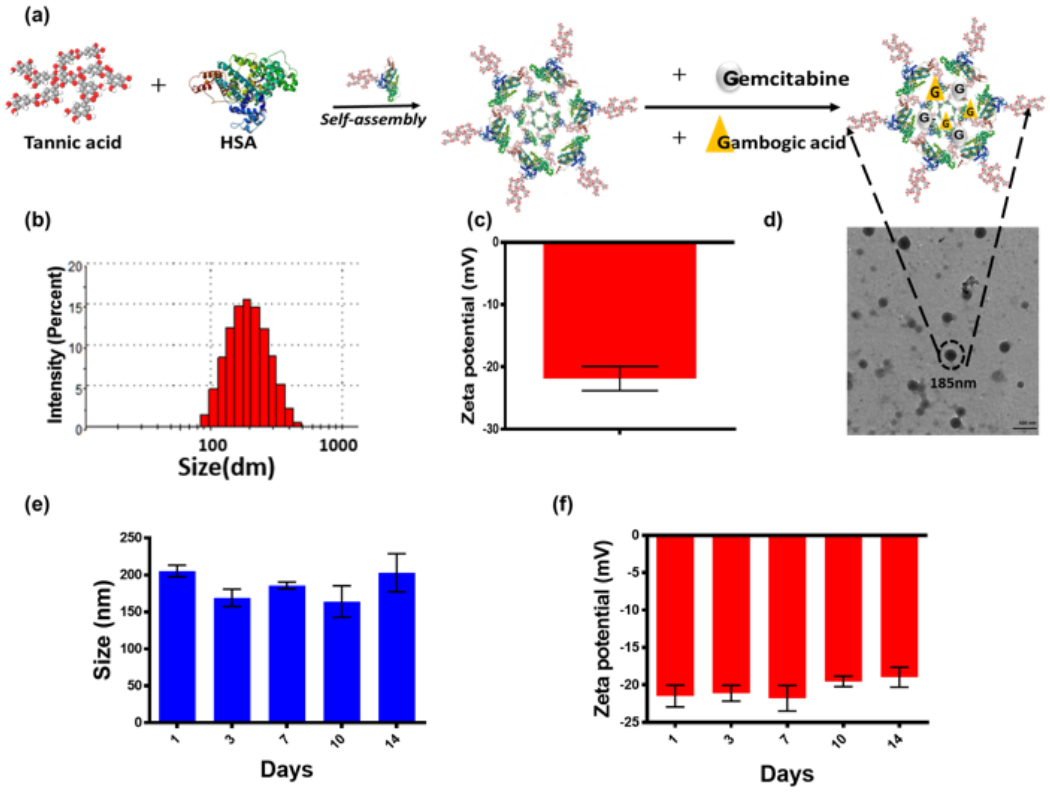

Figure 4-1. Characterization studies of G-G@HTA NPs.
(a)Schematic representation of G-G@HTA NPs preparation. (b) Size distribution, (c) Zeta potential, (d) Transmission electron microscopy TE. (e-f) Stability testing over time. (e) Size distribution and (f) zeta potential., (g) Fourier transform infrared spectroscopy (FTIR), (h) Fluorescence quenching. MFI=Mean fluorescence intensity.

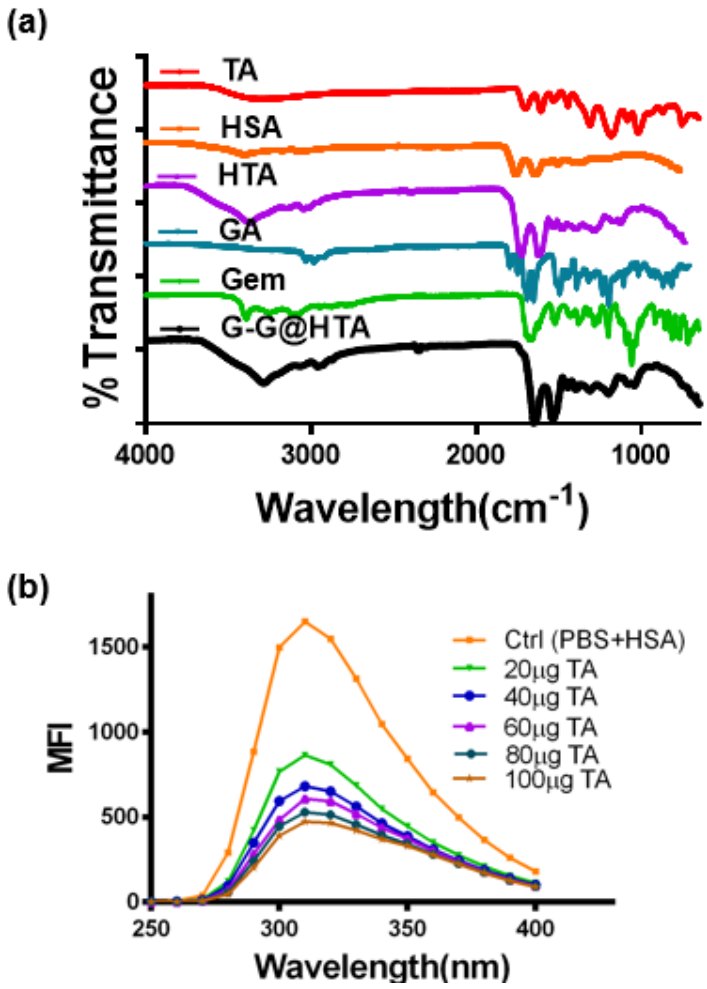

Figure 4-2. Spectral and biological confirmation of G-G@HTA NPs formation. (a) Fourier transform infrared spectroscopy (FTIR) demonstrate the characteristic peaks of excipients, representing the presence of all molecules in final formulation. (b) and fluorescence quenching of HSA and TA exhibits the instant binding of TA to HSA as measured by reduction of fluorescence intensity. MFI=Mean fluorescence intensity.

appears to be around 3280 Regarding HSA, alterations in the secondary structure of its two main amides were investigated by observing amide I and amide II bands. Amide I showed a characteristic peak at ~1652 cm^{-1} (N-H stretching) in native HSA that shifted slightly to ~1646 cm^{-1} in HTA and to ~ 1643 cm^{-1} in G-G@HTA, which is assigned to the absorption of an α-helix peak. Similarly, the amide II band moved to ~1534cm^{-1} in HTA and to ~1537cm^{-1} in G-G@HTA, compared to ~1527cm^{-1} in native HSA. Amide I band intensity corresponds to α-helix related C = O vibrational stretching, while amide II corresponds to N-H and C-N stretching. While other peaks in HTA and G-G@HTA coincide with characteristic peaks of GA, Gem and TA. This is a clear indication of successful development of HTA NPs and loading of Gem and GA on G-G@HTA nanoparticles.

Binding Affinity of Tannic Acid to Human Serum Albumin

A fluorescence quenching assay was employed to study the affinity of TA to HSA, two components of the HTA NPs. The degree of binding affinity was determined by the ability of TA to reduce HSA's tryptophan (Trp) residues[196]. A significant decrease in Trp fluorescence intensity was observed after additive titration of TA to HSA solution in PBS, indicating that the Trp residues were buried within TA layers upon binding of TA to the HSA molecule, leaving fewer uncovered Trp residues (**Figure 4-2b**). This finding is in agreement with our pervious finding in chapter one, where TA showed excellent binding affinity to lung fluid, which contains a large amount of HSA. The observed binding affinity is associated with hydrogen bonding and electrostatic interactions occurring between HSA and TA.

Cellular Uptake of HTA NPs by NSCLC

The quantitative and qualitative assessment of HTA NP uptake by NSCLC cells was performed by treating the cells with green fluorescent dye (Coumarin-6)-tagged HTA NPs containing Coumarin-6. The cellular uptake of HTA NPs was examined in A549 and H1299 cells by flow cytometry analysis. Following an increase in concentration of NPs, a cell population gradually shifted towards higher fluorescence, showing a concentration-dependent increase in the cellular uptake of NPs compared to the unstained control cells (**Figure 4-3**). Similar results were observed after increasing the incubation time with a fixed concentration of the coumarin-6-HTA NPs, as the fluorescence intensity significantly increased with a higher incubation time (**Figure 4-4**). For instance, in A549 cell lines, the cells treated with 2.5 and 5 μg /mL NPs had a mean fluorescence intensity of (9.2×10^5 and 15.5×10^5), respectively, whereas cells treated with 10 μg/ mL NPs had the highest mean fluorescence intensity (37×10^5), associated with higher cellular uptake. When treated with 5 μg /mL NPs for 1 and 3 h, cells had a mean fluorescence intensity of (8.9×10^5 and 15.6×10^5), respectively, whereas cells treated for 6 h had the highest mean fluorescence intensity (37.7×10^5), illustrating a higher cellular uptake. Moreover, successful internalization of the coumarin-6-HTA NPs (green fluorescent-tagged NPs) in cells was further evidenced by the representative

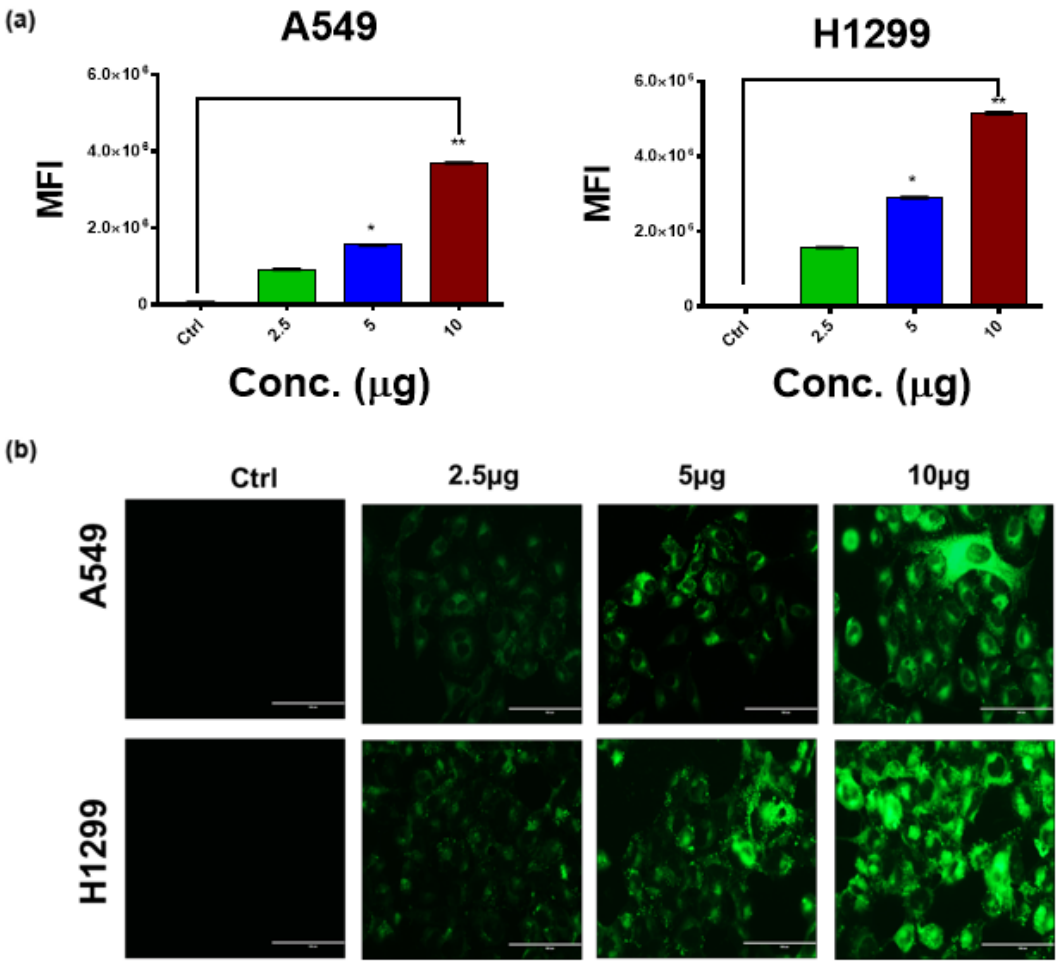

Figure 4-3. Dose dependency intracellular uptake of HTA NPs NSCLC. (Cellular uptake of HTA nanoparticles tagged fluorescence dye (Coumarin 6) in A549 and H1299 cell lines in a dose dependent manner (2.5, 5, 10µg) after 3 h incubation, (a) Graphical representation of quantitative analysis, (b). Representative fluorescence microscopic images of cellular uptake of fluorescently labeled were imaged under EVOS 214 FL Imaging System in a GFP channel. All statistical analysis was performed using a student's t test. Bars represent mean ± SEM. The significance level was * $p < 0.05$. MFI =Mean fluorescence intensity.

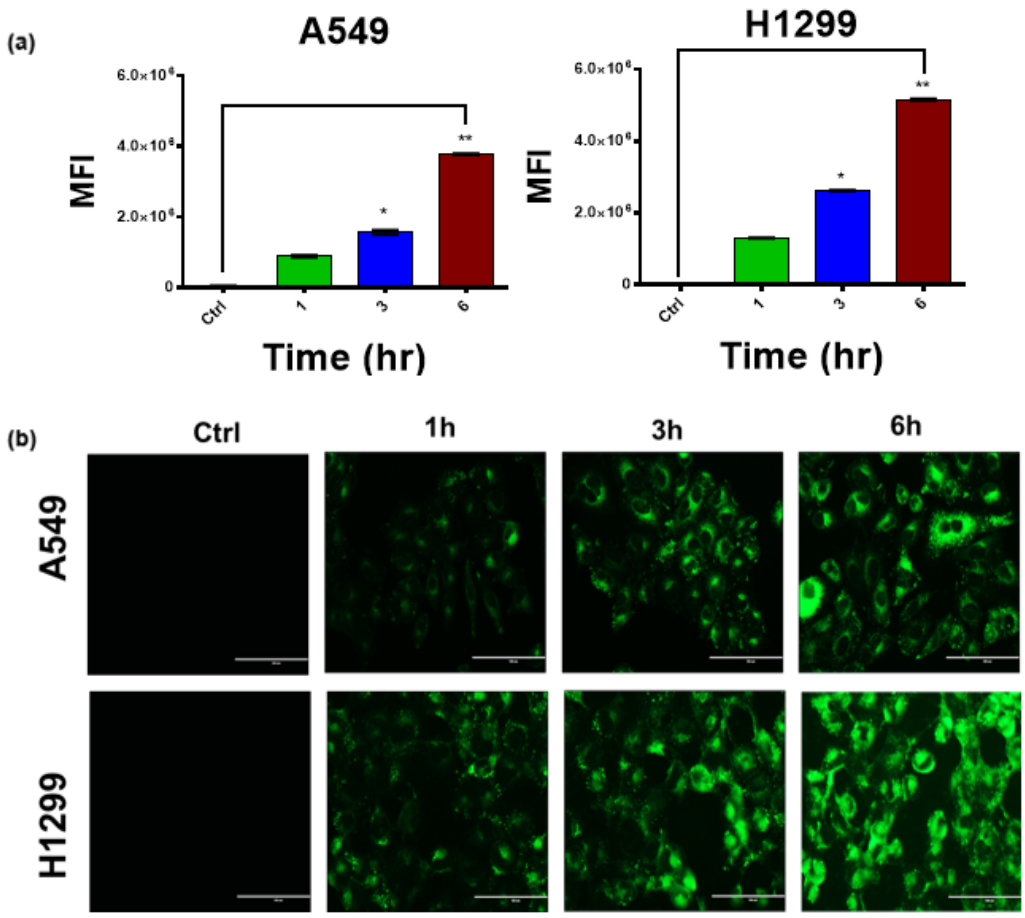

Figure 4-4. Time dependency intracellular uptake of HTA NPs NSCLC. (Cellular uptake of HTA nanoparticles tagged fluorescence dye (Coumarin 6) in A549 and H1299 cell lines in a time dependent manner (1,3,6h) incubated with 5µg of HTA NPS (a) Graphical representation of quantitative analysis, (b). Representative fluorescence microscopic images of cellular uptake of fluorescently labeled were imaged under EVOS 214 FL Imaging System in a GFP channel (Magnification 20X). All statistical analysis was performed using a student's t test. Bars represent mean ± SEM. The significance level was * $p < 0.05$. MFI =Mean fluorescence intensity.

fluorescent images of the cells in dose (**Figure 4-3**) and time (**Figure 4-4**) dependency manner. In control cells, no fluorescence was observed, whereas cells treated with different concentrations of coumarin-6-loaded NPs demonstrated a concentration-dependent enhancement in mean fluorescence intensity, corresponding to an increased concentration of internalized HTA NPs.

Superior Inhibition Effect of G-G@HTA on NSCLC Cells Proliferation

The effect of G-G@HTA NPs on the viability of A549 and H1299 NSCLC cells was quantitatively studied by MTT assay and qualitatively by taking representative images. The assay revealed that the viability of the cells decreased gradually with increasing concentration of G-G@HTA as compared to control cells, single drugs and combination treatment, as shown in **Figure 4-5**, which may be correlated with the successful and sufficient delivery of GA and Gem into NSCLC cells. For example, at 0.1nM GA and 0.1nM of Gem and the equivalent combination concentration treatments, the percent proliferation remained at ~89%, 49%, and 30%, respectively, in A549 cells. The percent proliferation of G-G@HTAs at the same concentration was prominently reduced to ~17%, respectively, suggesting that cytotoxicity is highly influenced by the implementation of nano-carriers. Treatment with G-G@HTA NPs clearly and systematically resulted in dose-dependent cell death, indicating the development of a suitable drug delivery system. Moreover, bare HTA NPs were also examined for their ability to induce cytotoxicity in NSCLC. The bare HTA NPs were found to be non-toxic (cell viability > 95%) as shown in **Figure 4-5**, confirming the biocompatibility of the bare nanocarrier. However, when loaded with GA and Gem, NP treatment resulted in significantly higher ($p<0.001$) cytotoxicity than that of free GA or Gem alone and cotreatment with the free drugs. Greater cytotoxicity is primarily attributed to the enhanced nanoparticle-mediated internalization of drugs (GA and Gem) *via* endocytosis pathways, as well as improved water solubility and stability of GA, which could protect the drug from hydrolysis and fast clearance, thereby leading to the enhancement of therapeutic function. Hence, based on a significant reduction in the percentage of cell viability, it can be suggested that the therapeutic potential of G-G@HTA NPs is not due to the carrier, but due to the encapsulated anticancer agents.

Treatment with G-G@HTA Reduces NSCLC Cells Colony Formation Ability *in Vitro*

To investigate the inhibitory effect of GA and Gem co-treatment compared to HTA NPs loaded with GA and Gem (G-G@HTA) on colony formation ability of NSCLC metastasis, colony formation assay was investigated on A549 and H1299 cell lines.

In these experiments, NSCLC cell lines were treated with 50nM of GA and 50nM of Gem, in addition to equivalent drug concentrations loaded into HTA NPs (G-G@HTA), (**Figure 4-6**). Our results indicate that G-G@HTA significantly reduces the ability of NSCLC cells to form colonies and reduce them by 76% and 84% in A549 and

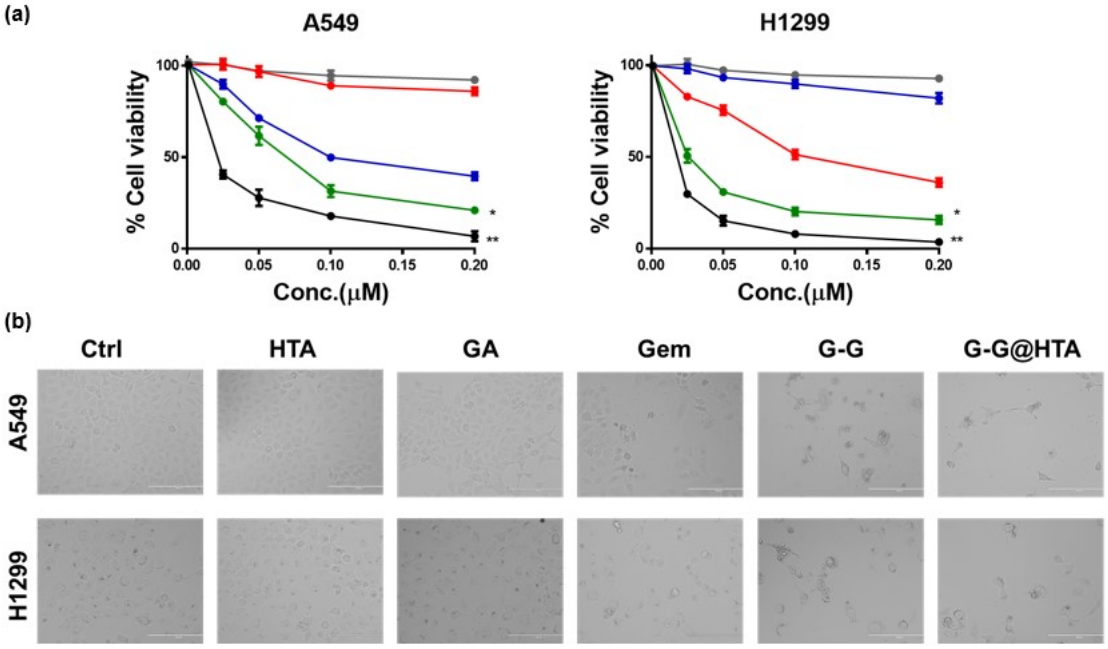

Figure 4-5. Anti-proliferative efficacy of G-G@HTA NPs in NSCLC cancer cells. Cell proliferation measured by MTT assay. (a) G-G@HTA NPs inhibited proliferation of non-small cell lung cancer (A549 and H1299) after treatment with 25-200nM Gem and GA or equivalent amount of drugs for G-G and G-G@HTA NPs for 48h. Untreated cells were used as control, as well as HTA NPs as a vehicle control. (b) Representative images for highest dosage taken after 48h.

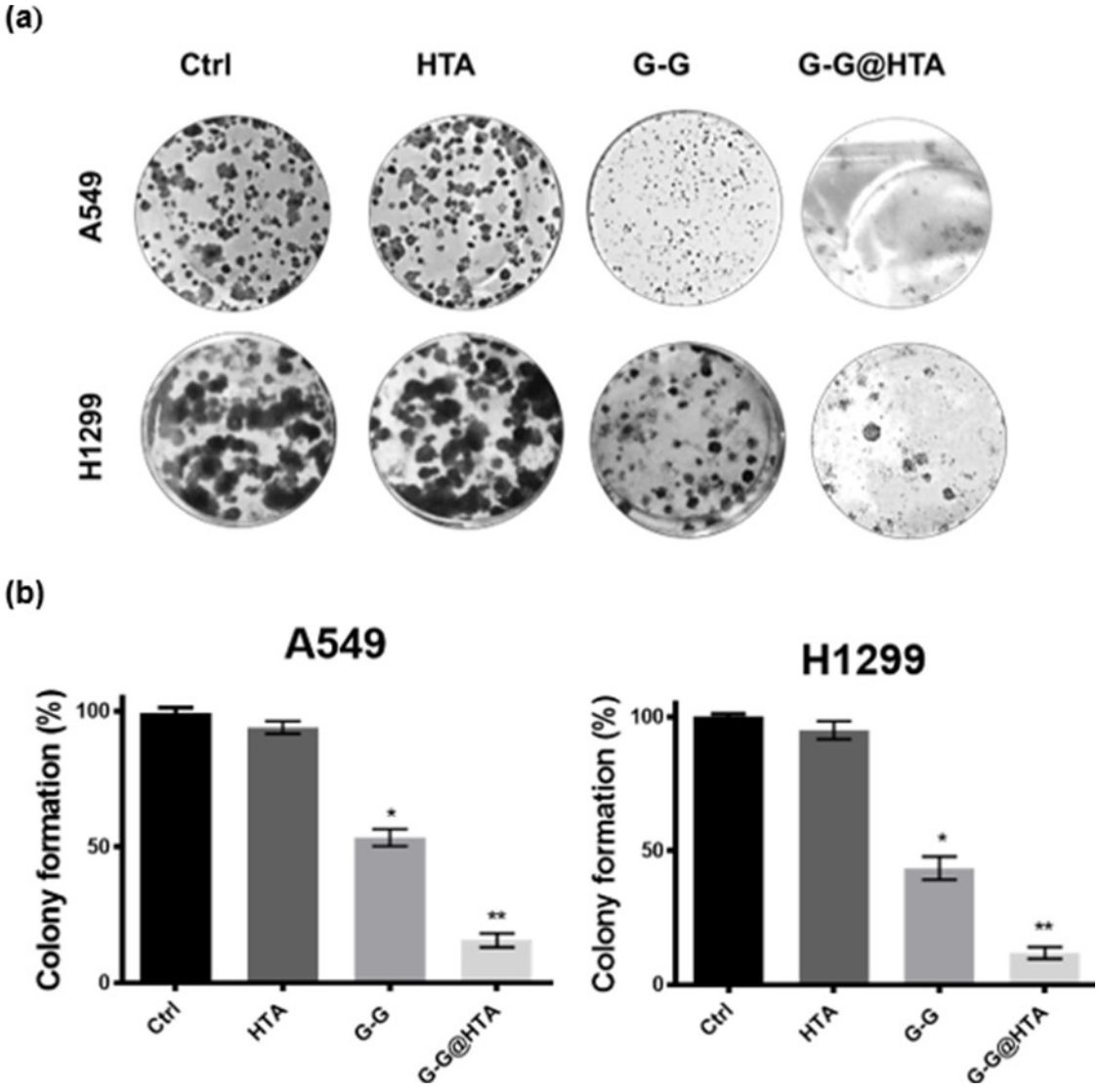

Figure 4-6. Anti-clonogenic potency of G-G@HTA NPs.
(a) Representative images of the effect of Gem and GA, co-treatment(G-G) and G-G@HTA NPs (equivalent to 25nM of Gem and 25nM of GA) on A549 and H1299 cells after 15 days for the colony forming ability on NSCLC. b) Quantities analysis: number of colonies formed in presence of each treatment groups; untreated cells (control) were considered as 100 % clonogenicity. HTA NPS used as a vehicle control. All statistical analysis was performed using a student's t test. Bars represent mean ± SEM. * and ** represent the level of significance with P (<0.05, 0.01) with respect to control.

H1299, respectively, relative to the untreated group. Collectively, as expected, G-G@HTA could significantly inhibit the colony formation ability of A549 and H1299 cell lines *in vitro*.

G-G@HTA Can Significantly Suppress NSCLC Cells Invasion and Migration

To investigate the inhibitory effect of co-treatment with GA and Gem compared to HTA NPs loaded with GA and Gem (G-G@HTA) in NSCLC metastasis, cell migration and invasion were investigated by Boyden chamber and transwell invasion assays, respectively.

In these experiments, NSCLC cell lines (A549 and H1299) were treated with 50nM of GA and 50nM of Gem, in addition to equivalent drug concentrations loaded into HTA NPs (G-G@HTA). Our results indicate that G-G@HTA significantly reduces the ability of NSCLC cells to invade neighboring cells by 88% and 94% in A549 and H1299, respectively, relative to the untreated group (**Figure 4-7**).

Furthermore, similar results were observed in respect to cell migration ability, as shown in **Figure 4-8** G-G@HTA significantly reduces the ability of NSCLC cells to migrate to neighboring cells by 86 and 92% in A549 and H1299, respectively, relative to the untreated group. Collectively, as expected, G-G@HTA could significantly inhibit the migration and invasion ability of A549 and H1299 cell lines *in vitro*.

G-G@HTA NPs Induce Regression of A549 Tumor Xenografts

A xenograft *in vivo* model was designed to confirm the synergistic effect of GA and Gem as achieved in *in vitro* studies. These compounds were tested against tumor growth on a subcutaneous xenograft model using A549 cells to develop a tumor in (nu/nu) mice. Our data demonstrate that GA combined with Gem showed a greater reduction in tumor growth compared to single agents (**Figure 4-9a**). In the same pattern, tumor volumes in the treatment group showed greater reduction than in the control group (**Figure 4-9b**); however, the degree of inhibition in the different groups varied. In the GA single agent group, as expected, tumor growth inhibition was not significant, while GA in combination with Gem yielded significantly smaller tumor volumes than Gem used alone. At 36 days, the mean tumor volume in the control group was $1002 \pm 75 mm^3$. Further, the bare HTA-treated group (a vehicle control) had no significant difference compared to the untreated group ($989 \pm 70 mm^3$), illustrating that tumor regression was unrelated to the HTA vehicle. In comparison to the control group, the tumor inhibition rates were 85 %, 49 %, 29 %, and 19 % in the GA, GEM, combination and G-G@HTA groups, respectively. Graphed tumor weight measurements (**Figure 4-9b**) and net tumor growth (**Figure 4-9c**) were also persistent with those of tumor size. These results demonstrate that GA and Gem combination therapy could act synergistically against NSCLC tumors in an *in vivo* model, and among all groups, tumor regression and growth inhibition was significantly enhanced with G-G@HTA NPs.

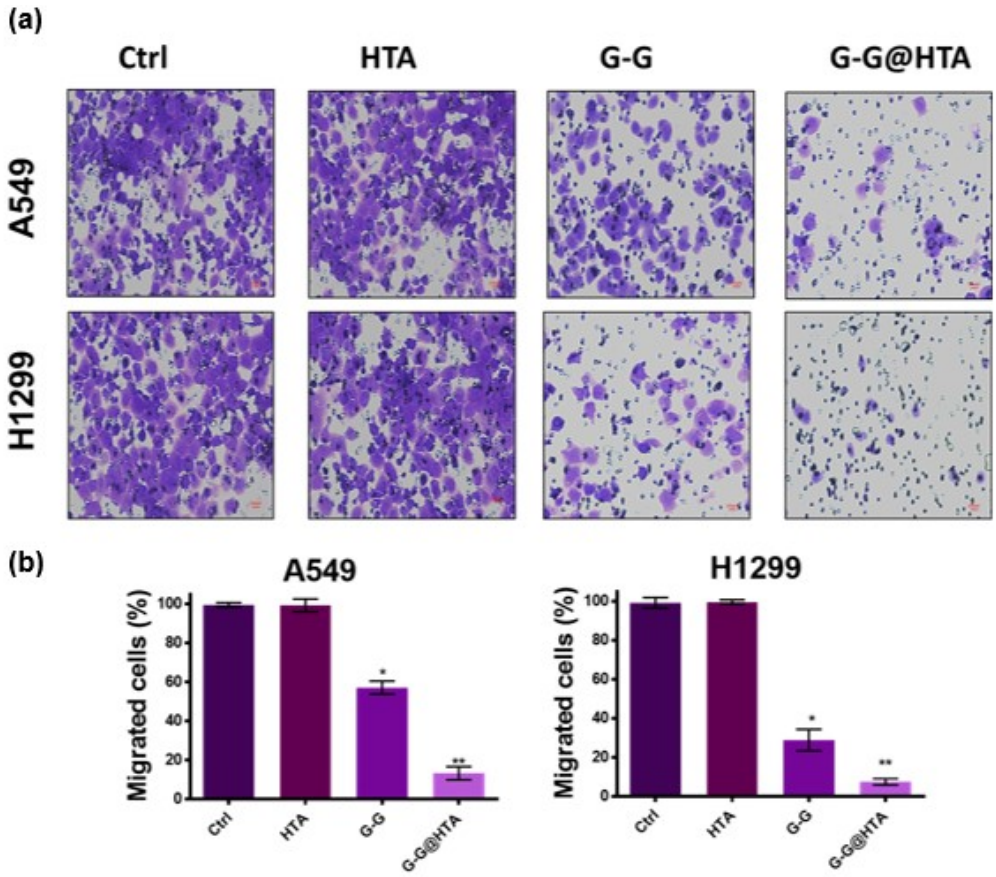

Figure 4-7. Anti-metastatic potential of G-G@HTA NPs measured by migration assays.

Migration assay to determine inhibition potential of NSCLC cell lines (A549 and H1299) after exposure to co treatment of 50nM of GA and 50nM of Gem or G-G@HTA NPs (GA and Gem equivalent) for 24h. (a) Representative images, taken by a Keyence microscope BZ-X800(Itasca, IL, USA) imaging System. (b) Quantitative graphical representation. Data represented as mean ±SEM of the mean (n = 3). Bars represent mean ± SEM. * and **represent the level of significance with P (<0.05, 0.01) with respect to control.

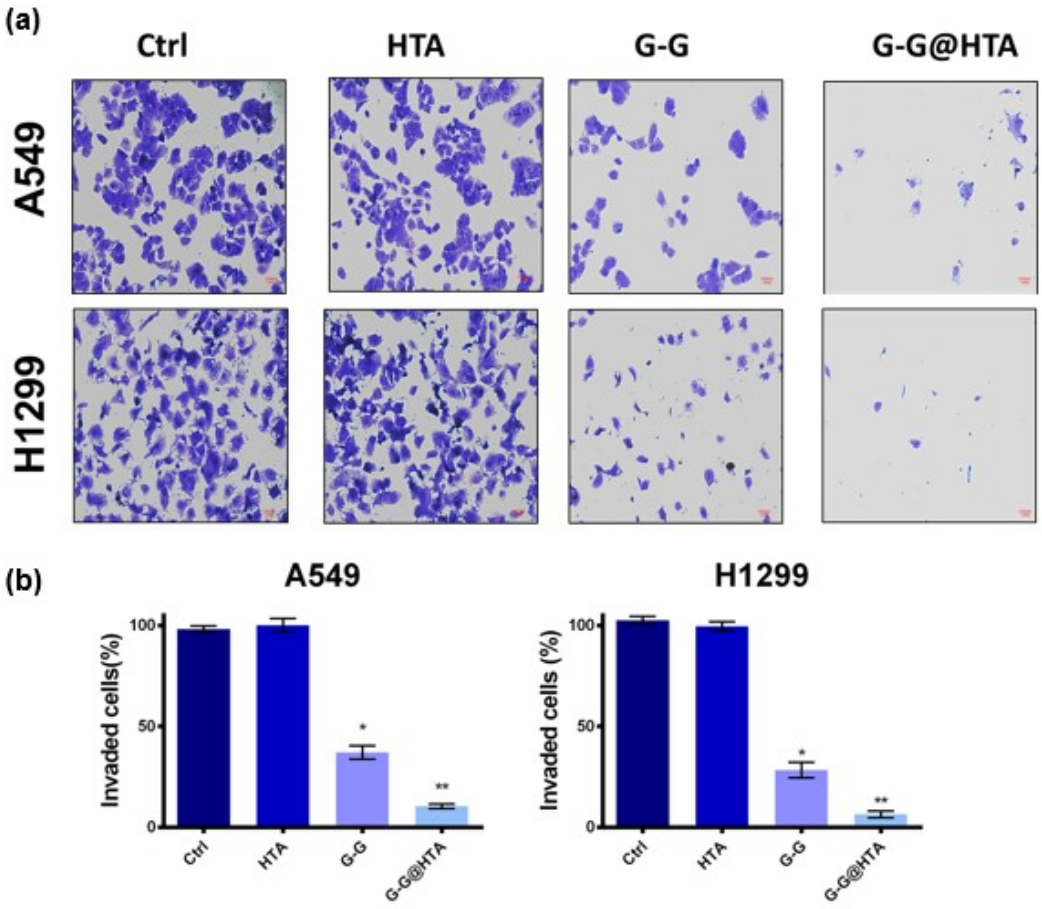

Figure 4-8. Anti-metastatic potential of G-G@HTA NPs measured by invasion assays.

Matrigel Invasion assay demonstrating similar effects, upon treatment with G-G@HTA NPs and GA+Gem (co-treatment of 50nM GA +50nM Gem and G-G@HTA equivalent to GA+Gem concentration)for 24h. (c) Representative images, taken by a Keyence microscope, (d) respective Quantitative graphical representation. Bar graphs represents the number of invaded cells with each treatment group, untreated cells served as control and was considered as 100% and other treatment groups expressed as percentage with respect to the invaded control cells, and HTA NPs treated group served as a NP vehicle. Data represented as mean ±SEM of the mean (n = 3). Bars represent mean ± SEM. * and **represent the level of significance with P (<0.05, 0.01) with respect to control.

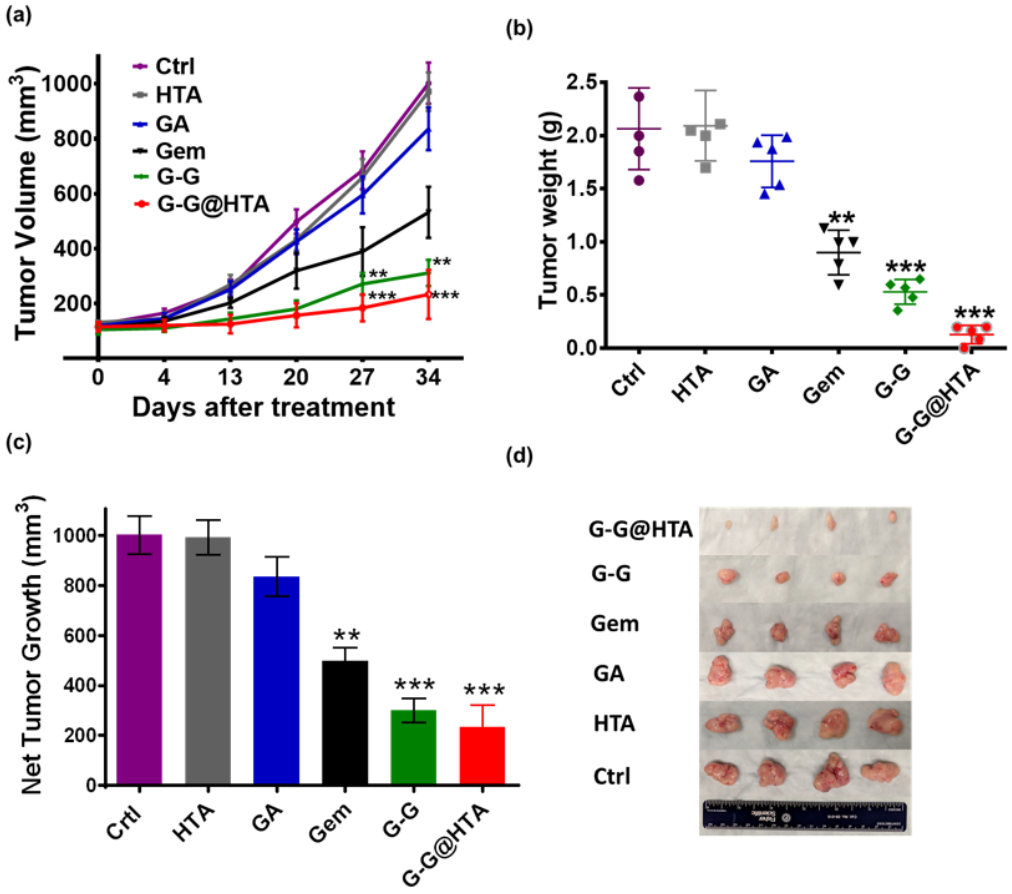

Figure 4-9. Anti-tumor activity of G-G@HTAs in mice bearing A549 xenograft tumors.

Effect of GA, Gem, GA+Gem(G-G) and G-G@HTA NPs on A549 derived xenograft tumors in athymic nude mice, untreated group representing control and HTA treated group present NP vehicle group. Mice were randomly divided into four treatment groups, including a PBS only control group: nanoparticle control (HTA only), GA (2 mg kg^{-1}), Gem (20 mg kg^{-1}) and a combination equivalent (GA +Gem). Respective dual-loaded nanoparticles (G+G@HTA) were administered biweekly *via* the intraperitoneal route, for four subsequent weeks: (a) Tumor volume(mm^3); (b) tumor weights(g); (c) Net tumor growth(mm3), (d) Excised tumor images from treated mice; (e) Immunohistochemistry studies (IHC) of GA, Gem and GA+Gem(G-G) and G-G@HTA NPs treated A549 NSCLC xenografts. Paraffin-embedded sections of A549 bearing tumors in nude mice were processed and IHC was done. IHC of Bcl2, MDR1, BAK, and RRM2, representative of three independent experiments. Data presented as mean ± SEM, each performed in triplicate. All statistical analysis was performed using student's t test. Bars represent mean ± SEM. *, ** and *** represent the level of significance with P (<0.05, 0.01, and 0.005) with respect to control.

Chemistry panels showing markers such as alanine transaminase (ALT), aspartate aminotransferase (AST), alkaline phosphatase test (ALP), gamma-glutamyl transpeptidase (GGT), glutamate dehydrogenase (GLDH), blood urea nitrogen (BUN), albumin (ALB), total bilirubin (Tbili), creatinine (Create), and glucose (Glu), which measures liver and kidney function, were in the acceptable range and did not show any significant abnormalities. Chemistry panel values for the G-G@HTA NP group were within reference range values, which further demonstrated supportive data for the safety of G-G@HTA NPs (**Table 4-1**).

Taken together, our results illustrate that G-G@HTA NPs treatment could efficaciously, safely, and synergistically restrict tumor growth in NSCLC cancer mouse model.

G-G@HTA Promoted Apoptosis and Restrained Tumor Proliferation *in Vivo*

To elucidate the mechanism of G-G@HTA on *in vivo* tumor growth, tissue sections from each group were collected and assayed for various biomarkers. **Figure 4-10**, demonstrates the significant upregulation of the apoptotic marker, Bak, and downregulation of survival markers, Bcl-2 and MDR1, in the G-G@HTA treatment group compared to the control group, single agent groups and the combination group. Moreover, RRM2, a biomarker associated with Gem resistance, was significantly downregulated in the G-G@HTA treatment group.

Furthermore, the H&E staining images(**Figure 4-11**) revealed no obvious damage to major organs in the G-G@HTA group, which suggests a lack of systemic toxicity following treatment. Likewise, the image shown in **Figure 4-12** provides evidence of the hemocompatibility of our formulation with red blood cell (RBC) membranes in mice. These pictures show comparable results for RBC morphologies among HTA, G-G@HTA, and control groups. Taken together, these results indicate that the administration of G-G@HTA two times per week, for four continuous weeks, can be considered safe.

In Vivo Biodistribution of HTA NPs

To Examine and evaluate the *in vivo* biodistribution and tumor targeting ability of the HTA NPs, the IVIS XRMS was employed to visualize and quantify the amount of HTA NPs that accumulated in nude mice bearing A549 tumors. ICG that fluoresces at the near infra-red (NIR) region was encapsulated within HTA NPs. Due to unspecific distribution, free ICG mice showed fluorescence that circulated throughout the body at initial hours a, gradually diminishing after 6 h. However, the fluorescence in groups injected with ICG-tagged HTA NPs was slowly detected throughout the mouse body. We speculate that these findings are due to a prolonged circulation time and slow distribution, known advantages when using NPs. A strong fluorescence intensity (FI) was observed in

Table 4-1. Chemistry panel analysis of the plasma serum of mice after treatments: hepatic and kidney function enzymes.

Parameters	References		Treatment groups					
	Normal range	Units	Control	HTA NPs	GA	Gem	G-G	G-G @HTA
Alb	2.5-3.5	g/dL	2.7±0.2	3.4±1.3	3.42±1.2	2.53±0.3	3.05±0.01	3±0.03
ALP	35-96	U/L	30±0.32	56±3.2	43±23.1	21±1.2	50±17.1	38±12.3
ALT	17-77	U/L	39±1.2	45.34±13.5	61.5±11.3	26.25±5.2	168±1.3	45±10.3
AST	54-298	U/L	226±0.2	188.34±65	174.5±65.3	86.25±21.3	145±56.3	246±35.5
BUN	8-33	mg/dL	16.67±0.9	18.5±3.2	18.5±4.2	20.5±1.3	22±6.01	15.5±0.3
Creat	0.2-0.9	mg/dL	0.67±2.72	0.33±0.1	0.425±0.1	0.67±0.1	0.625±0.3	0.47±0.03
Glu	62-175	mg/dL	131.67±0.9	168.3±45.3	214±13.2	224.75±28.32	317±41.3	136.5±29.3
TBili	0.0-0.9	mg/dL	0.125±0.3	0.13±0.02	0.125±0.1	0.125±0.1	0.15±0.1	0.125±0.006
TP	3.5-7.2	g/dL	4.87±0.5	5.64±0.9	6.65±3.2	5.5±0.3	6.6±0.1	5.6±2.2

Note: ALT= alanine transaminase, AST=aspartate aminotransferase, ALP= alkaline phosphatase test, GGT= gamma-glutamyl transpeptidase, GLDH= glutamate dehydrogenase, BUN= blood urea nitrogen, ALB= albumin, Tbili= total bilirubin, Create= creatinine, and Glu= glucose.

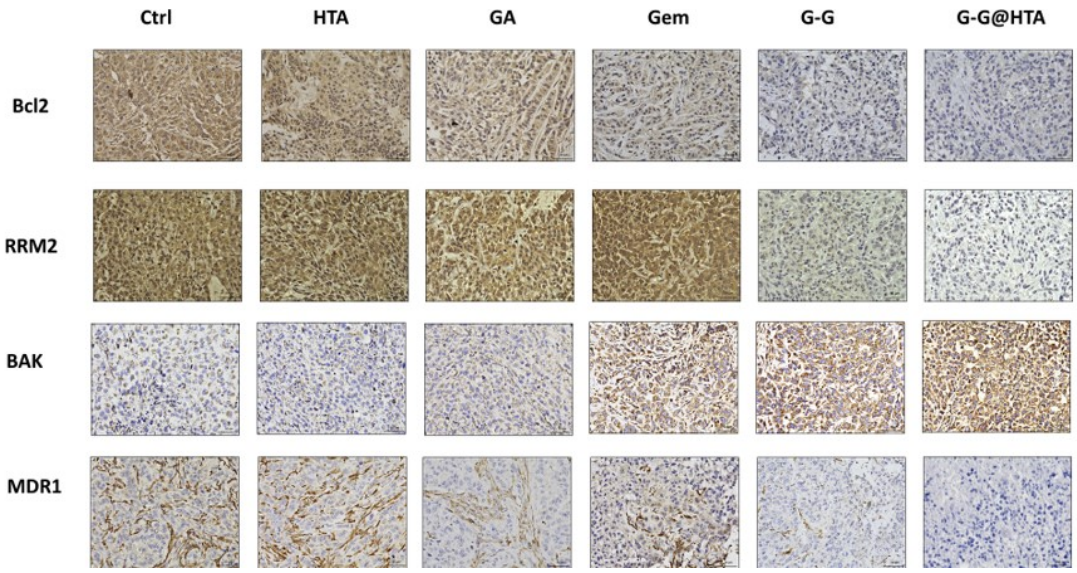

Figure 4-10. Immunohistochemistry and histopathologic examination. Immunohistochemistry studies (IHC) of GA, Gem and GA+Gem(G-G) and G-G@HTA NPs treated A549 NSCLC xenografts. Paraffin-embedded sections of A549 bearing tumors in nude mice were processed and IHC was done. IHC of Bcl2, MDR1, BAK, and RRM2, representative of three independent experiments.

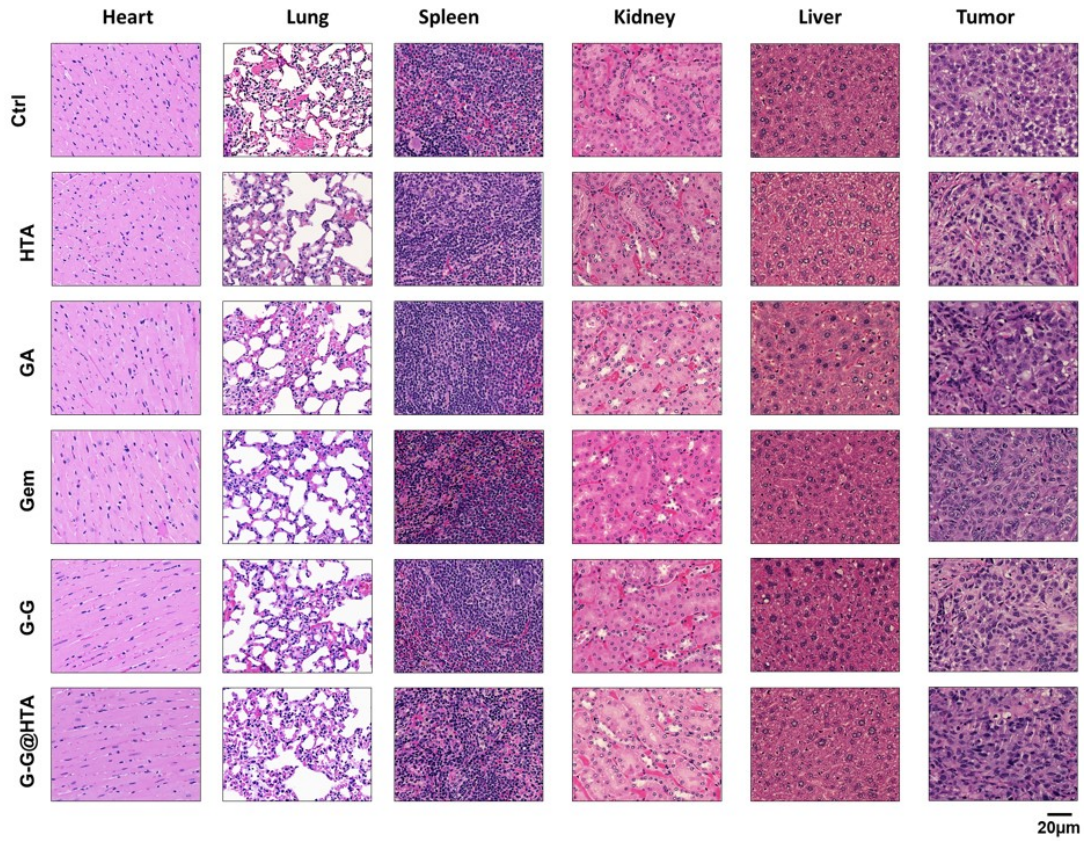

Figure 4-11. Biocompatible and toxicity studies of G-G@HTA NPs.
H&E staining of major organs (heart, spleen, lung, liver, and kidney) and tumors of mice treated with HTA vehicle, GA, Gem, both drugs in combination and G-G@HTA NPs.

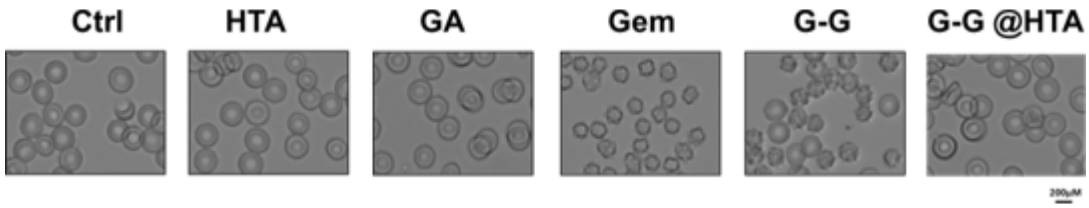

Figure 4-12. Hemocompatibility studies of G-G@HTA NPs.
Representative images of RBC morphology of mice blood treated with HTA vehicle, GA, Gem, both drugs in combination and G-G@HTA NPs.

tumor areas for all in the ICG-tagged HTA group after 6 h, which is imputed to the targeted accumulation of ICG-tagged HTA in tumor tissue *via* the enhanced permeability and retention effect. Moreover, FI signals on tumor sites increased from the 24h timepoint, whereas FI signals observed in the ICG group were slowly eliminated. The FI signal of the HTA group remained strong throughout the imaging study (72h). Hence, it can be proposed that HTA NPs assist and mediate the delivery of therapeutics into the tumor tissue with an extended retention period, which would improve and strengthen the antitumor efficacy. On another note, free ICG exhibited no accumulation at the tumor site during the imaging period, due to fast clearance and rapid diffusion after IP administration (**Figure 4-13**). For further evidence and a clear FI signal observation, the tumors and major organs (Heart, liver, kidney, lung and spleen) were collected at 72h post-injection. The *Ex Vivo* images of dissected organs and tumors are displayed in **Figure 4-13b**. As shown in the figures, zero FI signals were detected in tumors from the ICG group, while powerful FI signals are evident in tumor tissues from mice in the ICG-tagged HTA group. No significant fluorescent uptake was observed in the hearts, lungs, spleens, and kidneys. However, the FI signal from ICG-tagged HTAs was slightly detected in liver and lung tissue from all groups **Figure 4-13c**.

Discussion

Gem is an antimetabolite anticancer agent with an excellent record in clinical studies for various cancer types, including NSCLC. However, due to increasing drug resistance, its therapeutic efficacy has been compromised. At the same time, GA is a natural anticancer agent, potent apoptosis inducer, and chemo-sensitizer, making it an ideal candidate for combination with Gem.

The foundation of this study is built on the basis of our previous findings (Chapter 3), where we described a combinatorial dosage of GA and Gem and demonstrated their synergistic effect on NSCLC; GA sensitizes NSCLC to Gem therapy.

In order to overcome the water insolubility issue of GA and further reduce the development of Gem resistance, as well as avoid off-target side effects, we sought to design a human serum albumin-tannic acid nanoparticle and encapsulate GA and Gem for specific delivery to NSCLC (G-G@HTA NPs).

We have successfully developed and characterized HTA nanocarriers with dual loading properties for both hydrophobic and hydrophilic drugs; his drug delivery system (DDS) has several advantages features. Firstly, it is composed from safe excipients that are biodegradable and biocompatible. A cross-linked HSA with TA gives a stable platform that does not raise any immunogenicity issues. Secondly this carrier can simultaneously deliver both Gem and GA as its chemo-sensitizer. This cargo has relatively lower toxicity than other common combination therapies for NSCLC as GA is known to have a safe toxicity profile[65]. Thus, this nano carrier assist to overcome the resistance issue, deliver adequate quantities of drugs specifically to the tumor site *via* the EPR effect and internalizing them within the cancer cells through 60kDa glycoprotein

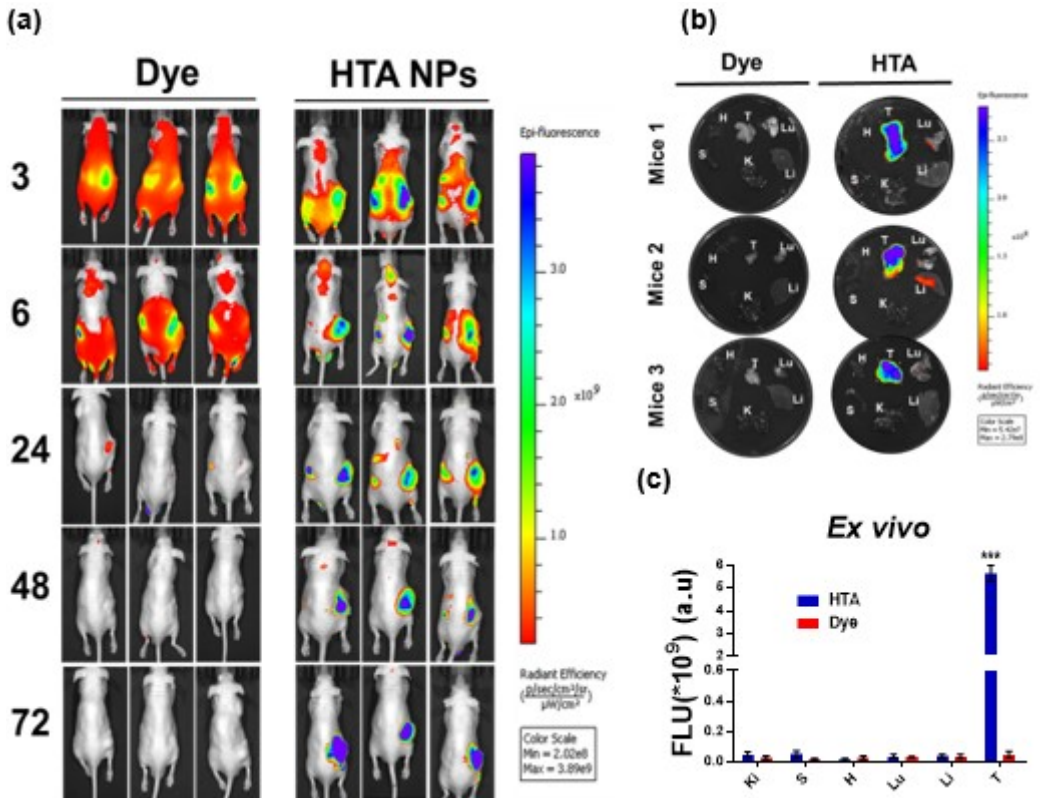

Figure 4-13. Tumor targeting ability of HTA NPs.
(a) *In vivo* fluorescent imaging of mice bearing A549 xenograft tumors treated with free dye (Indocyanine green (ICG)) and dye loaded nanoparticles (ICG-HTA NPs). The mice treated with dye and ICG labeled HTA NPs were imaged using the IVIS Lumina XRMS *in vivo* imaging system at various time intervals (3, 6, 24, 48, and 72h). (b) *Ex vivo* imaging of tumors and major organs (kidney(K), liver (Li), lung(Lu), heart, spleen(S) and tumor(T)) captured from euthanized mice treated with dye and ICG-HTA NPs after 72h. (c)Quantitative *ex vivo* analysis of the fluorescence signals of tumor and major organs, All statistical analysis was performed using a student's t test. Data is presented as mean ± standard error of the mean n = 3 for *in vivo* and *ex vivo* imaging. *** represent the level of significance with P (<0.001) with respect to control.

(gp60) and caveolin-1-mediated transcytosis receptors. Finally, this nanocarrier would prolong the circulation time of the drugs, increase their water solubility, lower incidence of side effects, decrease the required dosage of the drugs, and reduce the development resistance.[79]

HSA is an excellent platform for drug delivery as it is equipped with hydrophobic and hydrophilic domains, features which provide a dual loading capacity. In this study, G-G@HTA NPs were developed using the solvent evaporation method. This well-defined and common procedure not only has less complexity but also is time and cost efficient, as it involves less steps in and fewer chemicals in preparation technique as compared to other methods[124].

Additionally, tannic acid was utilized in this formulation to ensure formation of the self-assemblies in aqueous solution, thereby adding stability and improving biocompatibility [151] [234]. Accumulated evidence indicates that TA can be applied as a reducing agent to form homogenous nanoparticles [223] [234]. Furthermore, we have previously shown that TA has considerable and advantageous binding affinity with lung fluid[196], not to overlook its innate anticancer properties and intrinsic tumor targeting hallmarks [129] [76] [130] [230] [249]. Our approach was to take advantage of TA as crosslinker to facilitate the stable formation of HTA self-assemblies by hydrophobic interaction. Accumulated literature supports that, tannins especially TA promotes the precipitate of macromolecules such as proteins[250].

G-G@HTA nanoparticle (average size 185nm) could conveniently be utilized as a DDS for NSCLC therapy. These results correlate with previous preclinical and clinical trial findings, indicating that NPs in this size range not only are suitable for the recognition of tumor tissue, but also accumulation and retention within tumor tissue as opposed healthy tissue. For instance, Zhang et al. (2017) developed a co-assembly DDS for gefitinib and tripeptide tyroservatide with a size of approximately 200nm, where NPs efficiently internalize to NSCLC, and elevated antitumor efficacy in both *in vitro* and *in vivo* studies[251]. Furthermore, two FDA-approved nanomedicines currently used for lung cancer therapy, Abraxane (albumin bonded paclitaxel nanoparticle) and Genexol PM (paclitaxel encapsulated in PEG-PLA polymeric micelles) have similar particle size (~130 and 50nm respectively)[252] [253].

Successful formation of HTA NPs was confirmed with a quenching assay, FTIR studies and TEM. Binding of the excipients and their presence in the final (G-G@HTA) with uniform, spherical morphology was confirmed. Moreover, our HTA NPs have a zeta potential of -22 mV. A negative charge facilitates NP internalization into cancer cells, while also reducing the possibility of systemic toxicity.

Co-delivery of two drugs with NPs enhance the therapeutic efficacy of both anticancer drugs as compared to systemic delivery of them as single drugs or even in combination. For example, in a Phase II clinical trial investigation on NSCLC patients, results indicated that the co-delivery of cisplatin-gemcitabine by a liposomal NP showed significantly higher therapeutic efficacy with lower side effects (e.g. nephrotoxicity)

compared to free cisplatin-gemcitabine treatment group[254]. In previously conducted studies, GA has shown excellent chemo-sensitization potency *in vitro* and *in vivo* [179 191], but it is a hydrophobic agent. Thus, incorporation of GA in a nano-carrier can conquer this limitation, while prolonging circulation time and offering the controlled release profile for effective and targeted delivery.

Additionally, *in vitro* studies exhibited enhanced antitumor efficacy of the G-G@HTA NPs in comparison to the plain drugs. Moreover, the ability of cancer cells to invade and migrate—the main cause of cancer progression—was drastically decreased when NSCLC cell lines were treated with G-G@HTA NPs.

Further, as shown in our in vivo results (**Figure 4-9**), the G-G@HTA treatment showed a superior tumor regression effect compared to free drugs with equivalent concentrations and combination groups. As expected, the group treated with HTA alone did not show any effect on tumor regression. Thus, the primary cause for tumor regression in the group treated with G-G@HTA is presumably due to greater drug accumulation in cancer cells, facilitated by the nanocarrier. As a consequence of enhanced GA and Gem accumulation inside the cancer cells, the therapeutic effects of these agents are increased, which should lead to a substantial reduction in chemo-resistance, confirmed by a greater reduction in the expression level of MDR1 proteins on IHC slides from G-G@HTA NPs over plain treatments.

The elevated activation level of apoptosis at protein level was confirmed by IHC studies, confirming the successful delivery of GA and Gem encapsulated in HTA NPs, (by inhibition of the antiapoptotic biomarker, Bcl-2 and intracellular accumulation of BAK in tumor cells). Furthermore, RRM2, an important prognostic marker for NSCLC,[255 256] which also correlates to Gem-resistance and survival rates in NSCLC patients[36 255 39]was significantly downregulated in G-G@HTA treatment group. All together, these results illustrate the improved apoptotic potential of G-G@HTA NPs and also suggest that this novel formulation could ultimately lead to a reduction in chemo-resistance.

In vivo biodistribution investigation (**Figure 4-13**) was done as a proof- of concept for the tumor targeting ability of HTA NPs for clinical application and adoption. HTA NPs in mice bearing A549 tumors demonstrated superior tumor accumulation, even at 72h post-injection, and were able to bypass the swift elimination *via* the reticuloendothelial system.

We also analyzed the fate of these nanoparticles when they are in direct contact with blood cells. Blood chemistry panels and morphology analysis of blood cells provide a reliable basis for general wellness in biological systems. Hematological parameters were generally within the acceptable range of reference values, confirming a favorable safety profile for our NPs and their cargo. Another validation for this was H&E staining results, which did not show any obvious damage to major organs such as the heart, spleen, lungs, kidney or liver.

Conclusion

In summary, this study details the design of a novel nanocarrier and provides an optimized strategy for constructing dual-loaded nanoparticles using a biodegradable, non-toxic, human serum albumin-tannic acid-based platform for GA and Gem co-delivery in the treatment of NSCLC. The developed G-G@HTA NPs form mono-dispersed, spherical NPs, with favorable size and surface charge, ideal for internalization into cancer cells. These NPs show superior anticancer efficacy in *in vitro* and *in vivo* studies by eliminating the development of chemo-resistance and by utilizing chemo-sensitization in the setting of NSCLC.

CHAPTER 5. SUMMARY AND FUTURE DIRECTION

Summary

Originating from lung, bronchogenic carcinoma also known as lung cancer is the leading causes of cancer associated death in both men and women in the United States, with the majority of cases (85-90%) being NSCLC. Conventional chemotherapy is currently the most effective treatment for NSCLC patients with advanced invasive disease. The side effects of this type of therapy are often severe and intolerable, especially for unfit patients. However, Gem a pyrimidine nucleoside antimetabolite, with a relatively lower toxicity profile, has been used widely as an effective anticancer agent for patients with NSCLC as well as other cancers such as pancreatic, bladder, breast, and ovarian. But this treatment option often suffers from the rapid development of resistance, therefore combination therapies are being investigated as the therapeutic efficacy of combined agents together would potentially lead to an elevated level of anticancer potency and help to overcome the Gem resistance pitfall. In this regard, there is an emerging interest in combining chemotherapeutic agents with natural products, because of their anticancer properties with diverse molecular mechanism and safe profile; which leads to a robust anticancer efficacy while minimizing the undesirable side effects.

Here, we investigated the therapeutic effect of GA, a naturally occurring xanthonoid, in combination with Gem on NSCLC. Previous studies have shown that GA has anti-neoplastic, anticancer, and chemo-sensitization attributes[75 257 258]. However, to date, there have been no documented studies on its effects in combination with Gem on NSCLC. Our results revealed that a combined treatment of GA and Gem inhibited the growth and proliferation of NSCLC cells, induced apoptosis and inhibit the tube formation of HUVEC cells. Furthermore, GA sensitizes NSCLC to Gem therapy by blocking P-gp transporter. Our results highlight potentials of this treatment option for future NSCLC therapy.

Nevertheless, GA suffers from water solubility and its inorganic solvent may cause systemic toxicity issues. On the other hand, the utilization of the conventional drug delivery approach usually leads to off-target toxicity, thus, we designed the biodegradable and biocompatible stable NPs with low immunogenicity and low toxicity. Our *in vitro* and *in vivo* results demonstrated that our designed NDDS loaded with two anticancer agents (GA and Gem) significantly increased their therapeutic effect while decreased the off-target toxicity and side effects while prolongs the blood circulation as exhibited in a xenograft mouse model.

Future Research

Taken together, the results and findings of this project, illustrate the proof of concept that our uniquely designed dual loaded protein-based HTA NPs are capable of increasing the therapeutic effect of GA and Gem on NSCLC, and not only lead to tumor

regression but also have the tumor-targeting ability on a xenografic mouse model. Furthermore, successful tumor accumulation and biodistribution of HTA NPs provides strong supportive evidence for subsequent use in pre-clinical and clinical translation. It is further proven that this noncarrier is capable of co-deliver hydrophobic and hydrophilic drugs simultaneously and increase their antitumoral properties. However, this work can be considered as a decent attempt toward the production and development of finer nanomedicine in cancer therapy, some further research can strengthen this concept and project are as follows. Further detailed investigation of molecular mechanism would help to unraveling the involved signaling pathways to identifying the therapeutic target of GA and Gem combinations on NSCLC. Also, utilization of a high-pressure homogenizer in the process of preparation of the NPs, can assist with optimization and decreasing the batch to batch variation and increase the loading efficacy. Inspection of the loading efficacy and drug release profile of the G-G @HTA NPs is necessity. Moreover, to enhance the active targeting of these NPs, they can be conjugated with different ligands to target specific receptors abundant on cancer cells (e.g. EGFR).

Furthermore, the primary limitation of our *in vivo* study was utilization of xenograft animal model, and generation of tumor by subcutaneous techniques with just one subcategories of NSCLC, which cannot mimic the actual complex nature of NSCLC tumors, therefore considering this preliminary *in vivo* study as a concept validation, a more detailed and multidimensional model such as orthotopic mouse is required. Additionally, as the common administration route for protein-based NPs (e.g. Abraxane) is *via* intravenous injection, thus, further *in vivo* studies should take this in consideration for a smoother and more predictable transition to clinical trials.

LIST OF REFERENCES

1. Tan, W. L. *et al.* Novel therapeutic targets on the horizon for lung cancer. *Lancet Oncol.* **17**, e347–e362 (2016).

2. Mao, Y., Yang, D., He, J. & Krasna, M. J. Epidemiology of Lung Cancer. *Surg. Oncol. Clin. N. Am.* **25**, 439–445 (2016).

3. Dai, J., Yang, P., Cox, A. & Jiang, G. Lung cancer and chronic obstructive pulmonary disease: From a clinical perspective. *Oncotarget* **8**, 18513–18524 (2017).

4. Siegel, R. L., Miller, K. D. & Jemal, A. Cancer statistics, 2019. *CA. Cancer J. Clin.* **69**, 7–34 (2019).

5. Siegel, R. L., Miller, K. D. & Jemal, A. Cancer statistics, 2018. *CA. Cancer J. Clin.* **68**, 7–30 (2018).

6. Cutler, G. J. *et al.* women : The Iowa Women ' s Health Study. *Int. J.* **123**, 664–671 (2009).

7. Questions, G. Lung Cancer Biomarkers Guideline. *Hematol Oncol Clin North Am. 2017* **31**, 13–29 (2017).

8. American Cancer Society. Facts & Figures 2019. *Am. Cancer Soc.* (2019).

9. Yan, A., Yang, C., Chen, Z., Li, C. & Cai, L. MiR-761 promotes progression and metastasis of non-small cell lung cancer by targeting ING4 and TIMP2. *Cell. Physiol. Biochem.* **37**, 55–66 (2015).

10. Cheung, C. H. Y. & Juan, H. F. Quantitative proteomics in lung cancer. *J. Biomed. Sci.* **24**, 1–11 (2017).

11. Beckles MA1, Spiro SG, Colice GL, R. R. Initial Evaluation of the Patient With Lung Cancer. *Chest* **123**, 97S-104S (2007).

12. Hirsch, F. R. *et al.* Lung cancer: current therapies and new targeted treatments. *Lancet* **389**, 299–311 (2017).

13. Szabo, E., Mao, J. T., Lam, S., Reid, M. E. & Keith, R. L. Chemoprevention of Lung Cancer 3rd ed : American College of Chest Physicians. *Chest* **143**, e40S-e60S (2013).

14. Tan, W. L. *et al.* Novel therapeutic targets on the horizon for lung cancer. *Lancet Oncol.* **17**, e347–e362 (2016).

15. Srinivas, N. S. K., Verma, R., Kulyadi, G. P. & Kumar, L. A quality by design approach on polymeric nanocarrier delivery of gefitinib: Formulation, in vitro, and in vivo characterization. *Int. J. Nanomedicine* **12**, 15–28 (2017).

16. Miller, K. D. *et al.* Cancer treatment and survivorship statistics, 2016. *CA. Cancer J. Clin.* **66**, 271–289 (2016).

17. Steven, A., Fisher, S. A. & Robinson, B. W. Immunotherapy for lung cancer. *Respirology* **21**, 821–833 (2016).

18. The Lancet. Lung cancer: despite advances, prevention is still best. *Lancet* **388**, 533 (2016).

19. Wang, Y. *et al.* Lung cancer combination therapy: co-delivery of paclitaxel and doxorubicin by nanostructured lipid carriers for synergistic effect. *Drug Deliv.* **23**, 1398–1403 (2016).

20. Guy C. Jones, M.D., Jason D. Kehrer, DO, Jenna Kahn, MD, Bobby N. Koneru, MD, Ram Narayan, MD, Tarita O. Thomas, MD, PhD, Kevin Camphausen, MD, Minesh P Mehta, MD, and Aradhana Kaushal, M. Primary treatment options for high risk/medically inoperable early stage NSCLC patients. *Clin Lung Cancer* **25**, 1032–1057 (2017).

21. Leduc, C. & Quoix, E. Programmed death of chemotherapy in non-small-cell lung cancer? *Lancet* **389**, 227–228 (2017).

22. Natale, R. B. Gemcitabine-containing regimens vs others in first-line treatment of NSCLC. *Oncology (Williston Park).* **18**, 27–31 (2004).

23. Pilkington, G. *et al.* A systematic review of the clinical effectiveness of first-line chemotherapy for adult patients with locally advanced or metastatic non-small cell lung cancer. *Thorax* **70**, 359–367 (2015).

24. Leschinger, M. I., Helsberg, K., Langer, F. & Schuette, W. H. W. Gemcitabin in der first-line-therapie des lokal fortgeschrittenen und metastasierten nicht-kleinzelligen bronchialkarzinoms (NSCLC): Ergebnisübersicht randomisierter phase-III-studien. *Onkologie* **28**, 1–28 (2005).

25. Manegold, C. Gemcitabine (Gemzar®) in non-small cell lung cancer. *Expert Rev. Anticancer Ther.* **4**, 345–360 (2004).

26. Carmichael, J. The role of gemcitabine in the treatment of other tumours. *Br. J. Cancer* **78**, 21–25 (1998).

27. Toschi, L. & Cappuzzo, F. Gemcitabine for the treatment of advanced nonsmall cell lung cancer. *Onco. Targets. Ther.* **2**, 209–217 (2009).

28. Steward, W. P. Combination studies with gemcitabine in the treatment of non-small-cell lung cancer. *Br. J. Cancer* **78**, 15–19 (1998).

29. Toschi, L., Finocchiaro, G., Bartolini, S., Gioia, V. & Cappuzzo, F. Role of gemcitabine in cancer therapy. *Futur. Oncol.* **1**, 7–17 (2005).

30. Hagmann, W., Jesnowski, R. & Löhr, J. M. Interdependence of Gemcitabine Treatment, Transporter Expression, and Resistance in Human Pancreatic Carcinoma Cells. *Neoplasia* **12**, 740–747 (2015).

31. Seve, P. & Dumontet, C. Chemoresistance in Non-Small Cell Lung Cancer. *Curr. Med. Chem. Agents* **5**, 73–88 (2005).

32. Mackey, J. R. *et al.* Functional Nucleoside Transporters Are Required for Gemcitabine Influx and Manifestation of Toxicity in Cancer Cell Lines. *Cancer Res.* **58**, 4349–4357 (1998).

33. J., S. *et al.* The absence of human equilibrative nucleoside transporter 1 is associated with reduced survival in patients with gemcitabine-treated pancreas adenocarcinoma. *Clin. Cancer Res.* **10**, 6956–6961 (2004).

34. Achiwa, H. *et al.* Determinants of sensitivity and resistance to gemcitabine: The roles of human equilibrative nucleoside transporter 1 and deoxycytidine kinase in non-small cell lung cancer. *Cancer Sci.* **95**, 753–757 (2004).

35. Jia, Y. & Xie, J. Promising molecular mechanisms responsible for gemcitabine resistance in cancer. *Genes Dis.* **2**, 299–306 (2015).

36. Nakano, Y. *et al.* Gemcitabine chemoresistance and molecular markers associated with gemcitabine transport and metabolism in human pancreatic cancer cells. *Br. J. Cancer* **96**, 457–463 (2007).

37. Davidson, J. D. *et al.* An increase in the expression of ribonucleotide reductase large subunit 1 is associated with gemcitabine resistance in non-small cell lung cancer cell lines. *Cancer Res.* **64**, 3761–3766 (2004).

38. Chen, Z., Zheng, Y., Shi, Y. & Cui, Z. Overcoming tumor cell chemoresistance using nanoparticles: Lysosomes are beneficial for (stearoyl) gemcitabine-incorporated solid lipid nanoparticles. *Int. J. Nanomedicine* **13**, 319–336 (2018).

39. Grossi, F. *et al.* Expression of ribonucleotide reductase subunit-2 and thymidylate synthase correlates with poor prognosis in patients with resected stages I-III non-small cell lung cancer. *Dis. Markers* **2015**, (2015).

40. Ceppi, P. *et al.* ERCC1 and RRM1 gene expressions but not EGFR are predictive of shorter survival in advanced non-small-cell lung cancer treated with cisplatin and gemcitabine. *Ann. Oncol.* **17**, 1818–1825 (2006).

41. Lee, J. J. *et al.* The immunohistochemical overexpression of ribonucleotide reductase regulatory subunit M1 (RRM1) protein is a predictor of shorter survival to gemcitabine-based chemotherapy in advanced non-small cell lung cancer (NSCLC). *Lung Cancer* **70**, 205–210 (2010).

42. Zeng, C., Fan, W. & Zhang, X. RRM1 expression is associated with the outcome of gemcitabine-based treatment of non-small cell lung cancer patients–a short report. *Cell. Oncol.* **38**, 319–325 (2015).

43. Stubbe, J. Ribonucleotide reductases. *Adv. Enzymol. Relat. Areas Mol. Biol.* **63**, 349–419 (1990).

44. Samanta, K. *et al.* Gemcitabine combination nano therapies for pancreatic cancer. *Pharmaceutics* **11**, 1–25 (2019).

45. Ramirez, M. *et al.* Diverse drug-resistance mechanisms can emerge from drug-tolerant cancer persister cells. *Nat. Commun.* **7**, 1–8 (2016).

46. Nagesh, P. K. B. *et al.* PSMA targeted docetaxel-loaded superparamagnetic iron oxide nanoparticles for prostate cancer. *Colloids Surfaces B Biointerfaces* **144**, 8–20 (2016).

47. Yang, C. H. *et al.* Gemcitabine and cisplatin in a multimodality treatment for locally advanced non-small cell lung cancer. *Br. J. Cancer* **86**, 190–195 (2002).

48. d'Amato, T. A. *et al.* Chemotherapy resistance and oncogene expression in non-small cell lung cancer. *J. Thorac. Cardiovasc. Surg.* **133**, 352–363 (2007).

49. National Cancer Institute. Common Terminology Criteria for Adverse Events (CTCAE).v.5.0. *Cancer Ther. Eval. Progr.* 183 (1999).

50. Dias, D. A., Urban, S. & Roessner, U. A Historical overview of natural products in drug discovery. *Metabolites* **2**, 303–336 (2012).

51. Mirza, S., Vasaiya, A., Vora, H., Jain, N. & Rawal, R. Curcumin Targets Circulating Cancer Stem Cells by Inhibiting Self-Renewal Efficacy in Non-Small Cell Lung Carcinoma. *Anticancer. Agents Med. Chem.* **17**, (2016).

52. Lucas, I. K. & Kolodziej, H. Trans-Resveratrol Induces Apoptosis through ROS-Triggered Mitochondria-Dependent Pathways in A549 Human Lung Adenocarcinoma Epithelial Cells. *Planta Med.* **81**, 1038–1044 (2015).

53. Pelczynska, M. *et al.* Antiproliferative activity of vitamin D compounds in combination with cytostatics. *Anticancer Res.* **26**, 2701–2705 (2006).

54. Sadeghzadeh, H. *et al.* The Effects of Nanoencapsulated Curcumin-Fe3O4 on Proliferation and hTERT Gene Expression in Lung Cancer Cells. *Anticancer. Agents Med. Chem.* **17**, (2017).

55. Zhou, D. *et al.* Synthesis and Evaluation of Curcumin-Related Compounds Containing Inden-2-one for Their Effects on Human Cancer Cells. *Biol. Pharm. Bull.* **37**, 1977–1981 (2014).

56. Bhardwaj, V. & Mandal, A. K. A. Next-generation sequencing reveals the role of epigallocatechin-3-gallate in regulating putative novel and known microRNAs which target the MAPK pathway in non-small-cell lung cancer A549 cells. *Molecules* **24**, (2019).

57. Yang, J. *et al.* In vitro and in vivo antiangiogenic activity of caged polyprenylated xanthones isolated from garcinia hanburyi Hook. f. *Molecules* **18**, 15305–15313 (2013).

58. Zhang, T. *et al.* Inhalation treatment of primary lung cancer using liposomal curcumin dry powder inhalers. *Acta Pharm. Sin. B* **8**, 440–448 (2018).

59. Lee, S. H. *et al.* Quercetin enhances chemosensitivity to gemcitabine in lung cancer cells by inhibiting heat shock protein 70 expression. *Clin. Lung Cancer* **16**, e235–e243 (2015).

60. Mishra, B. B. & Tiwari, V. K. Natural products: An evolving role in future drug discovery. *Eur. J. Med. Chem.* **46**, 4769–4807 (2011).

61. Zhao, L., Guo, Q. L., You, Q. D., Wu, Z. Q. & Gu, H. Y. Gambogic acid induces apoptosis and regulates expressions of bax and Bcl-2 protein in human gastric carcinoma MGC-803 cells. *Biol. Pharm. Bull.* **27**, 998–1003 (2004).

62. Chen, B. *et al.* Mechanisms of Gambogic Acid-Induced Apoptosis in Non-Small Cell Lung Cancer Cells in Relation to Transferrin Receptors. *J. Chemother.* **21**, 666–672 (2014).

63. Xia, G. *et al.* Gambogic acid sensitizes gemcitabine efficacy in pancreatic cancer by reducing the expression of ribonucleotide reductase subunit-M2 (RRM2). *J. Exp. Clin. Cancer Res.* **36**, 107 (2017).

64. Banik, K. *et al.* Therapeutic potential of gambogic acid, a caged xanthone, to target cancer. *Cancer Lett.* **416**, 75–86 (2018).

65. Zhao, L. *et al.* General pharmacological properties, developmental toxicity, and analgesic activity of gambogic acid, a novel natural anticancer agent. *Drug Chem. Toxicol.* **33**, 88–96 (2010).

66. Chi, Y. *et al.* An open-labeled, randomized, multicenter phase IIa study of gambogic acid injection for advanced malignant tumors. *Chin. Med. J. (Engl).* **126**, 1642–1646 (2013).

67. Li, X. *et al.* Synthesis and anti-tumor evaluation of novel C-37 modified derivatives of gambogic acid. *Chinese J. Chem.* **30**, 1083–1091 (2012).

68. Zhang, X. J. *et al.* Studies on chemical-structure modification and structure-activity relationship of gambogic acid derivatives at carbon(34). *Chem. Biodivers.* **9**, 2295–2308 (2012).

69. Duan, D. *et al.* Gambogic acid induces apoptosis in hepatocellular carcinoma SMMC-7721 cells by targeting cytosolic thioredoxin reductase. *Free Radic. Biol. Med.* **69**, 15–25 (2014).

70. Wang, S., Wang, L., Chen, M. & Wang, Y. Gambogic acid sensitizes resistant breast cancer cells to doxorubicin through inhibiting P-glycoprotein and suppressing survivin expression. *Chem. Biol. Interact.* **235**, 76–84 (2015).

71. Inhibitors, P. Chemosensitizer Learn more about Chemosensitizer Multidrug Resistance in the Laboratory and Clinic. (2017).

72. Wang, S. *et al.* Fighting fire with fire: Poisonous Chinese herbal medicine for cancer therapy. *Journal of Ethnopharmacology* **140**, 33–45 (2012).

73. Tian, F. *et al.* A targeted nanoplatform co-delivering chemotherapeutic and antiangiogenic drugs as a tool to reverse multidrug resistance in breast cancer. *Acta Biomater.* **75**, 398–412 (2018).

74. Zhou, Y. *et al.* Daunorubicin and gambogic acid coloaded cysteamine-CdTe quantum dots minimizing the multidrug resistance of lymphoma in vitro and in vivo. *Int. J. Nanomedicine* **11**, 5429–5442 (2016).

75. Wang, X. *et al.* Gambogic acid as a non-competitive inhibitor of ATP-binding cassette transporter B1 reverses the multidrug resistance of human epithelial cancers by promoting ATP-binding cassette transporter B1 protein degradation. *Basic Clin. Pharmacol. Toxicol.* **112**, 25–33 (2013).

76. K.B. Nagesh, P. *et al.* Cross linked polyphenol-based drug nano-self assemblies engineered to blockade prostate cancer senescence. *ACS Appl. Mater. & Interfaces* **0**, null-null (2019).

77. Dai, Q. *et al.* Particle Targeting in Complex Biological Media. *Adv. Healthc. Mater.* **7**, 1–32 (2018).

78. Haley, B. & Frenkel, E. Nanoparticles for drug delivery in cancer treatment. *Urol. Oncol. Semin. Orig. Investig.* **26**, 57–64 (2008).

79. Yamashita, F. & Hashida, M. Pharmacokinetic considerations for targeted drug delivery. *Adv. Drug Deliv. Rev.* **65**, 139–147 (2013).

80. Hatami, E. *et al.* Development of Zoledronic Acid-Based Nanoassemblies for Bone-Targeted Anticancer Therapy. *ACS Biomater. Sci. Eng.* acsbiomaterials.9b00362 (2019). doi:10.1021/acsbiomaterials.9b00362

81. Ferrari, M. & Zhao, Y. The nano-plasma interface : implications of the protein corona. 17–24 (2015). doi:10.1016/j.colsurfb.2014.02.035.The

82. Gu, W., Wu, C., Chen, J. & Xiao, Y. Nanotechnology in the targeted drug delivery for bone diseases and bone regeneration. *Int. J. Nanomedicine* **8**, 2305–2317 (2013).

83. Wang, J., Sui, M. & Fan, W. Nanoparticles for Tumor Targeted Therapies and Their Pharmacokinetics. *Curr. Drug Metab.* **11**, 129–141 (2010).

84. Jain, R. K. & Stylianopoulos, T. Delivering nanomedicine to solid tumors. *Nat. Rev. Clin. Oncol.* **7**, 653–664 (2010).

85. Lian, H., Wu, J., Hu, Y. & Guo, H. Self-assembled albumin nanoparticles for combination therapy in prostate cancer. *Int. J. Nanomedicine* **12**, 7777–7787 (2017).

86. Singh, R. & Lillard, J. W. Nanoparticle-based targeted drug delivery. *Exp. Mol. Pathol.* **86**, 215–223 (2009).

87. Zhang, H., Zhai, Y., Wang, J. & Zhai, G. New progress and prospects: The application of nanogel in drug delivery. *Mater. Sci. Eng. C* **60**, 560–568 (2016).

88. Wang, W. *et al.* Lysosome-independent intracellular drug/gene co-delivery by lipoprotein-derived nanovector for synergistic apoptosis-inducing cancer-targeted therapy. *Biomacromolecules* acs.biomac.7b01549 (2018). doi:10.1021/acs.biomac.7b01549

89. Jiang, W., Cai, G., Hu, P. C. & Wang, Y. Personalized medicine in non-small cell lung cancer: A review from a pharmacogenomics perspective. *Acta Pharm. Sin. B* (2018). doi:10.1016/j.apsb.2018.04.005

90. Landesman-Milo, D., Ramishetti, S. & Peer, D. Nanomedicine as an emerging platform for metastatic lung cancer therapy. *Cancer Metastasis Rev.* **34**, 291–301 (2015).

91. Meng, H. *et al.* Use of a lipid-coated mesoporous silica nanoparticle platform for synergistic gmcitabine and pclitaxel dlivery to hman pncreatic cncer in mice. *ACS Nano* **9**, 3540–3557 (2015).

92. Elzoghby, A. O., Samy, W. M. & Elgindy, N. A. Albumin-based nanoparticles as potential controlled release drug delivery systems. *J. Control. Release* **157**, 168–182 (2012).

93. Ahmad, A. & Gadgeel Editors, S. M. *Lung Cancer and Personalized Medicine: Novel Therapies and Clinical Management*. **890**, (2016).

94. Chauhan, A. S. Dendrimers for Drug Delivery. *Molecules* **23**, (2018).

95. Walworth, K. *et al.* Dendrimer-based selective proteostasis-inhibition strategy to control NSCLC growth and progression. *PLoS One* **11**, 1–18 (2016).

96. Hardeep S. Oberoia, 1, Natalia V. Nukolovab, c, 1, Alexander V. Kabanovb, d,*, and T. K. B. Nanocarriers for delivery of platinum anticancer drugs. *Bone* **23**, 1–7 (2008).

97. Fantini, M. *et al.* Lipoplatin Treatment in Lung and Breast Cancer. *Chemother. Res. Pract.* **2011**, 1–7 (2011).

98. Stathopoulos, G. P. *et al.* Comparison of liposomal cisplatin versus cisplatin in non-squamous cell non-small-cell lung cancer. *Cancer Chemother. Pharmacol.* **68**, 945–950 (2011).

99. Zhao, M. *et al.* Quantitative proteomic analysis to the first commercialized liposomal paclitaxel nano-platform Lipusu revealed the molecular mechanism of the enhanced anti-tumor effect. *Artif. Cells, Nanomedicine Biotechnol.* **46**, S147–S155 (2018).

100. Zhang, Q., Huang, X. E. & Gao, L. L. A clinical study on the premedication of paclitaxel liposome in the treatment of solid tumors. *Biomed. Pharmacother.* **63**, 603–607 (2009).

101. Wang, X. *et al.* A phase I clinical and pharmacokinetic study of paclitaxel liposome infused in non-small cell lung cancer patients with malignant pleural effusions. *Eur. J. Cancer* **46**, 1474–1480 (2010).

102. Paraskar, A. S. *et al.* Harnessing structure-activity relationship to engineer a cisplatin nanoparticle for enhanced antitumor efficacy. *Proc. Natl. Acad. Sci. U. S. A.* **107**, 12435–12440 (2010).

103. Koizumi, F. *et al.* Novel SN-38-incorporating polymeric micelles, NK012, eradicate vascular endothelial growth factor-secreting bulky tumors. *Cancer Res.* **66**, 10048–10056 (2006).

104. Kim, H. J. *et al.* Phase II clinical trial of Genexol® (paclitaxel) and carboplatin for patients with advanced non-small cell lung cancer. *Cancer Res. Treat.* **43**, 19–23 (2011).

105. Kim, D. W. *et al.* Multicenter phase II trial of Genexol-PM, a novel Cremophor-free, polymeric micelle formulation of paclitaxel, with cisplatin in patients with advanced non-small-cell lung cancer. *Ann. Oncol.* **18**, 2009–2014 (2007).

106. Zhang, W. *et al.* Enhanced antitumor efficacy by Paclitaxel-loaded Pluronic P123/F127 mixed micelles against non-small cell lung cancer based on passive tumor targeting and modulation of drug resistance. *Eur. J. Pharm. Biopharm.* **75**, 341–353 (2010).

107. Ke, S. *et al.* Gold nanoparticles enhance TRAIL sensitivity through Drp1-mediated apoptotic and autophagic mitochondrial fission in NSCLC cells. *Int. J. Nanomedicine* **12**, 2531–2551 (2017).

108. Ann L Coker. Combination Therapy of NSCLC Using Hsp90 Inhibitor and Doxorubicin Carrying Functional Nanoceria. *Physiol. Behav.* **176**, 139–148 (2017).

109. Zhang, Y., Schwerbrock, N. M. J., Rogers, A. B., Kim, W. Y. & Huang, L. Codelivery of VEGF siRNA and gemcitabine monophosphate in a single nanoparticle formulation for effective treatment of NSCLC. *Mol. Ther.* **21**, 1559–1569 (2013).

110. Youngren-Ortiz, S. R. *et al.* Development of Optimized, Inhalable, Gemcitabine-Loaded Gelatin Nanocarriers for Lung Cancer. *J. Aerosol Med. Pulm. Drug Deliv.* **30**, 299–321 (2017).

111. Yardley, D. A. Nab-Paclitaxel mechanisms of action and delivery. *J. Control. Release* **170**, 365–372 (2013).

112. Wauthoz, N. *et al.* Safe lipid nanocapsule-based gel technology to target lymph nodes and combat mediastinal metastases from an orthotopic non-small-cell lung cancer model in SCID-CB17 mice. *Nanomedicine Nanotechnology, Biol. Med.* **11**, 1237–1245 (2015).

113. Sau Wai Hunga, Sean Marracheb, Shannon Cumminsc, Yangzom D. Bhutiaa, Hardik Modya, Shelley B. Hooksa, Shanta Dharb, and R. G. Defective hCNT1 Transport Contributes to Gemcitabine Chemoresistance in Ovarian Cancer Subtypes: Overcoming Transport Defects Using a Nanoparticle Approach. *Physiol. Behav.* **176**, 139–148 (2017).

114. Piyanuch Wonganan, Dharmika S. P. Lansakara-P, Saijie Zhu, Melisande Holzer, Michael A. Sandoval, Mangalika Warthaka, and Z. C. Just Getting Into Cells is Not Enough: Mechanisms Underlying 4-(N)-Stearoyl Gemcitabine Solid Lipid Nanoparticle's Ability to Overcome Gemcitabine Resistance Caused by RRM1 Overexpression. *Bone* **23**, 1–7 (2008).

115. piyanuch Wonganan, 1,† Woon-Gye Chung, 1,† saijie Zhu, 1 Kaoru Kiguchi, 2 John DiGiovanni2 and Zhengrong Cui. Silencing of ribonucleotide reductase subunit M1 potentiates the antitumor activity of gemcitabine in resistant cancer cells. *Cell Cycle* 1–5 (2012).

116. Lansakara-P., D. S. P., Rodriguez, B. L. & Cui, Z. Synthesis and in vitro evaluation of novel lipophilic monophosphorylated gemcitabine derivatives and their nanoparticles. *Int. J. Pharm.* **429**, 123–134 (2012).

117. He, Y. *et al.* Bisphosphonate-functionalized coordination polymer nanoparticles for the treatment of bone metastatic breast cancer. *J. Control. Release* **264**, 76–88 (2017).

118. Brian R. Sloat†,*, Michael A. Sandoval†,*, Dong Li‡, Woon-Gye Chung†, Dharmika S. P. Lansakara-P.†, Philip J. Proteau‡, Kaoru Kiguchi, John DiGiovanni, and Z. C. In vitro and in vivo anti-tumor activities of a gemcitabine derivative carried by nanoparticles. **409**, 278–288 (2012).

119. Khatri, N., Rathi, M., Baradia, D. & Misra, A. CRGD grafted siRNA Nano-constructs for chemosensitization of gemcitabine hydrochloride in lung cancer treatment. *Pharm. Res.* **32**, 806–818 (2015).

120. Ahn, H. K. *et al.* A phase II trial of Cremorphor EL-free paclitaxel (Genexol-PM) and gemcitabine in patients with advanced non-small cell lung cancer. *Cancer Chemother. Pharmacol.* **74**, 277–282 (2014).

121. Ding, D. *et al.* Novel self-assembly endows human serum albumin nanoparticles with an enhanced antitumor efficacy. *AAPS PharmSciTech* **15**, 213–222 (2014).

122. Vogel, S. M., Minshall, R. D., Pilipović, M., Tiruppathi, C. & Malik, A. B. Albumin uptake and transcytosis in endothelial cells in vivo induced by albumin-binding protein. *Am. J. Physiol. - Lung Cell. Mol. Physiol.* **281**, 1512–1522 (2001).

123. Park, C. R., Jo, J. H., Song, M. G., Park, J. Y. & Kim, Y. Theranostics Secreted protein acidic and rich in cysteine mediates active targeting of human serum albumin in U87MG xenograft mouse models. **9**, (2019).

124. Ma, P. & Mumper, R. J. Paclitaxel nano-delivery systems: A comprehensive review. *Journal of Nanomedicine and Nanotechnology* **4**, 6 (2013).

125. Leuner, C. & Dressman, J. Improving drug solubility for oral delivery using solid dispersions. *Eur. J. Pharm. Biopharm.* **50**, 47–60 (2000).

126. Abrantes, C. G., Duarte, D. & Reis, C. P. An Overview of Pharmaceutical Excipients: Safe or Not Safe? *J. Pharm. Sci.* **105**, 2019–2026 (2016).

127. Varanka, Z., Rojik, I., Varanka, I., Nemcsók, J. & Ábrahám, M. Biochemical and morphological changes in carp (Cyprinus carpio L.) liver following exposure to copper sulfate and tannic acid. *Comp. Biochem. Physiol. - C Toxicol. Pharmacol.* **128**, 467–477 (2001).

128. Chen, X. *et al.* Tannic acid is an inhibitor of CXCL12 (SDF-1α)/CXCR4 with antiangiogenic activity. *Clin. Cancer Res.* **9**, 3115–3123 (2003).

129. Nagesh, P. *et al.* Tannic Acid Induces Endoplasmic Reticulum Stress-Mediated Apoptosis in Prostate Cancer. *Cancers (Basel).* **10**, 68 (2018).

130. Chowdhury, P. *et al.* Tannic acid-inspired paclitaxel nanoparticles for enhanced anticancer effects in breast cancer cells. *J. Colloid Interface Sci.* **535**, 133–148 (2019).

131. Ghate, N. B. *et al.* An antioxidant extract of tropical lichen, Parmotrema reticulatum, induces cell cycle arrest and apoptosis in breast carcinoma cell line MCF-7. *PLoS One* **8**, (2013).

132. Noble, S. & Goa, K. L. Gemcitabine. A review of its pharmacology and clinical potential in non-small cell lung cancer and pancreatic cancer. *Drugs* **54**, 447–472 (1997).

133. Wang, C. *et al.* Enhanced expression of ten-eleven translocation 1 reverses gemcitabine resistance in cholangiocarcinoma accompanied by a reduction in P-glycoprotein expression. *Cancer Med.* **8**, 990–1003 (2019).

134. Arlt, A. *et al.* Role of NF-κB and Akt/PI3K in the resistance of pancreatic carcinoma cell lines against gemcitabine-induced cell death. *Oncogene* **22**, 3243–3251 (2003).

135. Yallapu, M. M., Ebeling, M. C., Chauhan, N., Jaggi, M. & Chauhan, S. C. Interaction of curcumin nanoformulations with human plasma proteins and erythrocytes. *Int. J. Nanomedicine* **6**, 2779–2790 (2011).

136. Wang, Y. *et al.* Comparative studies on biophysical interactions between gambogic acid and serum albumin via multispectroscopic approaches and molecular docking. *Journal of Luminescence* **205**, 210–218 (2019).

137. Gräfe, C. *et al.* Intentional formation of a protein corona on nanoparticles: Serum concentration affects protein corona mass, surface charge, and nanoparticle-cell interaction. *Int. J. Biochem. Cell Biol.* **75**, 196–202 (2016).

138. Yang, F., Zhang, Y. & Liang, H. Interactive association of drugs binding to human serum albumin. *Int. J. Mol. Sci.* **15**, 3580–3595 (2014).

139. An, Z., Lu, G., M??hwald, H. & Li, J. Self-assembly of human serum albumin (HSA) and L-??- dimyristoylphosphatidic acid (DMPA) microcapsules for controlled drug release. *Chem. - A Eur. J.* **10**, 5848–5852 (2004).

140. Boloker, G., Wang, C. & Zhang, J. Updated statistics of lung and bronchus cancer in United States (2018). *J. Thorac. Dis.* **10**, 1158–1161 (2018).

141. Athar, M., Khan, W. A. & Mukhtar, H. Effect of Dietary Tannic Acid on Epidermal, Lung, and Forestomach Polycyclic Aromatic Hydrocarbon Metabolism and Tumorigenicity in Sencar Mice. *Cancer Res.* **49**, 5784–5788 (1989).

142. Panzella, L. & Napolitano, A. Natural phenol polymers: Recent advances in food and health applications. *Antioxidants* **6**, 1–24 (2017).

143. Ogawa, S., Matsuo, Y., Tanaka, T. & Yazaki, Y. Utilization of flavonoid compounds from bark and wood. III. Application in health foods. *Molecules* **23**, 1–9 (2018).

144. Nepka, C., Asprodini, E. & Kouretas, D. Tannins, xenobiotic metabolism and cancer chemoprevention in experimental animals. *Eur. J. Drug Metab. Pharmacokinet.* **24**, 183–189 (1999).

145. Jackson, J. K. & Letchford, K. The Effective Solubilization of Hydrophobic Drugs Using Epigallocatechin Gallate or Tannic Acid-Based Formulations. *J. Pharm. Sci.* **105**, 3143–3152 (2016).

146. Xu, G. *et al.* Tannic acid anchored layer-by-layer covalent deposition of parasin i peptide for antifouling and antimicrobial coatings. *RSC Adv.* **6**, 14809–14818 (2016).

147. Yang, X. *et al.* Bioinspired Peptide-Decorated Tannic Acid for in Situ Remineralization of Tooth Enamel: In Vitro and in Vivo Evaluation. *ACS Biomater. Sci. Eng.* **3**, 3553–3562 (2017).

148. FRISCH, A. W. & CARSON, R. S. Mode of inactivation of influenza virus by tannic acid. *J. Bacteriol.* **66**, 576–580 (1953).

149. Shin, M. *et al.* DNA/tannic acid hybrid gel exhibiting biodegradability, extensibility, tissue adhesiveness, and hemostatic ability. *Adv. Funct. Mater.* **25**, 1270–1278 (2015).

150. Rahim, M. A., Hata, Y., Björnmalm, M., Ju, Y. & Caruso, F. Supramolecular Metal–Phenolic Gels for the Crystallization of Active Pharmaceutical Ingredients. *Small* **14**, 1–6 (2018).

151. Chung, K. T., Wong, T. Y., Wei, C. I., Huang, Y. W. & Lin, Y. *Tannins and human health: A review*. *Critical Reviews in Food Science and Nutrition* **38**, (1998).

152. Yallapu, M. M. *et al.* Implications of protein corona on physico-chemical and biological properties of magnetic nanoparticles. *Biomaterials* **46**, 1–12 (2016).

153. Yallapu, M. M., Ebeling, M. C., Jaggi, M. & Chauhan, S. C. Plasma proteins interaction with curcumin nanoparticles: implications in cancer therapeutics. *Curr. Drug Metab.* **14**, 504–15 (2013).

154. Chowdhury, P. *et al.* Development of polyvinylpyrrolidone/paclitaxel self-assemblies for breast cancer. *Acta Pharm. Sin. B* (2017). doi:10.1016/j.apsb.2017.10.004

155. Nagesh, P. K. *et al.* +1 (901) 448 2175. *Colloids Surf B Biointerfaces* **144**, 8–20 (2016).

156. Ghisaidoobe, A. B. T. & Chung, S. J. Intrinsic tryptophan fluorescence in the detection and analysis of proteins: A focus on förster resonance energy transfer techniques. *Int. J. Mol. Sci.* **15**, 22518–22538 (2014).

157. Casals, C., Miguel, E. & Perez-Gil, J. Tryptophan fluorescence study on the interaction of pulmonary surfactant protein A with phospholipid vesicles. *Biochem. J.* **296**, 585–593 (1993).

158. Gangadhar, T., Nandi, S. & Salgia, R. The role of chemokine receptor CXCR4 in lung cancer. *Cancer Biol. Ther.* **9**, 409–416 (2010).

159. Trial, I. Phase III Study of Erlotinib in Combination With Cisplatin and Gemcitabine in Advanced Non-Small-Cell Lung Cancer : The Tarceva Lung Cancer Phase III Study of Erlotinib in Combination With Cisplatin and Gemcitabine in Advanced Non – Small-Cell Lung Cancer. (2015). doi:10.1200/JCO.2005.05.1474

160. Wald, O., Shapira, O. M. & Izhar, U. CXCR4/CXCL12 axis in non small cell lung cancer (NSCLC) pathologic roles and therapeutic potential. *Theranostics* **3**, 26–33 (2013).

161. Socinski, M. A. Irinotecan in non-small-cell lung cancer: Status of ongoing trials. *Clin. Lung Cancer* **4**, S15–S20 (2002).

162. Nobuyuki, H. Carboplatin plus pemetrexed for the elderly incurable chemo-naive non-squamous non-small cell lung cancer: meta-analysis. 1–8 (2017). doi:10.1111/ajco.12837

163. Zheng, H.-C. The molecular mechanisms of chemoresistance in cancers. *Oncotarget* **8**, 59950–59964 (2017).

164. Sequist, L. V. *et al.* Genotypic and histological evolution of lung cancers acquiring resistance to EGFR inhibitors. *Sci. Transl. Med.* **3**, (2011).

165. Xu, L. *et al.* Gambogenic acid inhibits fibroblast growth factor receptor signaling pathway in erlotinib-resistant non-small-cell lung cancer and suppresses patient-derived xenograft growth article. *Cell Death Dis.* **9**, (2018).

166. Hayashi, H., Kurata, T. & Nakagawa, K. Gemcitabine: Efficacy in the treatment of advanced stage nonsquamous non-small cell lung cancer. *Clin. Med. Insights Oncol.* **5**, 177–184 (2011).

167. D'Amato, T. A., Landreneau, R. J., McKenna, R. J., Santos, R. S. & Parker, R. J. Prevalence of in vitro extreme chemotherapy resistance in resected nonsmall-cell lung cancer. *Ann. Thorac. Surg.* **81**, 440–447 (2006).

168. Bergman, A. M., Pinedo, H. M. & Peters, G. J. Determinants of resistance to 2′,2′-difluorodeoxycytidine (gemcitabine). *Drug Resist. Updat.* **5**, 19–33 (2002).

169. Chung, L.-Y. *et al.* Galectin-1 Upregulates CXCR4 to Promote Tumor Progression and Poor Outcome in Kidney Cancer. *J. Am. Soc. Nephrol.* **25**, 1486–1495 (2014).

170. Tian, F. *et al.* A targeted nanoplatform co-delivering chemotherapeutic and antiangiogenic drugs as a tool to reverse multidrug resistance in breast cancer. *Acta Biomater.* **75**, 398–412 (2018).

171. Zhang, X. *et al.* Gambogic acid inhibits the catalytic activity of human topoisomerase II by binding to its ATPase domain. *Mol. Cancer Ther.* **6**, 2429–2440 (2007).

172. Li, R. *et al.* Effects of gambogic acid on regulation of steroid receptor coactivator-3 in lung adenocarcinoma A549 cells. *Chinese J. Cancer Res.* **21**, 68–73 (2009).

173. Hua, X., Liang, C., Dong, L., Qu, X. & Zhao, T. Simultaneous determination and pharmacokinetic study of gambogic acid and gambogenic acid in rat plasma after oral administration of Garcinia hanburyi extracts by LC-MS/MS. *Biomed. Chromatogr.* **29**, 545–551 (2015).

174. Pfister, C., Pfrommer, H., Tatagiba, M. S. & Roser, F. Vascular endothelial growth factor signals through platelet-derived growth factor receptor β in meningiomas in vitro. *Br. J. Cancer* **107**, 1702–1713 (2012).

175. Xu, Y. *et al.* Nanoparticles with optimal ratiometric co-delivery of docetaxel with gambogic acid for treatment of multidrug-resistant breast cancer. *J. Biomed. Nanotechnol.* **12**, 1774–1781 (2016).

176. Zhao, T., Wang, H. J., Zhao, W. W., Sun, Y. L. & Hu, L. K. Gambogic acid improves non-small cell lung cancer progression by inhibition of mTOR signaling pathway. *Kaohsiung J. Med. Sci.* **33**, 543–549 (2017).

177. Zhu, M. *et al.* Gambogic Acid Shows Anti-Proliferative Effects on Non-Small Cell Lung Cancer (NSCLC) Cells by Activating Reactive Oxygen Species (ROS)-Induced Endoplasmic Reticulum (ER) Stress-Mediated Apoptosis. *Med. Sci. Monit.* **25**, 3983–3988 (2019).

178. Kang, Y. *et al.* Redox-responsive polymeric micelles formed by conjugating gambogic acid with bioreducible poly(amido amine)s for the co-delivery of docetaxel and MMP-9 shRNA. *Acta Biomater.* **68**, 137–153 (2018).

179. Wang, T. *et al.* Gambogic acid, a potent inhibitor of survivin, reverses docetaxel resistance in gastric cancer cells. *Cancer Lett.* **262**, 214–222 (2008).

180. Zou, Z. *et al.* Synergistic anti-proliferative effects of gambogic acid with docetaxel in gastrointestinal cancer cell lines. *BMC Complement. Altern. Med.* **12**, 1 (2012).

181. Wang, H. *et al.* Gambogic acid induces autophagy and combines synergistically with chloroquine to suppress pancreatic cancer by increasing the accumulation of reactive oxygen species 11 Medical and Health Sciences 1112 Oncology and Carcinogenesis 06 Biological Sciences 06. *Cancer Cell Int.* **19**, 1–15 (2019).

182. Wang, L. H. *et al.* Gambogic acid synergistically potentiates cisplatin-induced apoptosis in non-small-cell lung cancer through suppressing NF-κB and MAPK/HO-1 signalling. *Br. J. Cancer* **110**, 341–352 (2014).

183. Wei, J. *et al.* Gambogic acid potentiates the chemosensitivity of colorectal cancer cells to 5-fluorouracil by inhibiting proliferation and inducing apoptosis. *Exp. Ther. Med.* **13**, 662–668 (2017).

184. Liu, L., Qi, X. J., Zhong, Z. K. & Zhang, E. N. Nanomedicine-based combination of gambogic acid and retinoic acid chlorochalcone for enhanced anticancer efficacy in osteosarcoma. *Biomed. Pharmacother.* **83**, 79–84 (2016).

185. Na, K. *et al.* A solvent-assisted active loading technology to prepare gambogic acid and all-trans retinoic acid co-encapsulated liposomes for synergistic anticancer therapy. *Drug Deliv. Transl. Res.* (2019). doi:10.1007/s13346-019-00669-4

186. Bishayee, K., Dubey, V., Sadra, A. & Huh, S.-O. Targeting the difficult-to-drug CD71 and MYCN with gambogic acid and vorinostat an a class of neuroblastomas. *IBRO Reports* **6**, S426 (2019).

187. Shi, X. *et al.* Gambogic acid induces apoptosis in imatinib-resistant chronic myeloid leukemia cells via inducing proteasome inhibition and caspase-dependent bcr-abl downregulation AC. *Clin. Cancer Res.* **20**, 151–163 (2014).

188. Ning, R. *et al.* Gambogic acid potentiates clopidogrel-induced apoptosis and attenuates irinotecan-induced apoptosis through down-regulating human carboxylesterase 1 and -2. *Xenobiotica* **46**, 816–824 (2016).

189. Wang, C., Wang, W., Wang, C., Tang, Y. & Tian, H. Combined therapy with EGFR TKI and gambogic acid for overcoming resistance in EGFR-T790M mutant lung cancer. *Oncol. Lett.* **10**, 2063–2066 (2015).

190. Wang, S., Wang, L., Chen, M. & Wang, Y. Gambogic acid sensitizes resistant breast cancer cells to doxorubicin through inhibiting P-glycoprotein and suppressing survivin expression. *Chem. Biol. Interact.* **235**, 76–84 (2015).

191. Wang, J. & Yuan, Z. Gambogic Acid Sensitizes Ovarian Cancer Cells to Doxorubicin Through ROS-Mediated Apoptosis. *Cell Biochem. Biophys.* **67**, 199–206 (2013).

192. Wang, Y. *et al.* Methyl jasmonate sensitizes human bladder cancer cells to gambogic acid-induced apoptosis through down-regulation of EZH2 expression by miR-101. *Br. J. Pharmacol.* **171**, 618–635 (2014).

193. Liu, N. *et al.* Calcium channel blocker verapamil accelerates gambogic acid-induced cytotoxicity via enhancing proteasome inhibition and ROS generation. *Toxicol. Vitr.* **28**, 419–425 (2014).

194. He, D. *et al.* The NF-kappa B inhibitor, celastrol, could enhance the anti-cancer effect of gambogic acid on oral squamous cell carcinoma. *BMC Cancer* **9**, 343 (2009).

195. Jiang, X. L., Yao Zhang, Luo, C. L. & Wu, X. H. Targeting renal cell carcinoma with gambogic acid in combination with sunitinib in vitro and in vivo. *Asian Pacific J. Cancer Prev.* **13**, 6463–6468 (2012).

196. Hatami, E. *et al.* Tannic acid-lung fluid assemblies promote interaction and delivery of drugs to lung cancer cells. *Pharmaceutics* **10**, (2018).

197. Li, J., Pan, Y. Y. & Zhang, Y. Synergistic interaction between sorafenib and gemcitabine in EGFR-TKI-sensitive and EGFR-TKI-resistant human lung cancer cell lines. *Oncol. Lett.* **5**, 440–446 (2013).

198. Chou, T. C. Drug combination studies and their synergy quantification using the chou-talalay method. *Cancer Res.* **70**, 440–446 (2010).

199. Qin, Y. G. *et al.* Glycol chitosan incorporated retinoic acid chlorochalcone (RACC) nanoparticles in the treatment of Osteosarcoma. *Lipids Health Dis.* **14**, 1–10 (2015).

200. Florczyk, U. *et al.* Nrf2 regulates angiogenesis: effect on endothelial cells, bone marrow-derived proangiogenic cells and hind limb ischemia. *Antioxid. Redox Signal.* **20**, 1693–708 (2014).

201. Chowdhury, P. *et al.* Tannic acid-inspired paclitaxel nanoparticles for enhanced anticancer effects in breast cancer cells. *J. Colloid Interface Sci.* **535**, 133–148 (2019).

202. Khan, S. *et al.* MUC13 interaction with receptor tyrosine kinase HER2 drives pancreatic ductal adenocarcinoma progression. *Oncogene* **36**, 491–500 (2017).

203. Nagesh, P. K. B. *et al.* miRNA-205 nanoformulation sensitizes prostate cancer cells to chemotherapy. *Cancers (Basel).* **10**, (2018).

204. Hsu, C. P. *et al.* Mechanisms of grape seed procyanidin-induced apoptosis in colorectal carcinoma cells. *Anticancer Res.* **29**, 283–289 (2009).

205. Hafeez, B. Bin *et al.* Ormeloxifene Suppresses Prostate Tumor Growth and Metastatic Phenotypes via Inhibition of Oncogenic β-catenin Signaling and EMT Progression. *Mol. Cancer Ther.* **16**, 2267–2280 (2017).

206. Nagesh, P. *et al.* Tannic Acid Induces Endoplasmic Reticulum Stress-Mediated Apoptosis in Prostate Cancer. *Cancers (Basel).* **10**, 68 (2018).

207. Kim, S.-A., Kang, O.-H. & Kwon, D.-Y. Cryptotanshinone Induces Cell Cycle Arrest and Apoptosis of NSCLC Cells through the PI3K/Akt/GSK-3β Pathway. *Int. J. Mol. Sci.* **19**, 2739 (2018).

208. Twentyman, P. R., Rhodes, T. & Rayner, S. A comparison of rhodamine 123 accumulation and efflux in cells with P-glycoprotein-mediated and MRP-associated multidrug resistance phenotypes. *Eur. J. Cancer* **30**, 1360–1369 (1994).

209. Khan, M. A. *et al.* Gemcitabine triggers angiogenesis-promoting molecular signals in pancreatic cancer cells: Therapeutic implications. *Oncotarget* **6**, (2015).

210. Wang, H. *et al.* Gambogic acid induces autophagy and combines synergistically with chloroquine to suppress pancreatic cancer by increasing the accumulation of reactive oxygen species 11 Medical and Health Sciences 1112 Oncology and Carcinogenesis 06 Biological Sciences 06. *Cancer Cell Int.* **19**, 1–15 (2019).

211. Zou, Z. *et al.* Synergistic anti-proliferative effects of gambogic acid with docetaxel in gastrointestinal cancer cell lines. *BMC Complement. Altern. Med.* **12**, 1 (2012).

212. Lyu, L. *et al.* Cell-penetrating peptide conjugates of gambogic acid enhance the antitumor effect on human bladder cancer EJ cells through ROS-mediated apoptosis. *Drug Des. Devel. Ther.* **12**, 743–756 (2018).

213. Gao, G. *et al.* Gambogic acid regulates the migration and invasion of colorectal cancer via microRNA-21-mediated activation of phosphatase and tensin homolog. *Exp. Ther. Med.* **16**, 1758–1765 (2018).

214. Wen, C. *et al.* Gambogic acid inhibits growth, induces apoptosis, and overcomes drug resistance in human colorectal cancer cells. *Int. J. Oncol.* **47**, 1663–1671 (2015).

215. Zhu, M. *et al.* Gambogic Acid Induces Apoptosis of Non-Small Cell Lung Cancer (NSCLC) Cells by Suppressing Notch Signaling. *Med. Sci. Monit.* **24**, 7146–7151 (2018).

216. Barton-Burke, M. Gemcitabine: A pharmacologic and clinical overview. *Cancer Nursing* **22**, 176–183 (1999).

217. Goan, Y. G., Zhou, B., Hu, E., Mi, S. & Yen, Y. Overexpression of ribonucleotide reductase as a mechanism of resistance to 2,2-difluorodeoxycytidine in the human KB cancer cell line. *Cancer Res.* **59**, 4204–4207 (1999).

218. Montano, R. *et al.* Cell cycle perturbation induced by gemcitabine in human tumor cells in cell culture, xenografts and bladder cancer patients: implications for clinical trial designs combining gemcitabine with a Chk1 inhibitor. *Oncotarget* **8**, 67754–67768 (2017).

219. Robert S. DiPaola. To Arrest or Not To G2-M Cell-Cycle Arrest. *Clin. cancer Res.* **8**, 3311–3314 (2002).

220. Huang, J. *et al.* Role of gambogic acid and NaI131 in A549/DDP cells. *Oncol. Lett.* **13**, 37–44 (2017).

221. Wen, J. *et al.* Gambogic acid exhibits anti-psoriatic efficacy through inhibition of angiogenesis and inflammation. *J. Dermatol. Sci.* **74**, 242–250 (2014).

222. Ernsting, M. J. *et al.* A docetaxel-carboxymethylcellulose nanoparticle outperforms the approved taxane nanoformulation, Abraxane, in mouse tumor models with significant control of metastases. *J. Control. Release* **162**, 575–581 (2012).

223. Ranoszek-Soliwoda, K. *et al.* The role of tannic acid and sodium citrate in the synthesis of silver nanoparticles. *J. Nanoparticle Res.* **19**, (2017).

224. Yuee Cai, 1 Jinming Zhang, 1 Nelson G. Chen, 2 Zhi Shi, 3 Jiange Qiu, 3 Chengwei He, 1 andMeiwan Chen1. Recent Advances in Anticancer Activities andDrug Delivery Systems ofTannins. *Med. Res. Rev.* **36**, 705–748 (2016).

225. Kebebe, D. *et al.* Dimeric c(RGD) peptide conjugated nanostructured lipid carriers for efficient delivery of Gambogic acid to breast cancer . *Int. J. Nanomedicine* **Volume 14**, 6179–6195 (2019).

226. Mini, E., Nobili, S., Caciagli, B., Landini, I. & Mazzei, T. Cellular pharmacology of gemcitabine. *Ann. Oncol.* **17**, 7–12 (2006).

227. Bunschoten, A. *et al.* Targeted non-covalent self-assembled nanoparticles based on human serum albumin. *Biomaterials* **33**, 867–875 (2012).

228. Langer, K. *et al.* Optimization of the preparation process for human serum albumin (HSA) nanoparticles. *Int. J. Pharm.* **257**, 169–180 (2003).

229. Preparation of sub-100 nm human serum albumin nanospheres using a ph-coacervation method. *J. Drug Target.* **1**, 237–243 (1993).

230. Hatami, E. *et al.* Mannose-decorated hybrid nanoparticles for enhanced macrophage targeting. *Biochem. Biophys. Reports* **17**, 197–207 (2019).

231. Nagesh, P. K. B. *et al.* Cross-Linked Polyphenol-Based Drug Nano-Self-Assemblies Engineered to Blockade Prostate Cancer Senescence. *ACS Appl. Mater. Interfaces* (2019). doi:10.1021/acsami.9b14738

232. Sadhukha, T. & Prabha, S. Encapsulation in Nanoparticles Improves Anti-cancer Efficacy of Carboplatin. *AAPS PharmSciTech* **15**, 1029–1038 (2014).

233. Liang, Y. *et al.* Tumor-targeted polymeric nanostructured lipid carriers with precise ratiometric control over dual-drug loading for combination therapy in non-small-cell lung cancer. *Int. J. Nanomedicine* **12**, 1699–1715 (2017).

234. Lopes, L. C. S. *et al.* Silver and gold nanoparticles from tannic acid: Synthesis, characterization and evaluation of antileishmanial and cytotoxic activities. *An. Acad. Bras. Cienc.* **90**, 2679–2689 (2018).

235. Dong, G. *et al.* Antimicrobial and anti-biofilm activity of tannic acid against Staphylococcus aureus. *Nat. Prod. Res.* **32**, 2225–2228 (2018).

236. Chowdhury, P. *et al.* Development of polyvinylpyrrolidone/paclitaxel self-assemblies for breast cancer. *Acta Pharm. Sin. B* **8**, 602–614 (2018).

237. Leung, K. Cy5.5-Gly-Pro-Leu-Gly-Val-Arg-Gly-Cys-gold nanoparticles. 1–5 (2004).

238. Zhao, J. & Stenzel, M. H. Entry of nanoparticles into cells: The importance of nanoparticle properties. *Polym. Chem.* **9**, 259–272 (2018).

239. Huang, J. *et al.* Biodegradable self-assembled nanoparticles of poly (d,l-lactide-co-glycolide)/hyaluronic acid block copolymers for target delivery of docetaxel to breast cancer. *Biomaterials* **35**, 550–566 (2014).

240. Target, A. N. & Lung, N. C. The CXCR4 / SDF-1 Chemokine Receptor Axis. *JTO Acquis.* **3**, 1379–1383 (2008).

241. Eisenach, P. A., Schikora, F. & Posern, G. Inhibition of arginyltransferase 1 induces transcriptional activity of myocardin-related transcription factor a (mrtf-a) and promotes directional migration. *J. Biol. Chem.* **289**, 35376–35387 (2014).

242. Oh, B. Y., Hong, H. K., Lee, W. Y. & Cho, Y. B. Animal models of colorectal cancer with liver metastasis. *Cancer Lett.* **387**, 114–120 (2017).

243. Helbig, G. *et al.* NF-κB promotes breast cancer cell migration and metastasis by inducing the expression of the chemokine receptor CXCR4. *J. Biol. Chem.* **278**, 21631–21638 (2003).

244. Takeuchi, Y. *et al.* In vivo effects of short- and long-term MAPK pathway inhibition against neuroblastoma. *J. Pediatr. Surg.* **53**, 2454–2459 (2018).

245. Sompuram, S. R., Vani, K., Schaedle, A. K., Balasubramanian, A. & Bogen, S. A. Quantitative assessment of immunohistochemistry laboratory performance by measuring analytic response curves and limits of detection. *Arch. Pathol. Lab. Med.* **142**, 851–862 (2018).

246. Jansch, M., Stumpf, P., Graf, C., Rühl, E. & Müller, R. H. Adsorption kinetics of plasma proteins on ultrasmall superparamagnetic iron oxide (USPIO) nanoparticles. *Int. J. Pharm.* **428**, 125–133 (2012).

247. Feng, Q. *et al.* Self-Assembly of Gold Nanoparticles Shows Microenvironment-Mediated Dynamic Switching and Enhanced Brain Tumor Targeting. *Theranostics* **7**, 1875–1889 (2017).

248. Joseph, E., Singhvi, G. & Ions, I. Multifunctional nanocrystals for cancer Multifunctional nanocrystals for cancer therapy: a potential nanocarrier.

249. Hatami, E. *et al.* Abstract LB-400: Tannic acid induces prostate cancer cell death via unfolded protein response (UPR) and modulation of CHOP. *Cancer Res.* **78**, LB-400 LP-LB-400 (2018).

250. Smith, R. A., Walker, R. C., Levit, S. L. & Tang, C. Single-step self-assembly and physical crosslinking of PEGylated chitosan nanoparticles by tannic acid. *Polymers (Basel).* **11**, (2019).

251. Zhang, Z. *et al.* Construction of a Supramolecular Drug–Drug Delivery System for Non-Small-Cell Lung Cancer Therapy. *ACS Appl. Mater. Interfaces* **9**, 29505–29514 (2017).

252. Kim, T. Y. *et al.* Phase I and pharmacokinetic study of Genexol-PM, a Cremophor-free, polymeric micelle-formulated paclitaxel, in patients with advanced malignancies. *Clin. Cancer Res.* **10**, 3708–3716 (2004).

253. Miele, E., Spinelli, G. P., Miele, E., Tomao, F. & Tomao, S. Albumin-bound formulation of paclitaxel (Abraxane® ABI-007) in the treatment of breast cancer. *International Journal of Nanomedicine* **4**, 99–105 (2009).

254. Mylonakis, N. *et al.* Phase II study of liposomal cisplatin (Lipoplatin^{TM}) plus gemcitabine versus cisplatin plus gemcitabine as first line treatment in inoperable (stage IIIB/IV) non-small cell lung cancer. *Lung Cancer* **68**, 240–247 (2010).

255. Mah, V. *et al.* Ribonucleotide reductase subunit M2 predicts survival in subgroups of patients with non-small cell lung carcinoma: Effects of gender and smoking status. *PLoS One* **10**, 1–15 (2015).

256. Wang, L., and Meng, L., and Wang, X., and Ma, G. & and Chen, J. Expression of RRM1 and RRM2 as a novel prognostic marker in advanced non-small cell lung cancer receiving chemotherapy. *Tumor Biol.* **35**, 1899–1906 (2014).

257. Rong, J. J. *et al.* Gambogic acid down-regulates MDM2 oncogene and induces p21Waf1/CIP1 expression independent of p53. *Cancer Lett.* **284**, 102–112 (2009).

258. Wang, J. & Yuan, Z. Gambogic Acid Sensitizes Ovarian Cancer Cells to Doxorubicin Through ROS-Mediated Apoptosis. *Cell Biochem. Biophys.* **67**, 199–206 (2013).

259. U.S. National Library of Medicine. https://clinicaltrials.gov/ct2 accessed October 19, 2019.

VITA

Elham Hatami was born in Tehran, Iran, in 1984 to Ali Hatami and Aghdas Hatami. She graduated with Bachelor of Science degree in chemistry, from university of Tarbiaat Moalem, Tehran, Iran in 2008. She came to the United States in December 2013, and enrolled in University of Utah and earned her second Bachelor degree in biology in December 2015. She joined Ph.D. program in Pharmaceutical Sciences department at the University of Tennessee Health Science Center (UTHSC), Memphis, TN in fall 2016. She expects to receive her Doctorate degree in May 2020.

She has presented her projects in various regional and national conferences and published a number of scientific manuscripts in peer- reviewed journals.